Investigations into Smart Antennas for CDMA Wireless Systems

by

Salman Durrani

A thesis submitted in the
School of Information Technology & Electrical Engineering
in fulfillment of the requirements
for the degree of

Doctor of Philosophy

at the

The University of Queensland,
Brisbane, Australia.

August 2004

Investigations into Smart Antennas for CDMA Wireless Systems

Copyright © 2004 by Salman Durrani.

All Rights Reserved.

This thesis is dedicated to my parents, Karam Elahi Durrani and Samia Durrani, to whom I owe my love of learning.

Statement of Originality

The work presented in the thesis is, to the best of my knowledge and belief, original and my own work except as acknowledged in the text. The material has not been submitted, either in whole or in part, for a degree at the University of Queensland or any other university.

_____

Salman Durrani

August 2004

Abstract

Over the last few years, wireless cellular communications has experienced rapid growth in the demand for provision of high data rate wireless multimedia services. This fact motivates the need to find ways to improve the spectrum efficiency of wireless communication systems. Smart or adaptive antennas have emerged as a promising technology to enhance the spectrum efficiency of present and future wireless communications systems by exploiting the spatial domain. The aim of this thesis is to investigate smart antenna applications for Direct Sequence Code Division Multiple Access (DS-CDMA) systems. CDMA is chosen as the platform for this thesis work since it has been adopted as the air-interface technology by the Third Generation (3G) wireless communication systems.

The main role of smart antennas is to mitigate Multiple Access Interference (MAI) by beamforming (i.e. spatial filtering) operation. Therefore, irrespective of a particular wireless communication system, it is important to consider whether a chosen array configuration will enable optimal performance. In this thesis an initial assessment is carried out considering linear and circular array of dipoles, that can be part of a base station antenna system. A unified and systematic approach is proposed to analyse and compare the interference rejection capabilities of the two array configurations in terms of the Signal to Interference Ratio (SIR) at the array output. The theoretical framework is then extended to include the effect of mutual coupling, which is modelled using both analytical and simulation methods. Results show that when the performance is averaged over all angles of arrival and mutual coupling is negligible, linear arrays show similar performance as circular arrays. Thus in the remaining part of this thesis, only linear arrays are considered.

In order to properly evaluate the performance of smart antenna systems, a realistic channel model is required that takes into account both temporal and spatial propagation char-

acteristics of the wireless channel. In this regard, a novel parameterized physical channel model is proposed in this thesis. The new model incorporates parameters such as user mobility, azimuth angle of arrival, angle spread and Doppler frequency, which have critical influence on the performance of smart antennas. A mathematical formulation of the channel model is presented and the proposed model is implemented in software using Matlab. The statistics of the simulated channels are analysed and compared with theory to confirm that the proposed model can accurately simulate Rayleigh and Rician fading characteristics.

To assist system planners in the design and deployment of smart antennas, it is important to develop robust analytical tools to assess the impact of smart antennas on cellular systems. In this thesis an analytical model is presented for evaluating the Bit Error Rate (BER) of a DS-CDMA system employing an array antenna operating in Rayleigh and Rician fading environments. The DS-CDMA system is assumed to employ noncoherent M-ary orthogonal modulation, which is relevant to IS-95 CDMA and cdma2000. Using the analytical model, an expression of the Signal to Interference plus Noise Ratio (SINR) at the output of the smart antenna receiver is derived, which allows the BER to be evaluated using a closed-form expression. The proposed model is shown to provide good agreement with the (computationally intensive) Monte Carlo simulation results and can be used to rapidly calculate the system performance for suburban and urban fading environments.

In addition to MAI, the performance of CDMA systems is limited by fast fading. In this context, a hybrid scheme of beamforming and diversity called Hierarchical Beamforming (HBF) is investigated in this thesis to jointly combat MAI and fading. The main idea behind HBF is to divide the antenna elements into widely separated groups to form sub-beamforming arrays. The performance of a hierarchical beamforming receiver, applied to an IS-95 CDMA system, is compared with smart antenna (conventional beamforming) receiver and the effect of varying the system and channel parameters is studied. The simulation results show that the performance of hierarchical beamforming is sensitive to the operating conditions, especially the value of the azimuth angle spread.

The work presented in this thesis has been published in part in several journals and refereed conference papers, which reflects the originality and significance of the thesis contributions.

Acknowledgements

First, I would like to express my deepest appreciation and sincerest gratitude to my advisor, Prof. Dr. Marek E. Bialkowski, for his encouragement, advice and generous financial support during the course of my PhD. This thesis would not have been possible without his invaluable technical insight and continuous guidance.

I would like to thank all my senior colleagues at the University of Queensland, in particular Dr. John Homer, Dr. Nicholas Shuley and Prof. John L. Morgan (Warden, St John's College) for their advice. I thank my office mates and PhD colleagues Eddie Tsai, Januar Janapsatya and Serguei Zagriatski for their enjoyable company and discussions, both technical and non-technical. Many thanks are also due to Mr. Richard Taylor (School Technical Infrastructure Manager) for providing the extra computer systems support and facilities for the simulation work in the thesis.

Special thanks are due to Emad Abro and Ishaq Burney for their friendship and sense of humour which kept me sane over the past three and a half years.

I would like to acknowledge the support of the Australian government and the School of Information Technology & Electrical Engineering (ITEE), The University of Queensland, Brisbane, for provision of an International Postgraduate Research Scholarship (IPRS) and a School of ITEE International Scholarship respectively.

Last but not the least, I would like to thank my family; my sisters Sarah and Sameera for their love and patience and my parents for their continuous encouragement and moral support.

Thesis Publications

The work presented in this thesis has been published, in part, in the following journals and refereed conference proceedings:-

Refereed Journal Papers

- **S. Durrani** and M. E. Bialkowski, "Analysis of the error performance of adaptive array antennas for CDMA with noncoherent *M*-ary orthogonal modulation in nakagami fading," *to appear in IEEE Communications Letters*, vol. 9, no. 2, Feb. 2005.
- **S. Durrani** and M. E. Bialkowski, "Effect of mutual coupling on the interference rejection capabilities of linear and circular arrays in CDMA systems," *IEEE Transaction on Antennas and Propagation*, vol. 52, no. 4, pp. 1130-1134, Apr. 2004.
- **S. Durrani** and M. E. Bialkowski, "An investigation into the interference rejection capability of a linear array in a wireless communications system," *Microwave and Optical Technology Letters*, vol. 35, no. 6, pp. 445-449, Dec. 2002.
- **S. Durrani** and M. E. Bialkowski, "Interference rejection capabilities of different types of antenna arrays in cellular systems," *IEE Electronics Letters*, vol. 38, pp. 617-619, June 2002.

Refereed International Conference Papers

- **S. Durrani** and M. E. Bialkowski, "A simple model for performance evaluation of a smart antenna in a CDMA system," in *Proc. IEEE International Symposium on Spread Spectrum Techniques and Applications (ISSSTA)*, Sydney, Australia, Aug. 30 - Sep. 2, 2004, pp. 379-383.
- **S. Durrani** and M. E. Bialkowski, "Performance of hierarchical beamforming in a

Rayleigh fading environment with angle spread," in *Proc. International Symposium on Antennas (ISAP)*, vol. 2, Sendai, Japan, Aug. 17-21, 2004, pp. 937-940.

- **S. Durrani** and M. E. Bialkowski, "Effect of angular energy distribution of an incident signal on the spatial fading correlation of a uniform linear array," in *Proc. International Conference on Microwaves, Radar and Wireless Communications (MIKON)*, vol. 2, Warsaw, Poland, May 17-19, 2004, pp. 493-496.
- **S. Durrani** and M. E. Bialkowski, "Performance analysis of beamforming in ricean fading channels for CDMA systems," in *Proc. Australian Communications Theory Workshop (AusCTW)*, Newcastle, Australia, Feb. 4-6, 2004, pp. 1-5.
- **S. Durrani** and M. E. Bialkowski, "A smart antenna model incorporating an azimuthal dispersion of received signals at the base station of a CDMA system," in *Proc. IEEE International Multi Topic Conference (INMIC)*, Islamabad, Pakistan, Dec. 8-9, 2003, pp. 218-223.
- **S. Durrani** and M. E. Bialkowski, "BER performance of a smart antenna system for IS-95 CDMA," in *Proc. IEEE International Symposium on Antennas and Propagation (AP-S)*, vol. 2, Columbus, Ohio, June 22-27, 2003, pp. 855-858.
- **S. Durrani** and M. E. Bialkowski, "Simulation of the performance of smart antennas in the reverse link of CDMA system," in *Proc. IEEE International Microwave Symposium (IMS)*, vol. 1, Philadelphia, Pennsylvania, June 8-13, 2003, pp. 575-578.
- **S. Durrani**, M. E. Bialkowski and J. Janapsatya, "Effect of mutual coupling on the interference rejection capabilities of a linear array antenna, " in *Proc. Asia Pacific Microwave Conference (APMC)*, vol. 2, Kyoto, Japan, Nov. 19-22, 2002, pp. 1095-1098.
- **S. Durrani** and M. E. Bialkowski, "Investigation into the performance of an adaptive array in cellular environment," in *Proc. IEEE International Symposium on Antennas and Propagation (AP-S)*, vol. 2, San Antonio, Texas, June 16-21, 2002, pp. 648-651.
- **S. Durrani** and M. E. Bialkowski, "Development of CDMASIM: a link level simulation software for DS-CDMA systems," in *Proc. 14th International Conference on Microwaves, Radar and Wireless Communications (MIKON)*, Gdansk, Poland, May 20-22, 2002, pp. 861-864.

National Conference Abstracts

- **S. Durrani** and M. E. Bialkowski, "Influence of mutual coupling on the interference rejection capability of a smart antenna system," *8th Australian Symposium on Antennas (ASA)*, Sydney, pp. 20, Feb. 12-13, 2003.
- **S. Durrani** and M. E. Bialkowski, "The performance of a smart antenna system in multipath fading environment for CDMA," *4th Australian Communications Theory Workshop (AusCTW)*, Melbourne, pp. 10, Feb. 5-7, 2003.

Project Awards

- **Highly Commended Student Presentation Award**, Eighth Australian Symposium on Antennas, CSIRO Telecommunications & Industrial Physics Centre, Sydney, Australia, Feb. 2003.
  (one first prize and two honourable mention prizes were awarded at the conference.)
- **Richard Jago Memorial Prize**, School of Information Technology & Electrical Engineering, The University of Queensland, 2001.
  (prize awarded for the purpose of furthering research by attendance at a conference.)

Contents

List of Figures

List of Tables

List of Abbreviations

1-D	One-Dimensional
2-D	Two-Dimensional
1G	First Generation
2G	Second Generation
3G	Third Generation
3GPP	Third Generation Partnership Project
3GPP2	Third Generation Partnership Project Two
AOA	Angle of Arrival
AOD	Angle of Departure
AS	Angle Spread
AWGN	Additive White Gaussian Noise
BER	Bit Error Rate
BS	Base Station
CBF	Conventional Beamforming
CDMA	Code Division Multiple Access
dB	Decibels
EGC	Equal Gain Combining
FDD	Frequency Division Duplex
GSM	Global System for Mobile communications
HBF	Hierarchial Beamforming
IS-95	Interim Standard-95
LOS	Line-Of-Sight
MAI	Multiple Access Interference

MIMO	Multiple Input Multiple Output
MS	Mobile Station
NLOS	Non-Line-Of-Sight
OQPSK	Offset Quadrature Phase Shift Keying
pdf	Probability Density Function
PDP	Power Delay Profile
PSD	Power Spectral Density
PN	Pseudo-Noise
RMS	Root Mean Square
SCM	Spatial Channel Model
SDMA	Space Division Multiple Access
SFIR	Spatial Filtering for Interference Rejection
SINR	Signal to Interference plus Noise Ratio
SIR	Signal to Interference Ratio
SNR	Signal to Noise Ratio
TDD	Time Division Duplex
TDMA	Time Division Multiple Access
UCA	Uniform Circular Array
ULA	Uniform Linear Array
W-CDMA	Wideband-Code Division Multiple Access

List of Symbols

$\mathbf{a}(\theta)$	Array steering vector
$a^{(I)}(t)$	In-phase (I) channel spreading sequence
$a^{(Q)}(t)$	Quadrature (Q) channel spreading sequence
$a_k(t)$	kth user long code sequence
$\mathcal{A}$	Array manifold
BW_{ir}	Interference reduction beamwidth
c	Velocity of light (3×10^8 m/s)
$\mathbf{C}$	Coupling matrix
$\mathbf{d}(\theta)$	Gradient of array steering vector
d	Inter-element distance for ULA
D_k	Distance between the kth MS and the BS
E_b/N_o	Ratio of bit energy to noise power spectral density
F	Number of hierarchical beamforming sub-arrays
f	Frequency
$f_{AOA}(\theta)$	Probability density function of AOA
f_c	Carrier frequency (900 MHz)
f_D	Doppler frequency
$g_k(\theta_1, \theta_k)$	Normalised interference power from kth interferer
$G_{avg}(\theta_1)$	Spatial interference suppression coefficient
$\mathbf{h}(\theta)$	Channel vector
$h_{k,l,n}$	Channel response for lth multipath of kth user at nth antenna
j	Complex number
κ	Number of in-beam interferers

k	User index
K	Number of users
K_R	Rice factor
$\mathcal{K}$	Wave number
l	Multipath index
L	Number of resolvable multipaths per user
m	Hadamard-Walsh symbol index
M	M-ary Hadamard-Walsh symbol
M_c	Number of Monte Carlo simulation drops
n	Antenna index
N	Number of antenna elements
N_c	Spreading gain of CDMA system
$p(t)$	Chip pulse shape
$P(\tau)$	Power Delay Profile
$P_b^{(1\text{-D})}$	Probability of bit error for 1-D RAKE (conventional) receiver
$P_b^{(2\text{-D})}$	Probability of bit error for 2-D RAKE receiver
Q	Oversampling factor
$\mathbf{R}_s$	Array spatial correlation matrix
R	Radius of UCA
$R(\tau)$	Autocorrelation function
s	Subpath index
$s_k(t)$	Signal transmitted by kth user
S	Number of subpaths per path
$\mathcal{S}_k$	Shadowing attenuation for the kth MS
t	Time
T_c	Chip time
T_o	Half chip delay for OQPSK signals
T_w	Walsh symbol time
$U_n(\theta)$	nth element antenna pattern

v	Velocity of MS
$\mathbf{w}$	Weight vector
$W_k^{(m)}$	mth Hadamard-Walsh symbol of the kth user
$x_n(t)$	Received signal at the nth antenna
$y_n(t)$	Array output signal at the nth antenna
$\mathbf{Z}$	Mutual Impedance matrix
$\alpha_{k,l}^{(s)}$	Complex amplitude of subpath
α_o	Attenuation factor for out-of-beam interferers
$\beta_{k,l}$	Overall channel gain of lth multipath of kth user
Γ_k	Random asynchronous delay of the kth user
Δ	Scattering angle for uniform distribution of AOA
$\Delta\theta$	AOA change per snapshot
ε	Path loss exponent
η	Additive White Gaussian Noise
θ_{BW}	Half of total beamwidth towards desired user
θ_k	AOA of the kth user
$\theta_{k,l}^{(s)}$	AOA of sth subpath for the lth path of the kth user
$\vartheta_{k,l}^{(s)}$	Angular deviation of sth subpath for the lth path of the kth user
λ	Wavelength of carrier frequency
Λ	Average SIR improvement at array output
ξ	Probability of an in-beam interferer
$\rho(D_k)$	Overall path loss including the effect of shadowing
ρ_s	Spatial envelope correlation coefficient
$\bar{\rho}(D_k)$	Average path loss for the kth user
σ_{DS}	RMS delay spread
σ_{AOA}	Standard deviation of the pdf in AOA
σ_{AS}	RMS angle spread
σ_I^2	Variance of self interference terms

σ_M^2	Variance of MAI terms
σ_N^2	Variance of noise terms
σ_S^2	Variance of the shadowing random variable
$\bar{\sigma}_I^2$	Modified variance of self interference terms
$\bar{\sigma}_M^2$	Modified variance of MAI terms
$\bar{\sigma}_N^2$	Modified variance of noise terms
$\bar{\tau}_{k,l}$	Delay of the lth path of the kth user
υ	Correction factor for in-beam interferer
$\phi_{k,l}^{(s)}$	Random phase of sth subpath for the lth path of the kth user
$\phi_{k,l}$	Overall random phase of lth multipath of kth user
$\varphi_{k,l,n}$	Overall phase for lth multipath of kth user at the nth antenna
ψ_n	Angular position of the nth UCA element on xy plane
$\Psi_{k,l}^{(s)}$	AOD of sth subpath for the lth path of the kth user, relative to the motion of the mobile
$\Omega_{k,l}$	Power of the lth path of the kth user.

$E[\cdot]$	Statistical averaging operator
$(\cdot)^T$	Transpose
$(\cdot)^H$	Hermitian transpose or complex conjugate transpose
$(\cdot)^*$	Complex conjugate
$\|\|(\cdot)\|\|$	Vector norm
$\Im\{\cdot\}$	Imaginary part of complex number
$\Re\{\cdot\}$	Real part of complex number
$I_n(x)$	nth order modified Bessel function of the first kind
$J_n(x)$	nth order Bessel function of the first kind

Chapter 1

Introduction

In this chapter, a brief introduction to the concept and application of smart antennas for Code Division Multiple Access (CDMA) systems is presented. Following some introductory remarks in Section 1.1, the basic definition and classification of smart antennas is presented in Section 1.2. Key system aspects influencing the performance of smart antennas are also addressed in this section. The aims of this thesis are then identified in Section 1.3. In light of the thesis aims, a literature survey is presented in Section 1.4 which forms the basis of the work presented in this thesis and covers the topics of (i) interference rejection capabilities of array antennas, (ii) channel modelling for smart antennas, (iii) performance analysis of smart antennas for CDMA systems, (iv) adaptive beamforming algorithms for smart antennas and (v) hybrid smart antenna applications. The main thesis contributions are presented in Section 1.5. Finally, the thesis organisation is described in Section 1.6.

1.1 Background

Wireless cellular communication systems have evolved considerably since the development of the first generation (1G) systems in the 70's and 80's, which relied exclusively on Frequency Division Multiple Access/Frequency Division Duplex (FDMA/FDD) and analog Frequency Modulation (FM) [1]. The second generation (2G) wireless communication systems, which make up most of today's cellular networks, use digital modulation formats and Time Division Multiple Access/Frequency Division Duplex (TDMA/FDD) and Code Division Multiple Access/Frequency Division Duplex (CDMA/FDD) multiple access tech-

niques [2]. Examples of 2G systems include Interim Standard-95 Code Division Multiple Access (IS-95 CDMA) which is used in American, Asian and Pacific countries including USA, South Korea and Australia [3, 4] and Global System for Mobile communications (GSM) which is widely used in European and Asian countries including China and Australia [5,6]. The 2G systems have been designed for both indoor and vehicular environments with an emphasis on voice communication. While great effort in current 2G wireless communication systems has been directed towards the development of modulation, coding and protocols, antenna related technology has received significantly less attention up to now [7]. However, it has to be noted that the manner in which radio energy is distributed into and collected from space has a profound influence on the efficient use of spectrum [8].

Over the last few years, wireless cellular communication has experienced rapid growth in the demand for wireless multimedia services such as internet access, multimedia data transfer and video conferencing. Thus the third generation (3G) wireless communications systems must provide a variety of new services with different data rate requirements under different traffic conditions, while maintaining compatibility with 2G systems. Examples of 3G standards include cdma2000 [4] which has been commercially launched in countries including USA and South Korea and Wideband-CDMA (W-CDMA) [9] which has been launched in Europe, Japan and Australia [10]. This increasing demand for high data rate mobile communication services, without a corresponding increase in radio frequency spectrum allocation, motivates the need for new techniques to improve spectrum efficiency. Smart or adaptive arrays have emerged as one of the most promising technologies for increasing the spectral efficiency and improving the performance of present and future wireless communication systems [11–13].

1.2 Smart Antennas for CDMA Cellular Systems

1.2.1 What is a Smart Antenna ?

A smart antenna is defined as an array of antennas with a digital signal processing unit, that can change its pattern dynamically to adjust to noise, interference and multipaths.

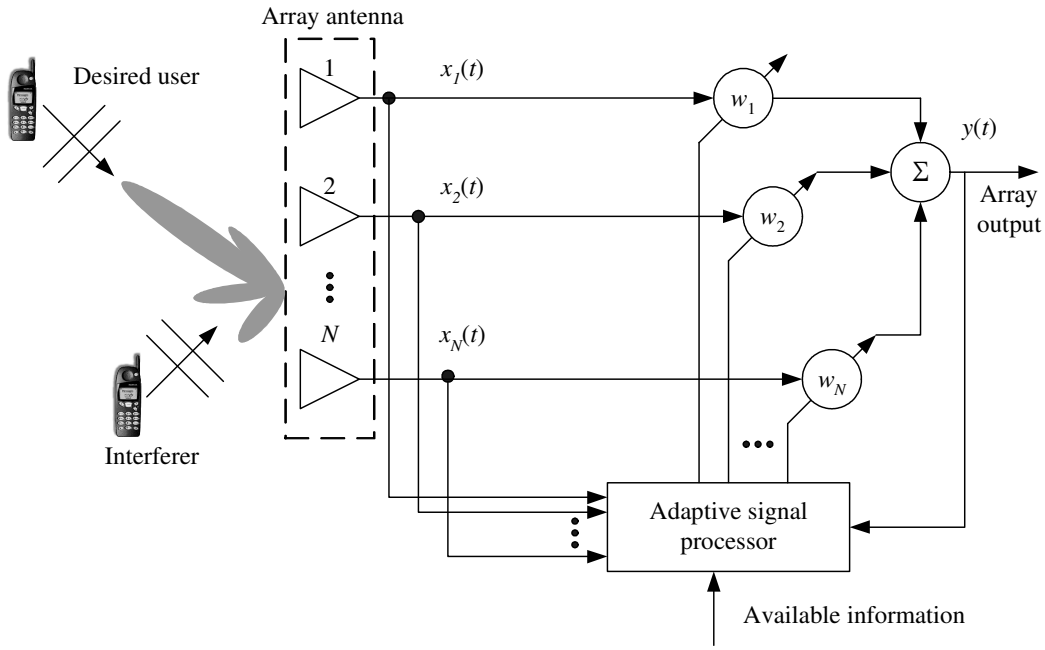

Figure 1.1: Block diagram of a smart antenna system.

The conceptual block diagram of a smart antenna system is shown in Figure 1.1. The following three main blocks can be identified: (i) array antenna (ii) complex weights and (iii) adaptive signal processor. The array antenna comprises of a Uniform Linear Array (ULA) or Uniform Circular Array (UCA) of antenna elements. The individual antenna elements are assumed to be identical, with omni-directional patterns in the azimuth plane. The signals received at the different antenna elements are multiplied with the complex weights and then summed up. The complex weights are continuously adjusted by the adaptive signal processor which uses all available information such as pilot or training sequences or knowledge of the properties of the signal to calculate the weights. This is done so that the main beam tracks the desired user and/or nulls are placed in the direction of interferers and/or side lobes towards other users are minimized. It should be noted that the term "smart" refers to the whole antenna system and not just the array antenna alone.

1.2.2 Classification

The fundamental idea behind a smart antenna is not new but dates back to the early sixties when it was first proposed for electronic warfare as a counter measure to jamming [14].

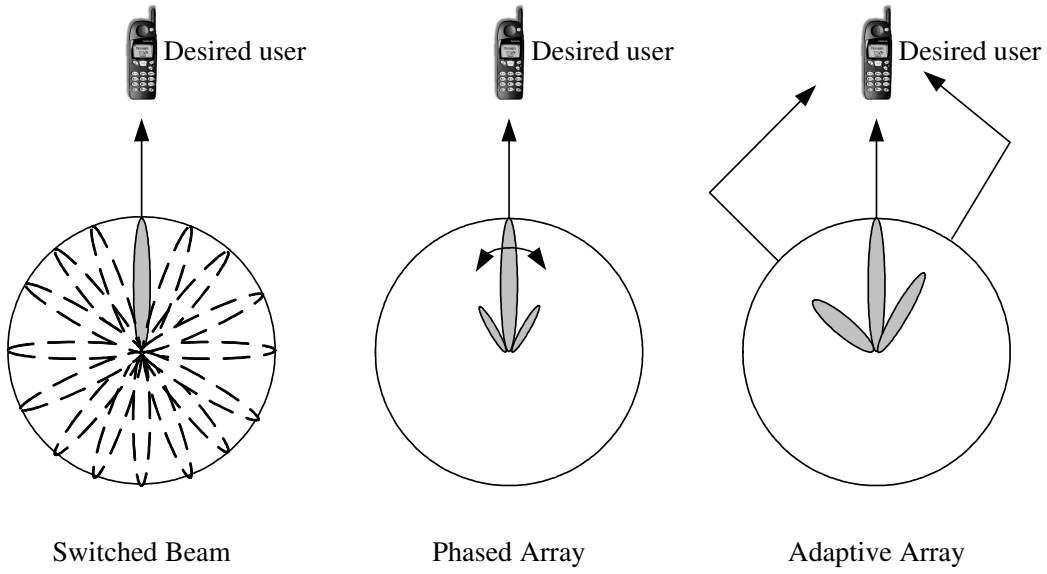

Figure 1.2: Different classifications of smart antenna systems.

Until recently, cost barriers have prevented the use of smart antennas in commercial systems. Thus in existing wireless communication systems, the base station antennas are either omni-directional which radiate and receive equally well in all azimuth directions, or sector antennas which cover slices of 60 or 90 or 120 degrees [15]. However, the advent of low cost Digital Signal Processors (DSPs), Application Specific Integrated Circuits (ASICs) and innovative signal processing algorithms have made smart antenna systems practical for commercial use [15–17].

The smart antenna systems for cellular base stations can be divided into three main categories, which are illustrated in Figure 1.2 [18]. These are (i) switched beam system (ii) phased arrays and (iii) adaptive arrays. It has to be noted that this division is not rigid and switched beam and phased array systems are simpler physical approaches to realising fully adaptive antennas. This step by step migration strategy has been used to lower the initial deployment costs to service providers. These categories are discussed in detail below:-

1.2.2.1 Switched Beam Systems

A switched beam antenna system consists of several highly directive, fixed, pre-defined beams which can be formed by means of a beamforming network [14] e.g., the Butler

matrix [19, 20] which consists of power splitters and fixed phase shifters. The system detects the signal strength and chooses one beam, from a set of several beams, that gives the maximum received power.

A switched beam antenna can be thought of as an extension of the conventional sector antenna in that it divides a sector into several micro-sectors [14]. It is the simplest technique and easiest to retro-fit to existing wireless technologies. However switched beam antenna systems are effective only in low to moderate co-channel interfering environments owing to their lack of ability to distinguish a desired user from an interferer, e.g. if a strong interfering signal is at the center of the selected beam and the desired user is away from the center of the selected beam, the interfering signal can be enhanced far more than the desired signal with poor quality of service to the intended user [14].

1.2.2.2 Phased Arrays

Phased arrays make use of the Angle of Arrival (AOA) information from the desired user to steer the main beam towards the desired user [14]. The signals received by each antenna element are weighted and combined to create a beam in the direction of the mobile. Only the phases of the weights are varied and the amplitudes are held constant.

Phased arrays improve upon the capabilities of a switched beam antenna. They can be considered as a generalization of the switched lobe concept and have an infinite number of possible beam directions [18]. The limitations of phased array can be overcome using fully adaptive arrays.

1.2.2.3 Adaptive Antennas

In an adaptive array, signals received by each antenna are weighted and combined using complex weights (magnitude and phase) in order to maximise a particular performance criterion e.g. the Signal to Interference plus Noise Ratio (SINR) or the Signal to Noise Ratio (SNR). Fully adaptive system use advanced signal processing algorithms to locate and track the desired and interfering signals to dynamically minimize interference and maximize intended signal reception [21].

The main difference between a phased array and an adaptive array system is that the former uses beam steering only, while the latter uses beam steering and nulling. For a given number of antennas, adaptive arrays can provide greater range (received signal gain) or require fewer antennas to achieve a given range [22]. However the receiver complexity and associated hardware increases the implementation costs.

1.2.3 Key System Aspects Influencing Smart Antenna Performance

The choice of a smart antenna receiver is highly dependent on the air interface and its parameters such as multiple access method, the type of duplexing, and pilot availability [17]. Besides the compatibility with the air interface, the number of antenna elements is also a very important consideration. These parameters, which are relevant to the work in this thesis, are discussed below:-

1.2.3.1 CDMA versus TDMA

The different air interface techniques have significant impact on the design and optimum approach for smart antennas because of the different interference scenarios [7]. In TDMA systems, the users are separated by orthogonal time slots. TDMA systems employ frequency reuse plan, which leads to a small number of strong interferers for both uplink and downlink [7]. By comparison, CDMA systems employ a total frequency reuse plan and the different users are multiplexed by distinct code waveforms. Thus in CDMA, each user's transmission is a source of interference for all other users.

The utilization of smart antennas in TDMA systems can be divided into two main stages. These are Spatial Filtering for Interference Reduction (SFIR) and Space Division Multiple Access (SDMA) [7]. SFIR uses the beam directivity from smart antennas to reduce the interference. Thus base stations with the same carrier frequencies can be put closer together, without violating the requirements for the signal to interference ratios. The increase in the capacity is then the decrease in the reuse factor [23]. With SDMA, the reuse factor remains unchanged compared to the conventional system. Instead, several users can operate within one cell on the same carrier frequency and the same time slot distinguished by their

angular position. The possible capacity gains for SDMA are larger than for spatial filtering. However, the required changes in the base station and base station controller software are more extensive and complicated [23].

For CDMA systems, there is less difference between SFIR and SDMA because any interference reduction provided by a smart antenna translates directly into a capacity or quality increase, e.g. more users in the system, higher bit rates for the existing users, improved quality for the existing users at the same bit rates, extended cell range for the same number of users at the same bit rates, or any arbitrary combination of these [24].

This thesis concentrates on smart antennas for CDMA since the Third Generation (3G) wireless communication systems are based on CDMA.

1.2.3.2 Downlink versus Uplink

Smart antennas are usually physically located at the Base Station (BS) only. Due to power consumption and size limitations, it is not practical to have multiple antennas at the Mobile Station (MS) in the downlink. Current 2G systems such as GSM and IS-95 CDMA are Frequency Division Duplex (FDD) systems. In FDD systems, the downlink channel characteristics are independent of the uplink characteristics due to the frequency difference. Thus the processing performed on the uplink cannot be exploited directly in the downlink without any additional processing [7]. By comparison in Time Division Duplex (TDD) systems, the uplink and downlink can be considered reciprocal, provided that the channel conditions have not changed considerably between the receive and transmit time slots. Under these conditions the weights calculated by the smart antenna for the uplink can also be used for the downlink. Application of smart antennas to the downlink transmission for current FDD systems is therefore one of the major challenges related to smart antenna technology [7]. In this regard, retrodirective arrays for both receive and transmit applications have recently been proposed [25].

Since future multimedia services will place higher demands on the downlink than on the uplink, it is important to find techniques that can boost the data rate of the downlink channel. Base station transmit diversity has been identified as an efficient way of improving the

data rate of the downlink channel without increasing the bandwidth [26, 27]. Transmit diversity using two antennas at the base station has been adopted for the W-CDMA standards being developed within the Third Generation Partnership Project (3GPP) [28]. Both open loop and closed loop transmit diversity are specified. The standards specify the transmission formats and certain performance requirements, but leave room for manufacturers and operators to implement individual data receiver solutions [29, 30].

Traditionally, diversity arrays are considered separate from smart antenna systems and fall outside the scope of this thesis. Therefore this thesis considers suitable receiving smart antenna architectures for base stations of CDMA wireless communication systems.

1.2.3.3 Pilot Availability

In IS-95 CDMA forward link, a common pilot channel is broadcast throughout the sector to provide cell identification, phase reference and timing information to the mobile stations. However, this common pilot cannot be used for channel estimation in smart antenna applications because the reference signal (pilot) used for channel estimation must go through the exact same path as the data [31]. The IS-95 CDMA reverse link has no pilot signal to maintain a coherent reference. Hence non-coherent demodulation is used in the reverse link [4].

Recognizing the potential of smart antennas in improving the performance of CDMA systems, some additional channels are dedicated in 3G wireless communication systems for potential use by smart antenna receivers, e.g. W-CDMA has connection dedicated pilot bits to assist in downlink beamforming while cdma2000 has auxiliary carriers to help with downlink channel estimation in forward link beamforming [2].

1.2.3.4 Array Size

The number of elements in the array antenna is a fundamental design parameter, as it defines the number of interference sources the array can eliminate and/or reduce and the additional gain the array will provide. The achievable improvement in system spectral efficiency increases with the number of elements in the array [8].

Because of practical considerations regarding costs, hardware implementation and installation, the number of horizontally separated antenna elements is usually in the range $4-12$ [8]. Typical element spacing used is half wavelength in order to minimise mutual coupling and avoid grating lobes [32]. This corresponds to an array size of approximately 1.2 m at 900 MHz and 60 cm at 2 GHz for an 8 element array antenna. Environmental issues may also have an impact on the array size, especially with recent growing public demand for reduced visible pollution and less visible base stations.

In light of the above considerations, this thesis generally considers the number of half wavelength spaced antenna elements in the range $4-8$.

1.3 Aims of this Thesis

This thesis aims at developing suitable analytical and simulation models for assessing the performance of a CDMA system which employs a smart antenna. The specific aims of the thesis concern:-

- Determining the interference rejection capabilities of linear and circular array antennas, when the effect of mutual coupling between array elements is first neglected and then taken into account.

- Developing a general channel model for use in the performance evaluation of a CDMA system employing a smart antenna.

- Determining the performance of a CDMA system with a smart antenna receiver using analytical methods and validating the obtained analytical model by simulations.

- Investigating the performance of a CDMA system which applies hierarchical beamforming (combination of diversity and beamforming) for array antennas and comparing its performance with the one using conventional smart antenna beamforming.

1.4 Literature Survey

The literature survey covers topics that form the basis of the work in this thesis. In light of the thesis aims identified in the previous section, these topics are considered in the following order (i) interference rejection capabilities of array antennas, (ii) channel modelling for smart antennas, (iii) performance analysis of smart antennas for CDMA systems, (iv) adaptive beamforming algorithms for smart antennas and (v) hybrid smart antenna applications. Each of these topics is addressed in detail below.

1.4.1 Interference Rejection and Mutual Coupling

In CDMA systems, all users communicate simultaneously in the same frequency band and hence Multiple Access Interference (MAI) is one of the major causes of transmission impairment. The interference rejection or Signal to Interference Ratio (SIR) improvement capability is, therefore, an important measure of performance of a CDMA cellular system employing BS array antennas. The figure of merit used to quantify this interference rejection capability is the spatial interference suppression coefficient [33]. The applications of the spatial interference suppression coefficient have appeared in a number of recent papers, e.g. it is employed in determining an expression for the theoretical bit error rate of a smart antenna system in [34] and it is used to find the capacity of a CDMA multi-antenna system in [35, 36]. It has to be noted that the above applications are only concerned with finding the mean value of the spatial interference suppression coefficient i.e. the value averaged over all angles of arrivals.

Many research papers have addressed the SIR improvement of linear arrays while neglecting mutual coupling between antenna elements [33, 37, 38]. Cellular base stations, however, are not restricted to linear array configurations. Before devising any beamforming algorithm, it is worthwhile to consider whether a chosen array configuration will enable optimal performance. Hence it is important to provide an assessment of performance for other configurations of arrays, e.g. uniform circular arrays.

In real arrays, mutual coupling is always present. The mutual coupling can be modelled

by using analytical techniques e.g., the Induced EMF method [32] as well as commercially available electromagnetic analysis packages e.g., FEKO [39]. A common assumption in the study of mutual coupling is that it will lead to degradation in the performance of the system. However this is not the case in general, e.g. it was found in [40] that by decreasing the amount of correlation between parallel channel, mutual coupling can in fact increase the channel capacity for Multiple Input Multiple Output (MIMO) systems. Studies ignoring mutual coupling may lead to less accurate system performance prediction results. Hence it is important to assess the SIR performance when mutual coupling between antenna elements is included in the array analysis.

1.4.2 Channel Modelling

Channel modelling is one of the most important and fundamental research areas in wireless communications. It plays a crucial role in the design, analysis and implementation of smart antennas in wireless communication systems [41–44]. In the past, classical channel models have focused mainly on the modelling of temporal aspects, such as fading signal envelopes, Doppler shifts of received signals and received power level distributions [45–48]. The use of smart antennas introduces a new spatial dimension in the channel models. The spatial properties of the channel, e.g. the angle of arrival and the distribution of arriving waves in azimuth, have an enormous impact on the performance of smart antenna systems and hence need to be accurately characterized [49].

The spatial channel models have received much attention in literature. A good overview of the spatial channel models for smart antennas is provided in [49] and for the case of MIMO systems in [50]. It has to be noted that all the channel models considered in this section are Two-Dimensional (2-D) in nature i.e. they assume that radio propagation takes place in the azimuth plane containing the transmitter and the receiver. Work has also been undertaken with regard to Three Dimensional (3-D) models [51–54].

The channel models for smart antennas can be divided into four main categories. These are (i) empirical models (ii) deterministic models (iii) geometric scatterer models and (iv) physical models. They are discussed in detail below:-

1.4.2.1 Empirical Models

Empirical or field measurement models are based on extensive sets of measurements. In such models, measurements are performed at the site of interest and suitable functions are fitted to the measurements [55–57].

The main advantage of empirical models is that the formulation of the model is quite simple to compute and the model can be used to extrapolate results for similar environments. However these models fail when used in a location that has different characteristics than those in which the measurements have been originally performed [58, Chapter 5].

1.4.2.2 Deterministic Models

Ray tracing is based on geometrical theory and considers direct, reflected and diffracted rays. Ray tracing produces deterministic channel models that operate by processing user-defined environments [59]. In recent years, many authors have investigated the application of ray tracing to predict the amplitudes, time delays, and arrival angles of the various multipath components for indoor and outdoor scenarios [60, 61].

The advantage of ray tracing models is that they offer great accuracy with site-specific results. However they are computationally intensive especially in complex environments. Also the detailed physical characteristics of the environment, e.g. terrain and building databases, must be known beforehand.

1.4.2.3 Geometric Scatterer Models

Geometric scatterer models are defined by a spatial scatterer density function. They assume that the propagation between the transmit and receive antennas takes place via single scattering from an intervening obstacle. Numerous scatterer models have been proposed e.g. a ring model [46, 62], discrete uniform model [63], Elliptical Scattering Model (ESM) [64] and the Circular Scattering Model (CSM) [65]. Each of these models is applicable to a specific application. For example, the ESM assumes that the scatterer density is constant within an elliptical region about the MS and BS and is suitable for micro or picocell environments. On the other hand, the CSM assumes a constant scatterer density within a circular region

about the MS and is suitable for macrocell environments. Recently, the versatile Gaussian Scatter Density Model (GSDM) was proposed which assumes a Gaussian distribution of scatterer density about the MS and BS [66]. It is applicable to both macrocell and picocell environments, depending on appropriate choice of input parameters. Comparison with measurements have shown that GSDM is superior to both CSM and ESM respectively [66].

The main advantage of scatterer models is that once the coordinates of the scatterers are drawn from a random process, all necessary spatial information can easily be derived. The main disadvantage is that a large number of scatterers are required for realistic fading simulation. Also consideration of continuously moving mobiles increases the complexity, which limits the applicability of these models for chip level simulations [67].

1.4.2.4 Physical Models

Physical models use important physical parameters to provide a reasonable description of the wireless channel characteristics and the surrounding scattering environment [68–70]. Of particular importance to this thesis is the Spatial Channel Model (SCM) [71], currently under consideration within the Third Generation Partnership Project Two (3GPP2) which is a standardisation body for 3G cellular systems. This detailed system level model is applicable for a variety of environments. Typical parameters used by the SCM model include array orientations, MS directions, shadow fading, path delays, delay spread, average path powers, angle of departures, angle of arrivals, angle spread and random phases. However a limitation of the above model is that it does not take into account MS mobility.

The main advantage of physical models, compared with scatterer models, is the reduced complexity and easier mathematical formulation of the channel model.

1.4.3 Performance Analysis of Smart Antennas

It is well known that array antennas with a suitable signal processing algorithm can improve the performance of Direct Sequence Code Division Multiple Access (DS-CDMA) systems by reducing the Multiple Access Interference (MAI) [72, 73]. In this regard, it is important to analyse the mean Bit Error Rate (BER) performance of a DS-CDMA system, with *M*-

ary orthogonal modulation and noncoherent detection, employing a smart antenna. This is because this type of modulation has been successfully used in the reverse link of IS-95 CDMA system (for details, see Appendix A) and is also specified in radio configurations 1 and 2 of the reverse link in cdma2000 standard [4]. A major challenge in the analysis is to derive closed-form expressions for the BER, which are a very important tool in the planning and design of smart antenna systems.

The BER analysis of CDMA systems with noncoherent M-ary orthogonal modulation has been done by a number of researchers [74–79]. In [74] and [75], the analysis was presented for an Additive White Gaussian Noise (AWGN) channel. Extensions to the case of a multipath fading channel for the Rayleigh distribution was presented in [77, 78] and for the case of more general Nakagami fading in [79] (the Nakagami distribution includes Rayleigh distribution as a special case and can also accurately approximate Rician fading). In both these papers, the mean Bit Error Rate (BER) was calculated by using the standard Gaussian Approximation (GA) [80] by first replacing the values of all the fading coefficients in the interference terms by their expectations and then using Stirling's formula [77] or averaging over a known fading distribution in order to reflect the effect of fading [79]. Recently, an analysis of multicode CDMA with noncoherent M-ary orthogonal modulation was published in [81]. It has to be noted that all the above considerations were restricted to the case of single antenna receivers.

An exact analysis of the BER of CDMA systems with array antennas is difficult. Thus different approximate analytical methods have been proposed to analyse the performance of CDMA smart antenna systems. Analytical results for a CDMA system with noncoherent M-ary orthogonal modulation and employing an array antenna operating in a Rayleigh fading environment were presented in [82], which used the analysis procedure given in [77]. No closed-form expression for the BER was given in [82]. This analysis procedure given in [77, 82] was also used to analyse the performance of a W-CDMA based smart antenna system in [83]. An alternative simplified technique utilising the interference suppression coefficient was proposed in [33, 84] and illustrated for the case of a cdma2000 based smart antenna system in [34].

Recently in [85, 86], a simple analytical method was described to analyse the performance of a DS-CDMA system employing an array antenna. The proposed method was shown to provide a more accurate assessment than the method of [33, 84]. However, the application of the proposed method was considered only for the simple case of coherent Binary Phase Shift Keying (BPSK) modulation.

1.4.4 Adaptive Beamforming Algorithms

Several adaptive beamforming algorithms have been proposed in literature for CDMA systems [73,84,87–95]. These algorithms generally fall into two main categories. These are (i) Maximum Signal to Interference plus Noise Ratio (SINR) beamforming and (ii) Maximum Signal to Noise Ratio (SNR) beamforming.

Maximum SINR beamforming is also called optimal combining. A technique to implement Maximum SINR beamforming, which utlilised the pre- and post-array correlation matrices, was first proposed in [87]. However the disadvantage of the above procedure was its heavy computational load. Recently, more simplified Maximum SINR beamforming algorithms have been proposed in [34].

Maximum SNR beamforming is also called Spatial Matched Filtering (SMF). This type of beamforming is comparatively simpler as it utilises post-array correlation matrices only. Simple smart antennas utilising Maximum SNR beamforming have been proposed based on Modified Conjugate Gradient Method (MCGM) [37], Lagrange multipliers [96] and power method [97] respectively. Maximum SNR beamforming is sub-optimal but computationally simpler. It was shown in [83] that for moderate number of interferers and/or multipaths per user and low to moderate angle spreads, the performance of antenna arrays with Maximum SNR beamforming is close to the performance with Maximum SINR beamforming.

From the point of view of theoretical performance evaluation of smart antenna systems, the actual adaptive beamforming algorithms used to determine the weights are not very important, as concluded in [34,83,88]. Thus the ideal solution for the weight vectors can be used in the analysis. This assumption is useful for performance evaluation and simulation studies and provides an estimate of the best possible system performance.

1.4.5 Hybrid Smart Antenna Applications

A smart antenna can mitigate Multiple Access Interference (MAI) by beamforming (spatial filtering) operation and consequently improve the performance of a CDMA system. However smart antennas may not be effective in all circumstances. This has led to the creation of novel hybrid applications of smart antennas. Recently smart antennas have been considered in combination with multi-user detectors/interference cancellation [98–100], PN code acquisition [101, 102] and power control [103, 104]. Of particular interest to this thesis is the combination of diversity and smart antennas. This is because in addition to MAI, the performance of CDMA systems is limited by multipath fast fading. Therefore further improvement in performance can be expected if efforts are made to jointly combat MAI and fading.

Diversity is a very effective technique which has been traditionally employed to combat fading. It uses multiple antennas to provide the receiver with multiple uncorrelated replicas of the same signal. The signals received on the disparate diversity branches can then be combined using various combining techniques, e.g. Equal Gain Combining (EGC) [105–107]. However diversity arrays have limited interference rejection and fail to eliminate the error probability floor in CDMA [72,108]. Diversity and beamforming also have conflicting requirements for optimum performance, e.g. diversity arrays employ widely spaced antenna elements (5λ or 20λ, where λ denotes the wavelength) while conventional beamforming arrays employ closely spaced antenna elements, with typical inter-element spacing of half wavelength.

A hybrid scheme of diversity and beamforming called Hierarchical Beamforming (HBF), was recently proposed in [109, 110]. In HBF, the array elements are divided into groups to form several sub-beamforming arrays. The inter-element spacing within a sub-array is assumed half wavelength, while the distance between the adjacent sub-arrays is large (e.g. 5λ or 20λ or more) to ensure independent fading between sub-arrays. The performance of a generic DS-CDMA system employing such an array in the downlink was analysed in [111]. However the analysis assumed zero angle spread. This assumption is reasonable in suburban areas where the coverage is from elevated BS antennas as the multipath rays arrive at

the BS with a small angle spread. However when the base stations are located within or near urban clutter, they can consequently experience a much larger angle spread than the elevated base stations [57]. Thus it is important to consider the effect of angle spread.

1.5 Thesis Contributions

The original contributions accomplished in this thesis stem from the literature review presented in Section 1.4 and include the following:-

- With regard to the optimal choices of the BS array antenna configurations, this thesis undertakes comparison between an array of dipoles arranged in equi-spaced linear and circular configurations. Two cases are considered; when mutual coupling between array elements is neglected and when it is taken into account by employing the Induced EMF method. An expression for the spatial interference suppression coefficient is derived for the first case and is then generalized to include the effect of mutual coupling. The results provide novel insights into the interference rejection capabilities of the investigated arrays.

- In view of the pros and cons of the various channel models considered in Section 1.4.2, this thesis constructs a parameterized physical channel model for evaluating the performance of smart antenna systems. The channel model assumes a single antenna at the mobile station and a uniform linear array of omni-directional antenna elements at the BS. It incorporates parameters such as azimuth angle of arrival, angle spread, power delay profiles and Doppler frequency, which have critical influence on the performance of smart antennas. A new feature of the channel model, in comparison with the SCM model described in Section 1.4.2.4, is a thorough framework for the incorporation of user mobility. The proposed model allows for efficient and accurate characterisation of Rayleigh and Rician fading multipath channels, which are relevant to urban and suburban fading environments.

- Because of the need for system planners to know how different design choices affect the overall performance of the smart antenna system, this thesis develops an analytical model for evaluating the mean BER of a DS-CDMA system employing a smart antenna. The analysis is performed assuming Rayleigh and Rician fading multipath environments. The DS-CDMA system is assumed to employ M-ary orthogonal modulation with noncoherent detection, which is relevant to IS-95 CDMA and cdma2000. A novel expression is derived of the Signal to Interference plus Noise Ratio (SINR) at the smart antenna receiver output, which allows the BER to be easily evaluated using a closed-form expression. The model provides rapid and accurate assessment of the performance of the DS-CDMA system employing a smart antenna. It is validated by comparison with Monte Carlo simulation results.

- Smart antennas can efficiently combat Multiple Access Interference (MAI) by forming a narrow beam towards the desired user and minimising side-lobes towards interferers. However, the performance of CDMA systems is limited by both fast fading and MAI. To this purpose, this thesis considers a hybrid scheme of beamforming and diversity called hierarchical beamforming. The novelty of the presented work is the analysis and comparison of the performance of hierarchical beamforming with conventional smart antenna beamforming in a Rayleigh fading multipath environment. The assessment takes into account the effect of azimuth angle spread at the base station. The results provide new insights into optimum receiver architectures including array antennas for the considered channel conditions.

The originality and significance of the above thesis contributions is reflected by publication of parts of this thesis in several journals and refereed conference proceedings. The work on the interference rejection capabilities has been published in [112–114]. The parameterized channel model has been reported in [115–117]. The performance evaluation of a DS-CDMA system employing a smart antennas has been presented in [116–118]. The performance analysis of hierarchical beamforming has been published in [119]. The con-

struction of the chip-level CDMA smart antenna simulation model, which is used to generate the simulation results and validate the analytical models proposed in this thesis, has been partially reported in [120]. Also the author's publications in [121–125] stem from the work presented in this thesis work.

1.6 Thesis Organisation

This chapter has provided an introduction to the concept and application of smart antennas for CDMA systems. It has explained the motivation behind this work and identified the aims and contributions of this thesis. The remainder of this thesis is organised as follows.

In Chapter 2, a signal model is developed for investigating the performance of linear and circular array antennas, in terms of the Signal to Interference Ratio at the array output. The model is extended to include the effect of mutual coupling. Performance analysis results are then provided to assess and compare the interference rejection capabilities of the two array geometries.

In Chapter 3, a parameterised physical channel model incorporating user mobility is presented for use in performance evaluation of smart antenna systems. The modelling of the various spatial and temporal parameters, which have a crucial influence on the performance of smart antennas, is described and these are then used to construct the mathematical formulation of the channel model. The proposed model is implemented in software and different Rayleigh and Rician fading channel simulation results are provided and discussed.

In Chapter 4, an analytical model is presented for evaluating the BER performance of a DS-CDMA system employing a smart antenna. The system and receiver model is presented in detail. The new model, which permits the BER to be readily evaluated using a closed-form expression, is described. The Monte Carlo simulation strategy and simulation assumptions employed to simulate the performance of smart antennas are discussed. The model is validated by comparison with the simulation results for suburban and urban fading environments.

In Chapter 5, a hybrid scheme of diversity and conventional beamforming called hierarchical beamforming is investigated. Its performance is compared with the conventional

smart antenna receiver, presented in Chapter 4, and the effect of varying the system and channel parameters is determined. Conclusions are drawn regarding the optimum receiver strategy for different fading environments.

In Chapter 6, the main thesis contributions are summarized and some suggestions for future work are presented.

Appendix A provides technical details of the reverse link of IS-95 CDMA system.

Finally, Appendix B provides a description of the customized chip-level simulation software, which has been developed in MATLAB [126] for the purpose of investigating the performance of CDMA smart antennas systems.

Chapter 2

Interference Rejection Capabilities of Array Antennas

In this chapter, the interference rejection capabilities of linear and circular array of half-wavelength spaced dipoles, that can be part of a CDMA cellular base station antenna system, are addressed. In Section 2.1, the modelling of the linear and circular array antennas is presented. In Section 2.2, the signal model for array antennas is described and an expression for the spatial interference suppression coefficient, which is the performance criteria for interference rejection, is derived. In Section 2.3, the modelling of mutual coupling is explained and the signal model is modified to include the effect of mutual coupling. Finally, results are presented in Section 2.4.

2.1 Modelling of Array Antennas

This section deals with the modelling of the Uniform Linear Array (ULA) and the Uniform Circular Array (UCA) antennas respectively.

2.1.1 Uniform Linear Array

A ULA consists of antenna elements placed uniformly along a straight line. It is the most commonly used array antenna in mobile communication systems because of its relative simplicity compared to other geometries.

Consider a linear array of N antenna elements located at the origin of the cartesian coordinate system and spaced a uniform distance $d = \lambda/2$ along the x-axis, as shown in

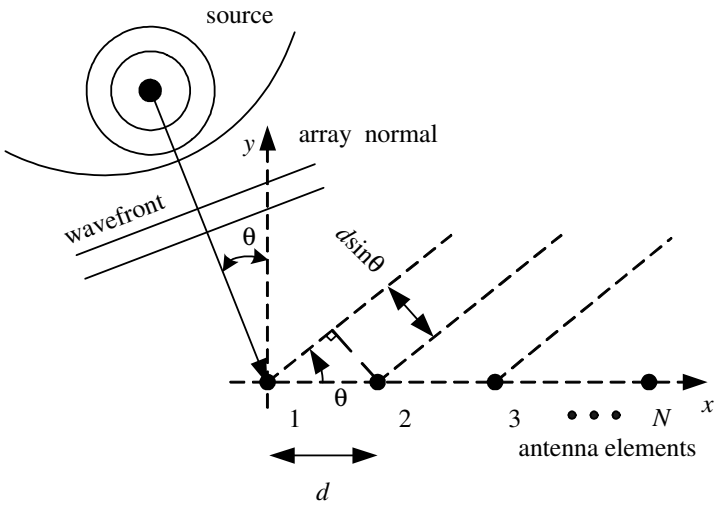

Figure 2.1: Uniform linear array geometry.

Figure 2.1. The spatial response of the array due to an incident plane wave from θ direction is modelled by the $N \times 1$ array steering vector $\mathbf{a}(\theta)$. In general, it is the product of antenna response and the geometrical array factor [127] and is given as

$$\mathbf{a}(\theta) = \left[U_1(\theta) \;\; U_2(\theta) e^{-j\mathcal{K}d\sin\theta} \;\; \cdots \;\; U_N(\theta) e^{-j\mathcal{K}(N-1)d\sin\theta} \right]^T \tag{2.1}$$

where $\mathcal{K} = 2\pi/\lambda$ is the wave number, $U_n(\theta)$ denotes the response of antenna element n and $(\cdot)^T$ denotes transpose operation. If mutual coupling between antenna elements is neglected and the individual element patterns are identical, then scaling them with respect to element number 1 reduces (2.1) to

$$\mathbf{a}(\theta) = \left[1 \;\; e^{-j\mathcal{K}d\sin\theta} \;\; \cdots \;\; e^{-j\mathcal{K}d(N-1)\sin\theta} \right]^T \tag{2.2}$$

2.1.2 Uniform Circular Array

A UCA consists of N antenna elements evenly spaced in a circle of radius R.

Consider a UCA of radius $R = \lambda/[4\sin(\pi/N)]$ in the xy plane, as shown in Figure 2.2. This radius is chosen to maintain an inter-element spacing of $d = \lambda/2$, equivalent to that used for the linear array [128]. For convenience, the center of the circle is selected as the phase reference.

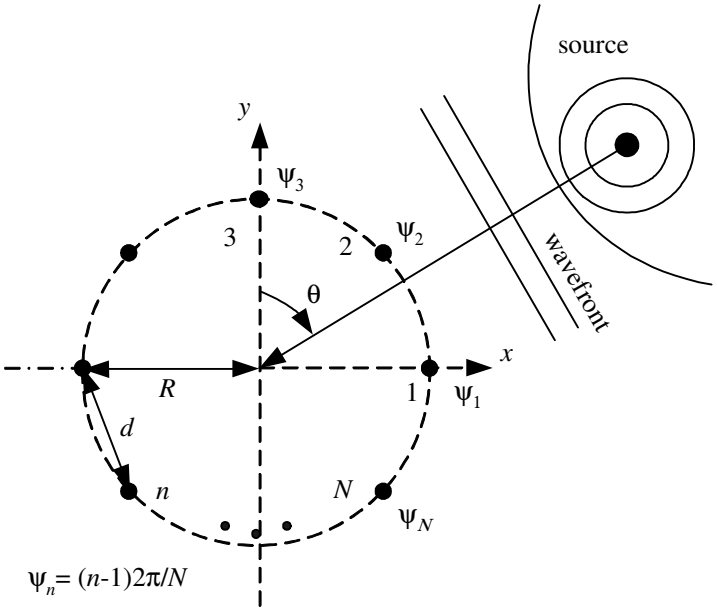

Figure 2.2: Uniform circular array geometry.

Assuming identical and omni-directional antenna elements, the array steering vector can then be written as [32]

$$\mathbf{a}(\theta) = \left[e^{j\mathcal{K}R\sin(\theta+\psi_1)} \;\; e^{j\mathcal{K}R\sin(\theta+\psi_2)} \;\; \ldots \;\; e^{j\mathcal{K}R\sin(\theta+\psi_N)} \right]^T \tag{2.3}$$

where $\psi_n = 2\pi(n-1)/N$ for $n = 1, 2, \ldots, N$ is the angular position of the nth element on the xy plane.

2.2 Signal Model

The signal model for investigating the interference rejection capabilities of array antennas is developed by considering the case of the ULA. The model is later extended for the case of the UCA.

2.2.1 Received Signal

Consider a ULA of N antenna elements located at the origin of the cartesian coordinate system and spaced a distance $d = \lambda/2$ along the x-axis. The array receives signals from K narrow-band mobile users, which are randomly distributed in the xy plane (azimuthal

direction) in the far-field of the array. In this case, the parameter that characterizes the location of each user is its Angle of Arrival (AOA) θ, which is conventionally measured from the array broadside ($\theta = 0^\circ$ is referred to as the broadside direction and $\theta = 90^\circ$ as the end-fire direction). For simplicity, mutual coupling is first ignored and the linear array is considered to be made of omni-directional antenna elements. Selecting the first element as the phase reference, the received signal at the nth antenna element can be expressed as

$$x_n(t) = \sum_{k=1}^{K} s_k(t)\, e^{-j\mathcal{K}d(n-1)\sin\theta_k} + \eta_n(t) \tag{2.4}$$

where $\mathcal{K}$ is the wave number $= 2\pi/\lambda$, $\lambda =$ wavelength of the carrier frequency of the signals, $d =$ uniform inter-element distance, $s_k(t) =$ signal transmitted by the kth source as received by the reference antenna, $\theta_k =$ AOA of the kth source as measured from the array broadside and $\eta_n(t) =$ Additive White Gaussian Noise (AWGN) at the antenna elements with zero mean and having variance σ^2. Using vector notation, the received signal can be expressed as

$$\mathbf{x}(t) = \sum_{k=1}^{K} \mathbf{a}(\theta_k) s_k(t) + \boldsymbol{\eta}(t) = \mathbf{A}(\theta)\,\mathbf{s}(t) + \boldsymbol{\eta}(t) \tag{2.5}$$

where $\mathbf{x}(t)$ is $N \times 1$ received signal vector, $\mathbf{s}(t)$ is $K \times 1$ transmitted signal vector, $\boldsymbol{\eta}(t)$ is $N \times 1$ noise vector, $\mathbf{a}(\theta_k)$ is the $N \times 1$ steering vector given in (2.2) which models the spatial response of the array due to an incident plane wave from the θ_k direction and $\mathbf{A}(\theta) = [\mathbf{a}(\theta_1), \mathbf{a}(\theta_2), \ldots, \mathbf{a}(\theta_K)]$ is $N \times K$ matrix whose columns are steering vectors of the sources. The collection of these steering vectors over the parameter set of interest $\mathcal{A} = \{\mathbf{a}(\theta) | \theta \in \Theta\}$ is called the array manifold, where Θ denotes the set of all possible parameter vectors. The array manifold is assumed to be unambiguous, i.e. the matrix $\mathbf{A}(\theta)$ has full rank for all distinct $\theta_k \in \Theta$. It can be shown that the uniform linear array manifold is unambiguous if the AOA's are confined to the set $\Theta = [-\pi/2, \pi/2]$ [129].

The array correlation matrix associated with vector $\mathbf{x}(t)$ contains information about how signals from each element are correlated with each other and is given by

$$\mathbf{R}_{xx} = E[\mathbf{x}(t)\,\mathbf{x}^H(t)] \tag{2.6}$$

where $E[\cdot]$ denotes expectation or statistical averaging operator and $(\cdot)^H$ denotes Hermitian transpose.

Let $s_1(t)$ be the desired user's signal arriving from direction θ_1 and consider the rest of the signals $s_k(t), k = 2,3,\ldots,K$ as interferences arriving from their respective directions. The array output is given by

$$y(t) = \mathbf{w}^H \mathbf{x}(t) \tag{2.7}$$

where $\mathbf{w}$ is the weight vector that is applied to the antenna array to produce a beam pattern with its main lobe in the direction of the desired user. Assuming that Maximum Signal to Noise Ratio (SNR) beamforming is performed, $\mathbf{w}$ is given by [37]

$$\mathbf{w} = \zeta_1 \mathbf{v}_{\max} \tag{2.8}$$

where $\mathbf{v}_{\max}$ is the eigenvector corresponding to the largest eigenvalue $\lambda_{\max}$ of $\mathbf{R}_{xx}$. It was shown in [37] that the eigenvector corresponding to the maximum eigenvalue of the array correlation matrix is approximately equal to the steering vector of the desired user when the desired signal is much stronger than the interferers at the receiver. Thus $\mathbf{w}$ is given by

$$\mathbf{w} = \zeta_1 \mathbf{a}(\theta_1) \tag{2.9}$$

where ζ_1 is a constant and is set to $1/N$. Substituting (2.9) in (2.7) and using (2.5) and simplifying, we get

$$\begin{aligned} y(t) &= \sum_{k=1}^{K} \mathbf{w}^H \mathbf{a}(\theta_k) s_k(t) + \mathbf{w}^H \boldsymbol{\eta}(t) \\ &= \mathbf{w}^H \mathbf{a}(\theta_1) s_1(t) + \sum_{k=2}^{K} \mathbf{w}^H \mathbf{a}(\theta_k) s_k(t) + \mathbf{w}^H \boldsymbol{\eta}(t) \\ &= \frac{1}{N} \mathbf{a}^H(\theta_1) \mathbf{a}(\theta_1) s_1(t) + \frac{1}{N} \sum_{k=2}^{K} \mathbf{a}^H(\theta_1) \mathbf{a}(\theta_k) s_k(t) + \frac{1}{N} \mathbf{a}^H \boldsymbol{\eta}(t) \\ &= s_1(t) + \frac{1}{N} \sum_{k=2}^{K} \mathbf{a}^H(\theta_1) \mathbf{a}(\theta_k) s_k(t) + \frac{1}{N} \mathbf{a}^H(\theta_1) \boldsymbol{\eta}(t) \end{aligned} \tag{2.10}$$

The mean output power of the processor is

$$\begin{aligned} P(t) &= E[y(t)y^*(t)] \\ &= E[|s_1(t)|^2] + \sum_{k=2}^{K} \frac{1}{N^2} |\mathbf{a}^H(\theta_1)\,\mathbf{a}(\theta_k)|^2 E[|s_k(t)|^2] + E[\frac{1}{N} |\mathbf{a}^H(\theta_1)\,\boldsymbol{\eta}(t)|^2] \\ &= E[|s_1(t)|^2] + \sum_{k=2}^{K} g_k(\theta_1,\theta_k) E[|s_k(t)|^2] + \frac{\sigma^2}{N} \end{aligned} \tag{2.11}$$

where the expectation is taken over time and the noise and signals are assumed to be uncorrelated. The first term on the right side in (2.11) is the desired signal power, whereas the second and third terms represent interference and noise power respectively.

2.2.2 Spatial Interference Suppression Coefficient

The coefficient $g_k(\theta_1,\theta_k) = \frac{1}{N^2} |\mathbf{a}^H(\theta_1)\mathbf{a}(\theta_k)|^2$ in (2.11) is a measure of how much undesired power is picked up from an interferer. This is due to the fact that the array is unable to form a perfect pencil beam radiation pattern towards the desired signal at $\theta = \theta_1$ so the side lobes pick up interfering signals.

The normalized amount of interference power seen from an interferer k at angle of arrival θ_k can be expressed in more general form as a scalar product of beamforming weight vector representing phased antenna elements and the array steering vector representing a plane wave as

$$g_k(\theta_1,\theta_k) = \left| \frac{\mathbf{w}^H \mathbf{a}(\theta_k)}{||\mathbf{w}^H||\;||\mathbf{a}(\theta_k)||} \right|^2 \tag{2.12}$$

where $||(\cdot)||$ denotes the Euclidean norm of a vector. Substituting the values from (2.2) and (2.9) and simplifying, we get

$$\begin{aligned} g_k(\theta_1,\theta_k) &= \frac{1}{N^2} |\mathbf{a}^H(\theta_1)\mathbf{a}(\theta_k)|^2 \\ &= \frac{1}{N^2} \frac{|\sin(\frac{\pi N}{2}(\sin\theta_1 - \sin\theta_k))|^2}{|\sin(\frac{\pi}{2}(\sin\theta_1 - \sin\theta_k))|^2} \end{aligned} \tag{2.13}$$

Assuming the interferers are uniformly distributed in the range $[-\pi/2, \pi/2]$, the mean value of $g_k(\theta_1,\theta_k)$ is given as

$$G_{avg}(\theta_1) = E[g_k(\theta_1,\theta_k)] = \frac{1}{\pi} \int_{-\pi/2}^{\pi/2} g_k(\theta_1,\theta_k)\, d\theta_k \tag{2.14}$$

where $G_{avg}(\theta_1)$ is the spatial interference suppression coefficient [33].

2.2.3 Performance Improvement in terms of SNR and SIR

Using (2.11), the Signal to Noise Ratio at the array output (SNR_o) can be written as

$$\begin{aligned}\text{SNR}_\text{o} &= \frac{E[|s_1(t)|^2]}{E[|\frac{1}{N}\mathbf{a}^H(\theta_1)\boldsymbol{\eta}(t)|^2]} \\ &= N\,\frac{E[|s_1(t)|^2]}{\sigma^2} \\ &= N\,(\text{SNR}_\text{in}) \end{aligned} \tag{2.15}$$

where σ^2 denotes noise power while SNR_in is the signal to noise ratio after PN despreading, when a single antenna element is employed. (2.15) shows that the SNR at the array output is improved by N times.

Similarly using (2.11), the instantaneous Signal to Interference Ratio at the array output (SNR_o) can be written as

$$\text{SIR}_\text{o} = \frac{E[|s_1(t)|^2]}{\sum_{k=2}^{K} g_k(\theta_1,\theta_k)E[|s_k(t)|^2]} \tag{2.16}$$

From the above equation, it can be observed that the Signal to Interference Ratio at the array output is a function of θ_1, the direction of the desired user. The mean SIR at the array output (SIR_o) can be written in terms of input SIR (SIR_in) as

$$\text{SIR}_\text{o} = \frac{\text{SIR}_\text{in}}{G_{avg}(\theta_1)} \tag{2.17}$$

The average improvement in SIR (Λ) at the array output is then given as

$$\Lambda = 10\log_{10}\left[\frac{1}{G_{avg}(\theta_1)}\right] = -10\log_{10}[G_{avg}(\theta_1)] \tag{2.18}$$

2.2.4 Circular Array

For a UCA, assuming the interferers are uniformly distributed in the range $[-\pi,\pi]$, $G_{avg}(\theta_1)$ is given by

$$G_{avg}(\theta_1) = \frac{1}{2\pi}\int_{-\pi}^{\pi} g_k(\theta_1,\theta_k)\,d\theta_k \tag{2.19}$$

where $g_k(\theta_1,\theta_k)$ is given in (2.12) as before, with the steering vector given in (2.3). Thus the interference rejection capabilities of the UCA can be investigated using (2.17) as for the case of a ULA.

2.3 Mutual Coupling

Thus far in this chapter, it has been assumed that the elements of the array antenna are independent isotropic point sensors that sample but do not reradiate the incident signal. However in a real system, each antenna element has some physical size and the elements sample and reradiate the incident signal. The reradiated signals interact with the surrounding elements causing the elements to be mutually coupled. Mutual coupling is the name given to this phenomenon that a current flowing in one antenna element can induce a voltage on a neighbouring antenna element.

To model the effects of mutual coupling, a mutual impedance matrix is used to characterize the interaction among the array antenna components [130]. Mathematically, the mutual impedance matrix $\mathbf{Z}$ is given by

$$\mathbf{Z} = \begin{pmatrix} Z_A & Z_{12} & \dots & Z_{1n} \\ Z_{21} & Z_A & \dots & Z_{2n} \\ \vdots & \vdots & \vdots & \vdots \\ Z_{n1} & Z_{n2} & \dots & Z_A \end{pmatrix} \tag{2.20}$$

where Z_A is the element's impedance in isolation (for $\lambda/2$ dipole, its value is $Z_A = 73 + j42.5$ ohm), Z_T is the impedance of the receiver at each element and is chosen as the complex conjugate of Z_A to obtain an impedance match for maximum power transfer.

In general, numerical techniques such as Method of Moments [131] or Full-Wave Electromagnetic Numerical Computation [132] can be used to obtain the mutual impedance matrix. For dipoles, however, $\mathbf{Z}$ can be easily determined using classical Induced Electromotive Force (EMF) method [32].

2.3.1 Induced EMF Method

Induced EMF method is a classical method of computing the self and mutual impedances of an antenna array. This method is restricted to straight and parallel elements in formation and does not account for the radii of the wires and the gaps at the feeds. However, the advantage of this method is that it leads to closed form solutions for the three classic cases of side-by-side, collinear and parallel-in-echelon configurations [36].

For the side-by-side configuration and dipole lengths $l = \lambda/2$, an element of the mutual impedance matrix Z_{mn}, where $1 \leq m,n \leq N$, is given by [32]

$$Z_{mn} = \begin{cases} 30[0.5772 + \ln(2\mathcal{K}l) - C_i(2\mathcal{K}l)] + \\ j[30\,S_i(2\mathcal{K}l)], & m = n \qquad (2.21a) \\ 30[2C_i(u_0) - C_i(u_1) - C_i(u_2)] - \\ j[30(2S_i(u_0) - S_i(u_1) - S_i(u_2))], & m \neq n \qquad (2.21b) \end{cases}$$

where $\mathcal{K}$ is the wave number, d_h is the horizontal distance between the two dipole antennas and

$$u_0 = \mathcal{K}d_h \qquad (2.22)$$

$$u_1 = \mathcal{K}(\sqrt{d_h^2 + l^2} + l) \qquad (2.23)$$

$$u_2 = \mathcal{K}(\sqrt{d_h^2 + l^2} - l) \qquad (2.24)$$

and $C_i(u)$ and $S_i(u)$ are the Cosine and Sine integrals respectively, defined as [133]

$$C_i(u) = \int_\infty^u \frac{\cos(x)}{x}\,dx \qquad (2.25)$$

$$S_i(u) = \int_0^u \frac{\sin(x)}{x}\,dx \qquad (2.26)$$

2.3.2 Modified Signal Model

In order to include effect of mutual coupling for both linear and circular arrays, a mutual coupling matrix is inserted in the model for the received signal, modifying (2.5) to

$$\mathbf{x}(t) = \sum_{k=1}^{K} \mathbf{C}\,\mathbf{a}(\theta_k)s_k(t) + \boldsymbol{\eta}(t) = \sum_{k=1}^{K} \mathbf{a}_{MC}(\theta_k)s_k(t) + \boldsymbol{\eta}(t) \qquad (2.27)$$

where $\mathbf{a}_{MC}(\theta_k) = \mathbf{C}\,\mathbf{a}(\theta_k)$ is the modified array steering vector and $\mathbf{C}$ is the coupling matrix of the antenna array, which can be written using fundamental electromagnetics and circuit theory as [134]

$$\mathbf{C} = (Z_A + Z_T)(\mathbf{Z} + Z_T\mathbf{I}_N)^{-1} \qquad (2.28)$$

where $\mathbf{I}_N$ is the $N \times N$ identity matrix and $\mathbf{Z}$ is the mutual impedance matrix in (2.21).

In addition, the beamforming weight vector is modified as

$$\mathbf{w}_{MC} = \frac{1}{N}\,\mathbf{C}\,\mathbf{a}(\theta_1) \tag{2.29}$$

Once the **C** matrix has been obtained, the capability of the array including mutual coupling effects can be assessed by finding the mean output power of the processor, as before, and identifying the signal, noise and interference power terms respectively. Repeating the analysis in the last section, it can be shown that with mutual coupling matrix taken into account the normalized amount of interference power seen from an interferer *k* at angle of arrival θ_k is

$$g_k(\theta_1,\theta_k) = \left|\frac{\mathbf{w}_{MC}^H\,\mathbf{a}_{MC}(\theta_k)}{||\mathbf{w}_{MC}^H||\;||\mathbf{a}_{MC}(\theta_k)||}\right|^2 \tag{2.30}$$

where $\mathbf{w}_{MC}$ is given in (2.29) and $\mathbf{a}_{MC}(\theta_k)$ in (2.27) respectively. The numerator in (2.30) after substituting the values becomes

$$\begin{aligned}\left|\mathbf{w}_{MC}^H\,\mathbf{a}_{MC}(\theta_k)\right|^2 &= \left|[\frac{1}{N}\,\mathbf{C}\,\mathbf{a}(\theta_1)]^H[\mathbf{C}\,\mathbf{a}(\theta_k)]\right|^2 \\ &= \frac{1}{N^2}\left|\mathbf{a}^H(\theta_1)\,\mathbf{C}^H\,\mathbf{C}\,\mathbf{a}(\theta_k)\right|^2 \end{aligned}\tag{2.31}$$

(2.30) is then substituted in (2.14) and (2.19) to get the spatial interference suppression coefficient for linear and circular arrays respectively.

2.4 Results

2.4.1 Mutual Impedance Matrix

When there is no mutual coupling, the matrix **Z** appearing in (2.20) is diagonal. In the presence of mutual coupling between antenna elements, there are non-zero elements off the diagonal. Figure 2.3 shows the plot of the magnitude of the normalized impedance matrix elements for an array of $N = 12$, $l = \lambda/2$ dipoles with terminating impedance $Z_T = Z_A$ for (a) linear and (b) circular geometries respectively. The figure shows that for a linear array, the coupling between the neighbouring elements is almost the same along the array. Also the magnitude of the coupling decreases quite rapidly as we move away from the diagonal. For a circular array, the magnitude also decreases initially but it increases again due to the circular symmetry of the geometry.

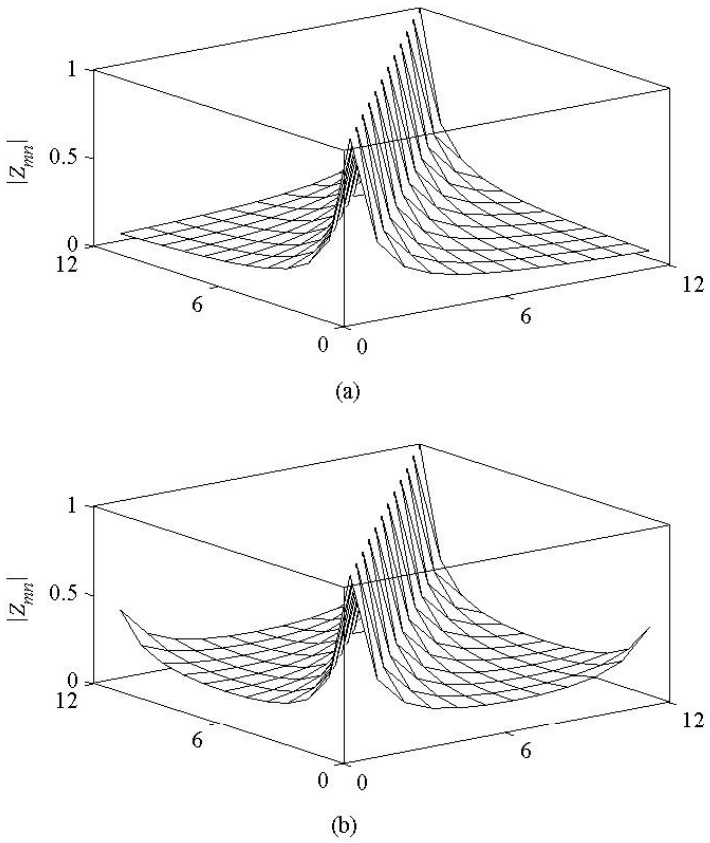

Figure 2.3: The magnitude of the normalized impedance matrix elements for an array of $N = 12$, $l = \lambda/2$ dipoles with (a) linear and (b) circular geometries.

2.4.2 Plot of Spatial Interference Suppression Coefficient for ULA

Figure 2.4 shows a plot of the spatial interference suppression coefficient $G_{avg}(\theta_1)$ for a linear array for different number of antenna elements N, without mutual coupling. The curves are U-shaped, with a broad minimum, implying that interference reduction is maximum over a certain range of Angle Of Arrival (AOA) θ_1, centered at $\theta_1 = 0^\circ$ (broadside).

2.4.3 Plot of Average Improvement in SIR vs. AOA for ULA

To gain more insight into the interference suppression capability, the average improvement in SIR (Λ) is plotted as a function of the AOA. This is shown in Figure 2.5 for an $N = 8$ element linear array under no mutual coupling assumption. It can be seen that the exact

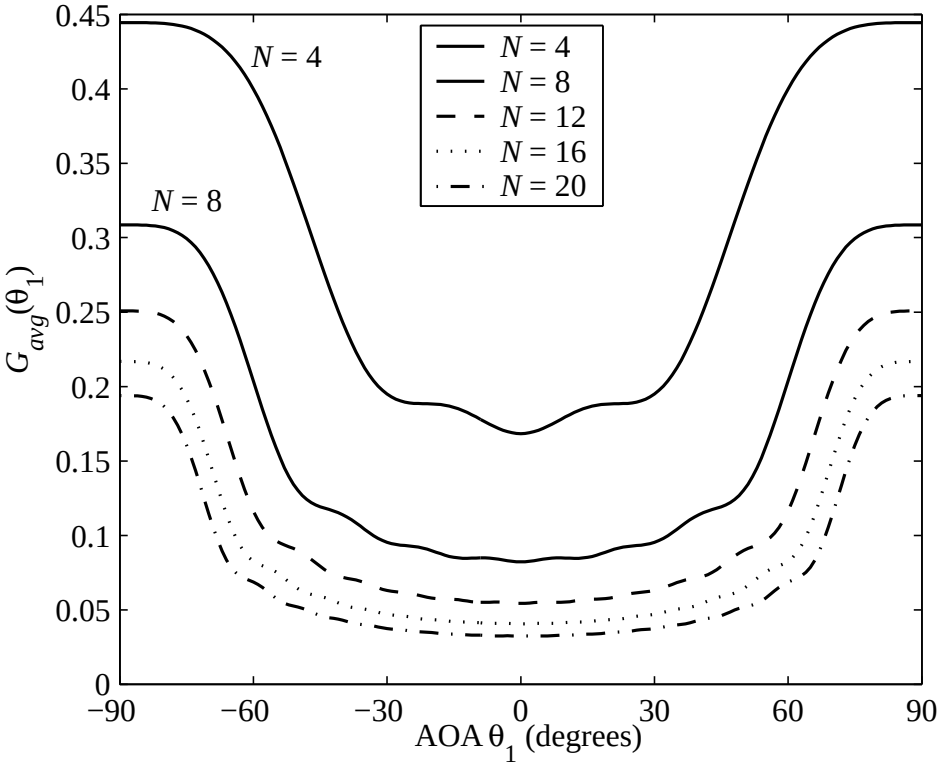

Figure 2.4: Variation of the spatial interference coefficient $G_{avg}(\theta_1)$ with AOA θ_1 for ULA antenna $(N = 4, 8, 12, 16, 20)$, without mutual coupling.

amount of SIR at the array output is dependent on AOA θ_1. The maximum SIR improvement of about 10.85 dB is achieved when DOA is $\theta = 0^\circ$. However this decreases by more than half to about 5.1 dB for end-fire incidence. The presented result confirms the expectation that for a linear array its discrimination against interferers (in terms of SIR) is best in the array's broadside direction and deteriorates in its end-fire directions.

2.4.4 Interference Reduction Beamwidth

To characterise this degradation in performance as we move from broadside to end-fire direction, we can define an 'Interference Reduction Beamwidth' (BW_{ir}) as the range of AOA θ_1 over which $G_{avg}(\theta_1)$ is within 3 dB of its maximum value at 0°. Figure 2.6 shows the variation of BW_{ir} with N. For $N = 4$, the beamwidth is approximately $\pm 51^\circ$ but increases to about $\pm 59^\circ$ for $N = 12$. The range is nearly the same when N increases further, with a small oscillation about this value, implying the onset of diminishing returns.

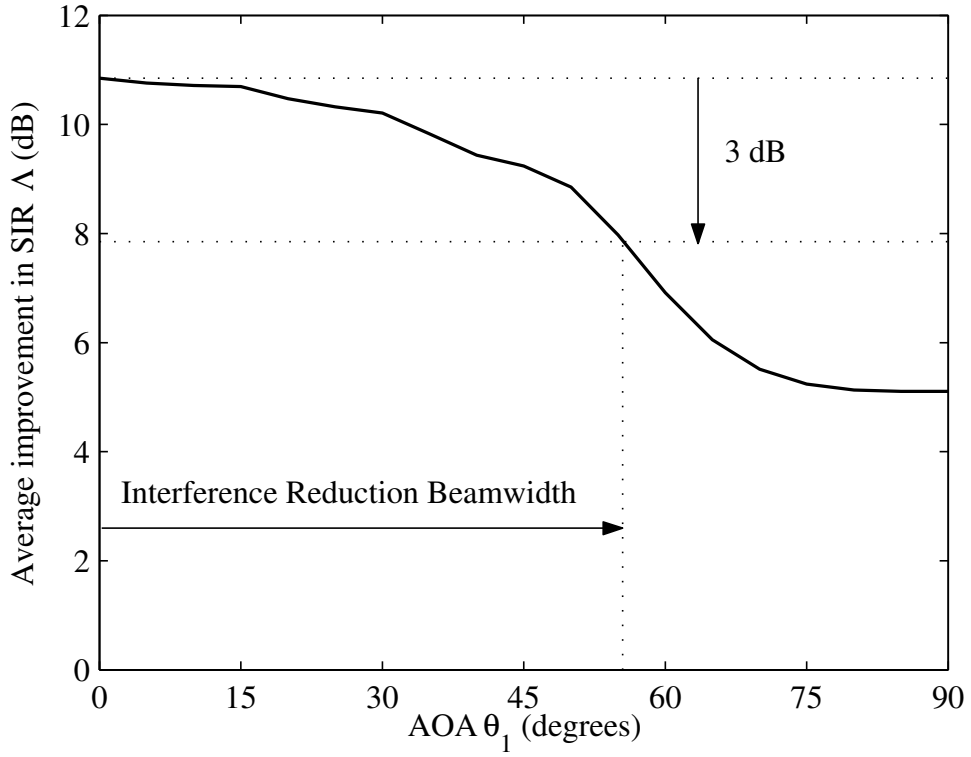

Figure 2.5: Plot of Average Improvement in SIR versus AOA θ_1 for $N = 8$ ULA antenna, under no mutual coupling assumption.

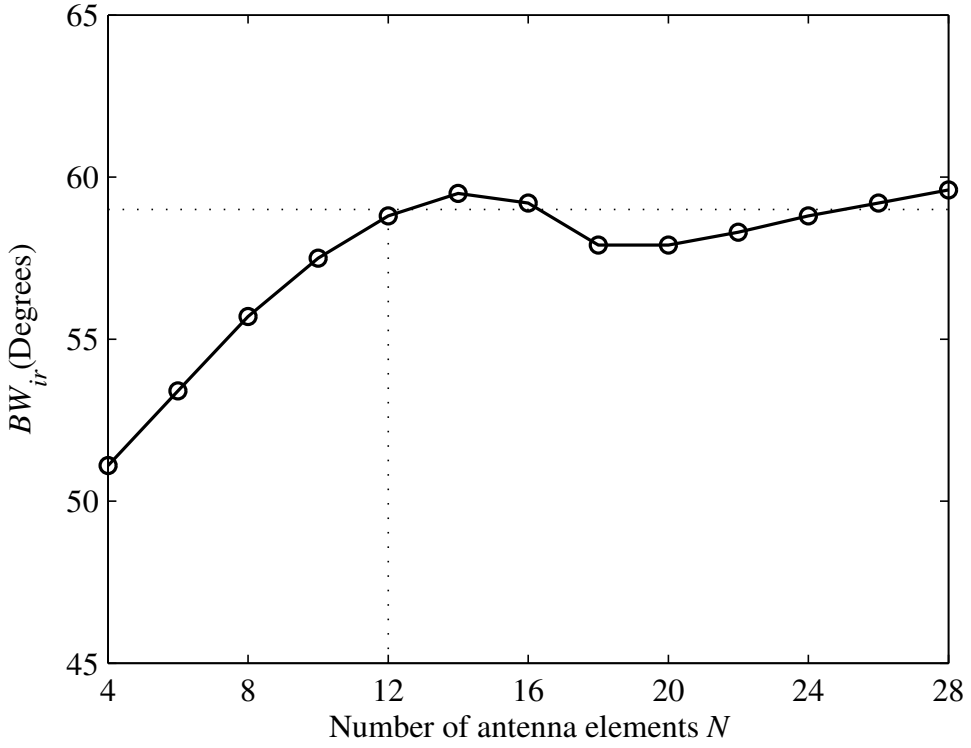

Figure 2.6: Plot of 'Interference Reduction Beamwidth' versus number of antenna elements N, for a ULA antenna under no mutual coupling assumption.

2.4.5 Effect of Mutual Coupling on Spatial Interference Suppression Coefficient for ULA

Figure 2.7 shows a plot of the spatial interference suppression coefficient $G_{avg}(\theta_1)$ for a linear array for different number of antenna elements N with mutual coupling. The $\mathbf{Z}$ matrix is obtained using the Induced EMF method. The figure shows that for a linear array, mutual coupling degrades the SIR improvement capability of the array. For larger scan angles, the performance is the same as for the case of no mutual coupling, but for broad-side incidence there is degradation due to mutual coupling.

2.4.6 Plot of Spatial Interference Suppression Coefficient for UCA

The plot of $G_{avg}(\theta_1)$ for circular array is shown in Figure 2.8. For a smaller number of antenna elements, the SIR improvement shows an oscillatory variation. However as N increases the curves flatten, indicating uniform SIR improvement over all angles.

For the case when mutual coupling is considered, the $\mathbf{Z}$ matrix is obtained using Induced EMF method and also using FEKO [39], which is a commercially available electromagnetic analysis package based on the Method of Moments (in FEKO simulations, frequency of 2 GHz and a wire radius of 0.5mm or $3.33 \times 10^{-3}\lambda$ are assumed). From the figure, it can be observed that contrary to the case of the linear array, a slight improvement in performance can be observed when mutual coupling is included, for all scan angles. The figure also shows that the curves obtained using $\mathbf{Z}$ determined from the Induced EMF method show a good agreement with the curves obtained using $\mathbf{Z}$ calculated from FEKO. The slight difference in the curves can be attributed to limitations of the Induced EMF method, e.g. it cannot take into account the gaps at the feed and the radius of the wires.

2.4.7 Variation of Mean of Spatial Interference Suppression Coefficient with N

Finally, Table 2.1 shows a comparison of mean of $G_{avg}(\theta_1)$ over AOA θ_1 for different N for linear and circular arrays, with and without mutual coupling. The mean is taken over 180° $(-\pi/2 \leq \theta \leq \pi/2)$ for linear array and 360° $(-\pi \leq \theta \leq \pi)$ for circular array.

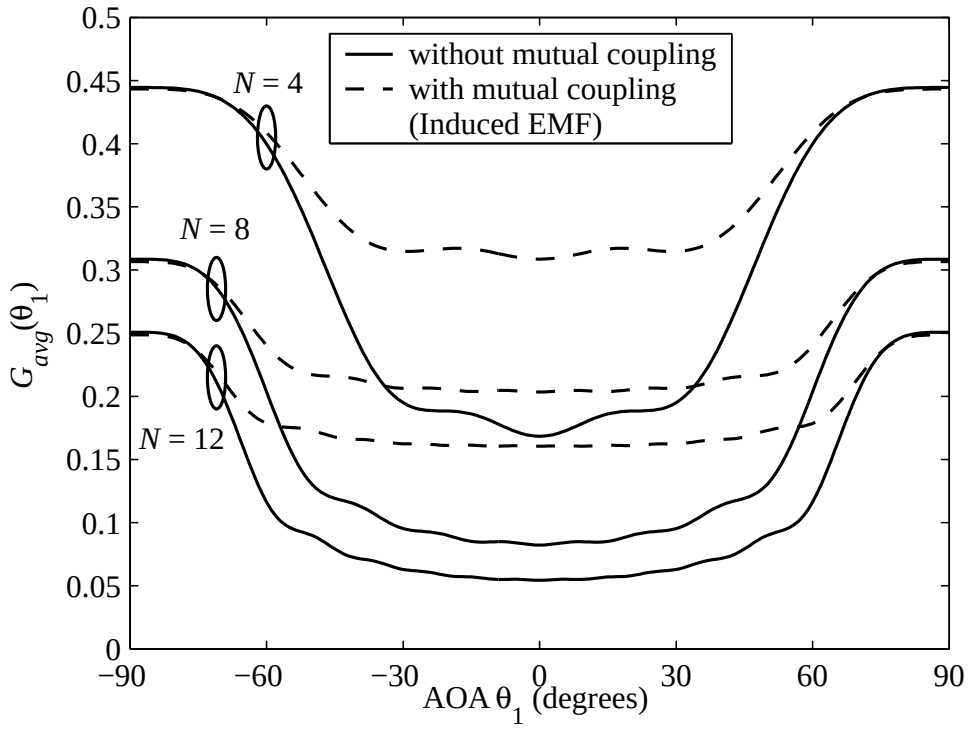

Figure 2.7: Variation of the spatial interference coefficient $G_{avg}(\theta_1)$ with AOA θ_1 for ULA antenna $(N = 4, 8, 12)$, with and without mutual coupling.

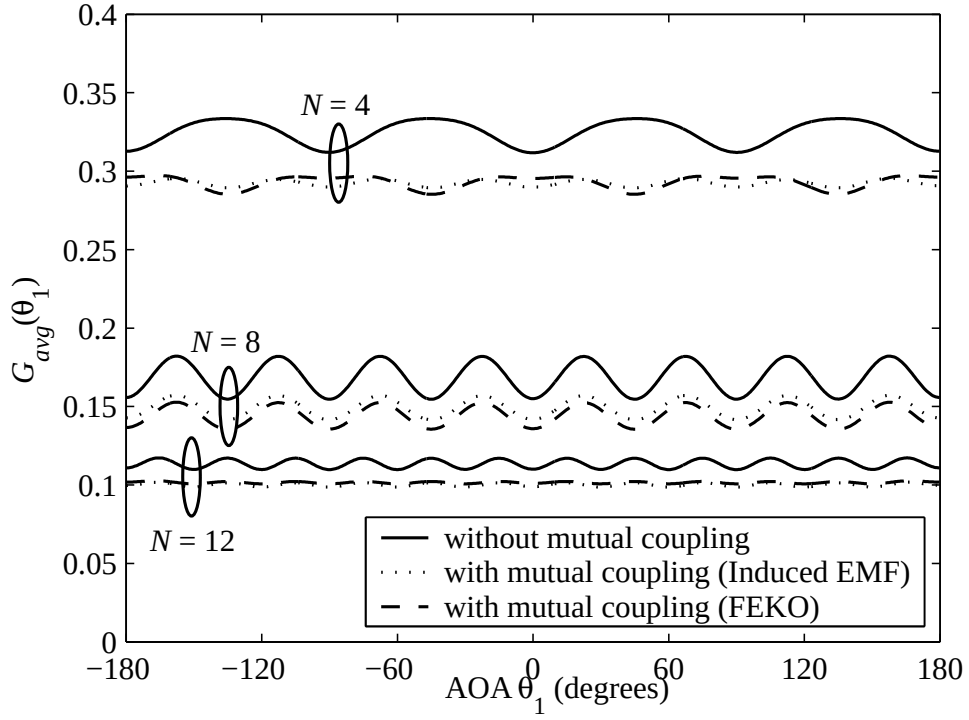

Figure 2.8: Variation of the spatial interference suppression coefficient $G_{avg}(\theta_1)$ with AOA θ_1 for UCA antenna $(N = 4, 8, 12)$, with and without mutual coupling.

Table 2.1: Mean of $G_{avg}(\theta_1)$ over AOA θ_1 for linear and circular arrays, with and without mutual coupling

N	Mean of $G_{avg}(\theta_1)$ over AOA θ_1			
	Linear		Circular	
	without coupling	with coupling	without coupling	with coupling
4	0.3021	0.3667	0.3241	0.2926
8	0.1668	0.2369	0.1683	0.1438
12	0.1176	0.1852	0.1134	0.0996
16	0.0917	0.1558	0.0915	0.0811
20	0.0756	0.1363	0.0774	0.0722

The table shows that when averaged over all values of AOA, both arrays show a similar performance for the case of no mutual coupling. This conclusion is in good agreement with the findings recently reported in [135]. However when mutual coupling is taken into account, the values are higher for a linear array indicating a degradation in performance while for a circular array the values are slightly reduced indicating a small improvement in performance. The values also confirm that for large N, the interference rejection capability reaches an asymptotic level both with or without mutual coupling.

2.5 Summary

This chapter has addressed the modelling of linear and circular array of half-wavelength spaced dipoles, which can be part of a base station of a CDMA cellular communication system. The performance of these two array antennas has been compared in terms of their interference rejection capabilities for the two cases of with and without mutual coupling. It has been shown that a circular array provides a more uniform improvement in terms of SIR than a linear array and is less susceptible to the effects of mutual coupling. However when the performance is averaged over all angles of arrival and mutual coupling is negligible, linear arrays show similar performance to circular arrays. Thus in the remaining chapters of this thesis, only linear arrays are considered.

Chapter 3

Description and Modelling of Wireless Channel

In this chapter a new spatio-temporal channel model, for use in the performance analysis of wireless communication systems incorporating smart antennas, is presented. As mentioned in Chapter 1, there are several ways to characterize the wireless propagation environment. This chapter describes the construction of a parameterized physical channel model for smart antennas and is organised as follows. In Section 3.1, modelling of the various spatial and temporal parameters of the channel model is described. In Section 3.2, these parameters are then combined into a single channel model and a mathematical description of the model is presented. Finally, the proposed model is implemented in software and Sections 3.3 and 3.4 present and discuss different Rayleigh and Rician fading channel simulations respectively.

3.1 Physical Channel Model Parameters

Consider the scenario where the Base Station (BS) is an elevated and separate structure that is located well above the surrounding scatterers. Without loss of generality, it is assumed that the BS employs a Uniform Linear Array (ULA) of N omni-directional antenna elements, with inter-element spacing $d = \lambda/2$. The Mobile Station (MS), however, moves on the street level (at a typical height of $1-2$ m) and is surrounded by local scattering structures (e.g., an urban or suburban environment). Furthermore, a few dominant and spatially well-separated reflectors, such as hills or large buildings, are located in the environment in the far-field of the array. The propagation scenario is illustrated in Figure 3.1.

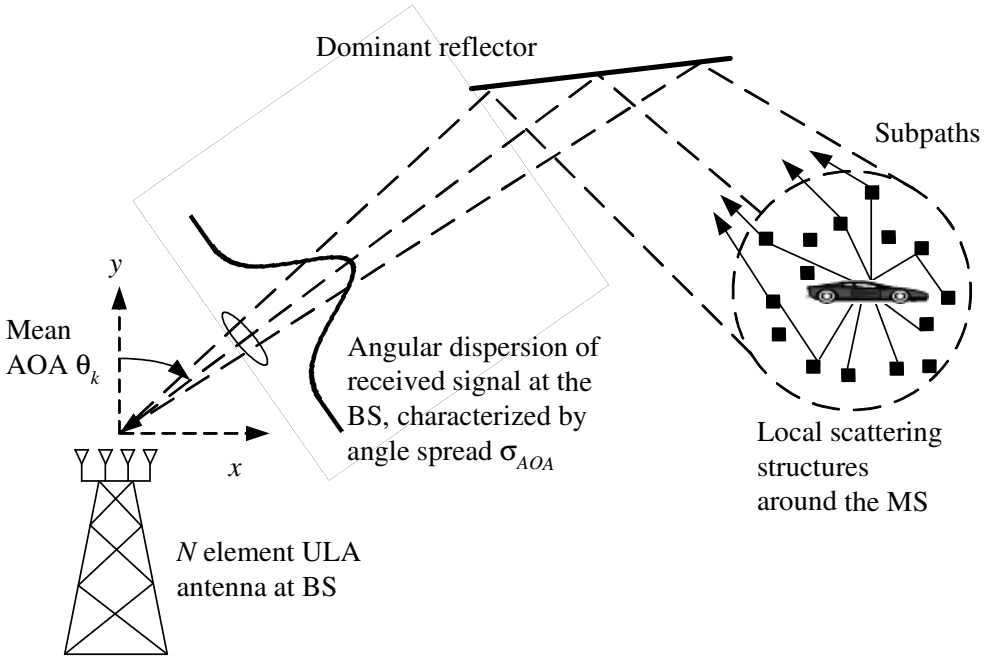

Figure 3.1: Illustration of wireless propagation environment.

The signal transmitted by the MS illuminates the local scattering structures around the MS. This generates numerous subpaths of the signal. The subpaths reach the BS either directly (line-of-sight propagation) or after undergoing further reflection from a dominant reflector (non-line-of-sight propagation), which gives rise to multipath propagation. Each propagation path arriving at the BS is itself composed of a large number of subpaths, which cannot be resolved by the receiver because their relative time delay is too small (i.e. less than one chip duration). Since the dominant reflectors are significantly separated, a different combination of the incoming subpaths is reflected at each reflector. Therefore independent fading is assumed for each path. In case of movement of the MS, the superposition of the subpaths results in time-correlated multipath fading.

Each propagation path is associated with its own power, time delay and angle of arrival. In general, the received signal at the BS arrives mainly from one given direction. In addition, a small angle spread of subpaths is observed at the BS as the MS is far away from the BS and the BS is well above the surrounding objects.

Various parameters of the physical model, that are used to characterise the wireless

channel between the MS and BS, can be grouped into the following two main categories:-

1. Temporal Parameters
   (a) Path loss.
   (b) Shadowing.
   (c) Multipath fading.
   (d) Power Spectral Density.
   (e) Power Delay Profile.
2. Spatial Parameters
   (a) Angle of Arrival.
   (b) Angular distribution of users.
   (c) pdf's in Angles of Departure and Angles of Arrival.
   (d) Spatial correlation.
   (e) MS mobility.

The modelling of these parameters is detailed in the following subsections.

3.1.1 Path Loss

Path loss is defined as an overall decrease in signal strength with distance between the transmitter and receiver [136]. Measurements show that the average received signal power decreases logarithmically with distance [2]. The average path loss $\overline{\rho}(D_k)$ can thus be expressed as

$$\overline{\rho}(D_k) = \overline{\rho}(D_0) + 10\,\varepsilon \log_{10}\left(\frac{D_k}{D_0}\right), \qquad \text{dB} \tag{3.1}$$

where ε is the path loss exponent that indicates the rate of signal power attenuation with distance, D_0 is the close-in reference distance which is determined from measurements close to the transmitter, D_k is the distance between the kth MS and the BS and $\overline{\rho}(D_0)$ is the average path loss at close-in reference distance [2]. The value of ε depends on the specific propagation environment, e.g. in free space $\varepsilon = 2$. For a typical urban macrocell environment, the value of ε ranges between 2 and 5, with a typical value of 4 [2].

3.1.2 Shadowing

Shadowing or slow fading represents the variation of average path loss in a local area (several tens of meters). It is caused by variation of propagation conditions due to buildings, roads, trees and other obstacles in a relatively small area [137].

Empirical studies show that the received signal levels at a specific transmitter-receiver separation have a Gaussian distribution about the distance dependent average path loss from (3.1), where the measured signal levels have values in dB units [2]. Thus considering shadowing, the overall path loss $\rho(D_k)$ is given by

$$\rho(D_k) = \bar{\rho}(D_k) + \mathcal{S}_k, \qquad \text{dB} \tag{3.2}$$

where $\bar{\rho}(D_k)$ is given in (3.1) and $\mathcal{S}_k$ is a zero mean Gaussian distributed random variable (in dB) with variance $\sigma_{\mathcal{S}}^2$ (also in dB). The variance usually lies in the range $4-12$ dB, depending upon the propagation environment. For urban macrocells, typical value for $\sigma_{\mathcal{S}}^2$ is 8 dB [107].

Shadowing and path loss both affect the mean power of the received signal and their combined effect changes slowly over time due to motion of the MS. It is assumed that these slow-fading effects are compensated for by the perfect power control system and are therefore not considered in the simulations.

3.1.3 Multipath Fading

When a radio signal is transmitted in a wireless channel, the waves propagate through the physical medium (atmosphere or free space) and interact with the physical objects that constitute the propagation environment such as buildings, hills, trees and moving vehicles, giving rise to many subpaths of the transmitted signal. Multipath fading is caused by the constructive and destructive combination of these randomly delayed, reflected, scattered and diffracted subpath signal components over distances of the order of a few wavelengths [42]. This type of fading is relatively fast and is therefore responsible for short-term signal variations.

Depending on the nature of the propagation environment, the multipath fading envelope can be described by different models [42]. In this thesis the Rayleigh (non-line-of-sight) and Rician (line-of-sight) fading models, which are most commonly used to describe the statistical time varying nature of the individual multipath envelopes, are considered [2].

3.1.3.1 Rayleigh Model

The Rayleigh distribution can be used to model the multipath fading in Non-Line-Of-Sight (NLOS) fading environments, i.e. when there is no direct Line-Of-Sight (LOS) path between the MS and BS. In this case, the channel fading amplitude α is distributed according to

$$f_\alpha(\alpha) = \frac{2\alpha}{\Omega} \exp\left(-\frac{\alpha^2}{\Omega}\right), \qquad \alpha \geq 0 \tag{3.3}$$

where $\Omega = E[\alpha^2]$ is the average envelope power and $E[\cdot]$ denotes expectation operator.

3.1.3.2 Rice Model

The Rice distribution is used to model the propagation paths consisting of one direct LOS component and many random weaker NLOS components. In this case, the channel fading amplitude is distributed according to [107]

$$f_\alpha(\alpha) = \frac{2\alpha}{b_0} \exp\left(-\frac{\alpha^2+s^2}{2b_0}\right) I_0\left(\frac{\alpha s}{b_0}\right), \qquad \alpha \geq 0 \tag{3.4}$$

where s^2 is the specular power, $2b_0$ is the scattered power and $I_0(\cdot)$ is the modified Bessel function of the first kind and zero order [133].

The Rice factor K_R is defined as the ratio of the specular power to the diffuse or scattered power. This ratio is commonly expressed in decibels as

$$K_R = 10\log_{10}\left(\frac{s^2}{2b_0}\right) \tag{3.5}$$

The Rice factor completely specifies the Rice distribution. In terms of the Rice factor, the specular and scattered powers can be written as [107]

$$s^2 = \frac{K_R\,\Omega}{K_R+1} \tag{3.6a}$$

$$2b_0 = \frac{\Omega}{K_R+1} \tag{3.6b}$$

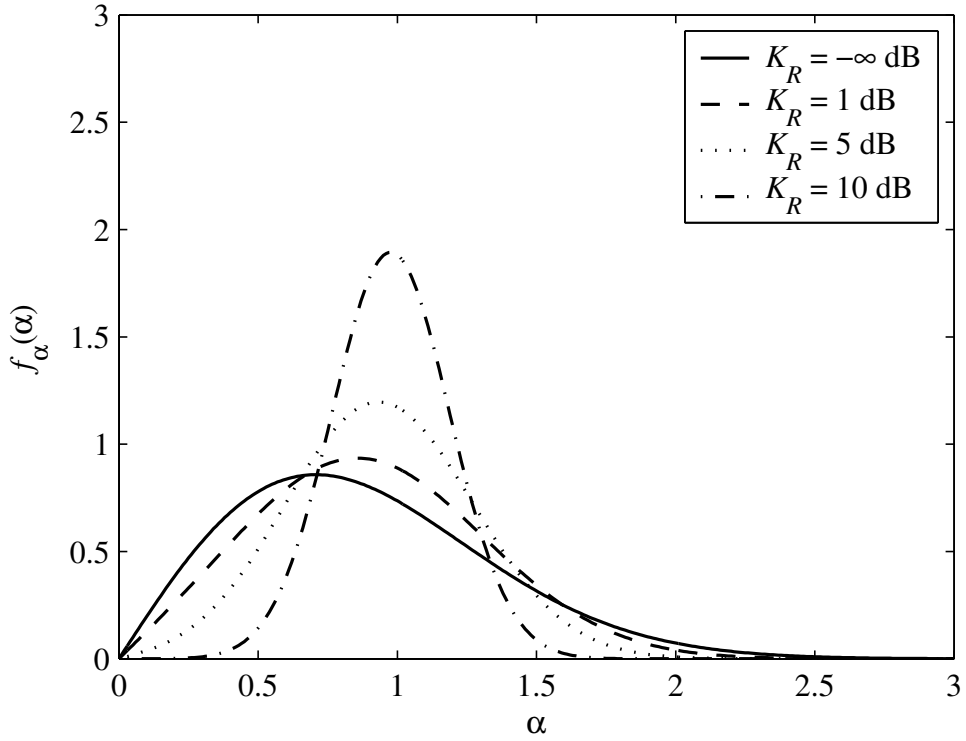

Figure 3.2: The Rice probability density function for Rice factors $K_R = -\infty, 1, 5, 10$ dB respectively.

where $\Omega = s^2 + 2b_0$ is the average envelope power. Using (3.6a) and (3.6b), the probability density function (pdf) of the Rice distribution can be written as [138]

$$f_\alpha(\alpha) = \frac{2\alpha(K_R+1)}{\Omega} \exp\left(-K_R - \frac{(K_R+1)\alpha^2}{\Omega}\right) I_0\left(2\alpha\sqrt{\frac{K_R(K_R+1)}{\Omega}}\right), \qquad \alpha \geq 0 \quad (3.7)$$

Figure 3.2 shows the Rice pdf for several values of K_R. The curve for $K_R = -\infty$ dB corresponds to the Rayleigh pdf. It can be seen that the Rician pdf degenerates to a Rayleigh pdf as the value of $K_R \to -\infty$ dB.

3.1.4 Power Spectral Density

Whenever relative motion exists between the transmitter and receiver, it causes an apparent shift in the frequency of the received signal due to the Doppler shift. The Doppler shift is different for every subpath as it depends on the Angle of Departure (AOD) of the subpath relative to the direction of movement of the MS. For the sum of all the scattered

and reflected subpaths, this yields a continuous spectrum of Doppler frequencies, called the Power Spectral Density (PSD). The inverse Fourier transform of the PSD is the autocorrelation function of the fading signal [107, 139].

The shape of the PSD determines the time domain fading signal and its temporal correlation properties. The proper selection of the fading spectrum is, therefore, very important in order to produce realistic fading signals that have proper temporal correlation behaviour. Depending upon the particular propagation environment and the underlying communication scenario, different PSD's have been proposed [42]. A popular choice for land mobile communications, which is also adopted this thesis, is the Jakes PSD [45, 46].

For the case of Rayleigh fading, the normalised Jakes PSD and the corresponding autocorrelation function are given by [42]

$$S(f) = \frac{1}{\pi f_D \sqrt{(1-(f/f_D)^2}}, \qquad |f| \leq f_D \tag{3.8a}$$

$$R(\tau) = J_0(2\pi f_D \tau) \tag{3.8b}$$

where $J_0(\cdot)$ is the zero-order Bessel function of the first kind and f_D is the maximum Doppler shift that the signal undergoes, given by

$$f_D = \frac{v}{\lambda} = \frac{v f_c}{c} \tag{3.9}$$

where v is the vehicle speed (in m/s), λ is the wavelength of the transmitted signal, c is the velocity of light and f_c is the carrier frequency.

In this thesis, the maximum Doppler frequency used is 100 Hz. This corresponds to a speed of $v = 120$ km/hr for $f_c = 900$ MHz and $v = 54$ km/hr for $f_c = 2$ GHz respectively (i.e. a fast vehicular channel). Figure 3.3 shows a plot of the autocorrelation function against the time delay assuming $f_D = 100$ Hz.

3.1.5 Power Delay Profile

The information about the multipath delays (τ_l) and powers ($\Omega_l = E[(\alpha_l)^2]$) is conveniently represented using the channel's Power Delay Profile (PDP), which is also referred to as the Multipath Intensity Profile (MIP). It shows the mean power present at different time delays.

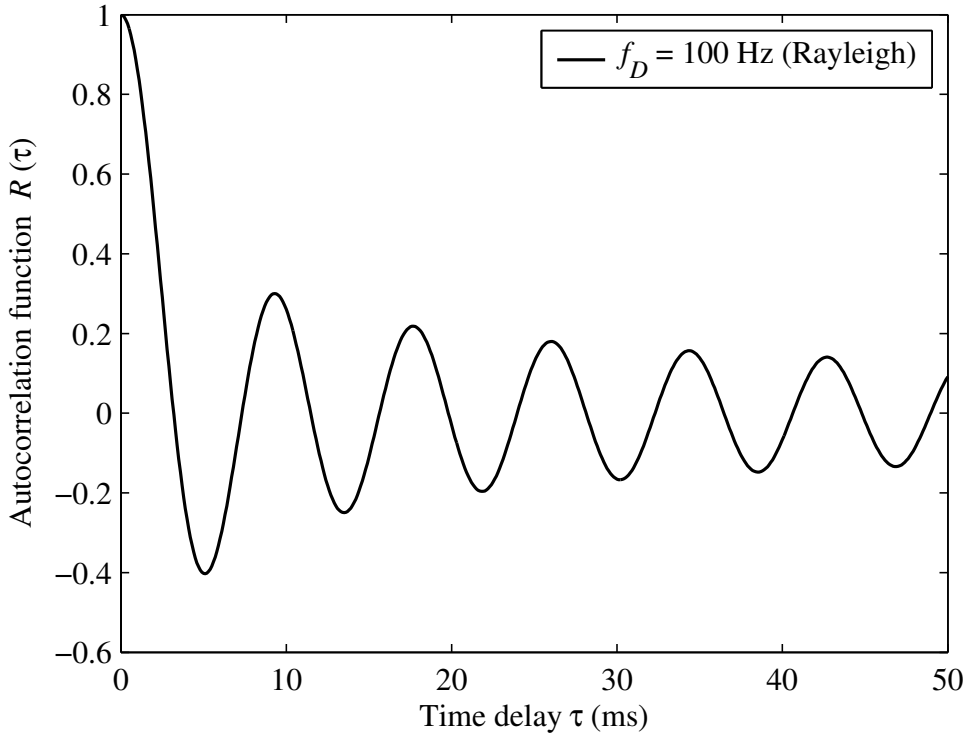

Figure 3.3: The autocorrelation function corresponding to the Jakes power spectral density for $f_D = 100$ Hz.

The PDP model can assume various forms, depending on the type of environment (indoor or outdoor) and the general propagation conditions [140]. In this work, the simplifying assumption is made that the time delays associated with the different resolvable multipaths are independent of the Angles of Arrival (AOA's) [71].

An important measure which characterizes the time dispersiveness of the channel is the RMS delay spread σ_{DS}. It is defined as the square root of the second central moment of the PDP and is given as [2]

$$\sigma_{DS} = \sqrt{\overline{\tau^2} - (\overline{\tau})^2} \tag{3.10}$$

where

$$\overline{\tau^2} = \frac{\sum_l \Omega_l (\tau_l)^2}{\sum_l \Omega_l} \tag{3.11}$$

and $\overline{\tau}$ is the first moment of the power delay profile called the mean excess delay. It is

Table 3.1: Typical RMS delay spread values reported in literature [141].

Environment	RMS Delay Spread (μs)
Suburban	$0.1-1$
Urban	$1-3$
Rural	$6-7$

defined as [2]

$$\bar{\tau} = \frac{\sum_l \Omega_l \tau_l}{\sum_l \Omega_l} \tag{3.12}$$

(3.11) and (3.12) do not rely on the absolute path powers but only on the relative amplitudes. The delays in the above equations are measured relative to the first path. Typical values for the RMS delay spread at 900 MHz reported in literature are shown in Table 3.1 [141].

In this thesis, a uniform PDP is assumed. The two-path model is often used for analytical treatments. The impulse response for this model can be written as [142]

$$h(t) = \alpha_1 \delta(t-\tau_1) + \alpha_2 \delta(t-\tau_2) \tag{3.13}$$

where τ_1 and τ_2 are the path delays and α_1 and α_2 are the complex fading coefficients. The PDP can be written as

$$P(\tau) = \Omega_1 \delta(t-\tau_1) + \Omega_2 \delta(t-\tau_2) \tag{3.14}$$

where Ω_1 and Ω_2 are the path powers respectively.

The two- and and three-path PDP's used in the work are shown in Figure 3.4 [2].

3.1.6 Mean Angle of Arrival

Each MS's incoming signal at the BS is described with a mean Angle of Arrival (AOA) θ_k. It is assumed that the AOA is the same for all the multipaths of a particular user, i.e. the spatial channel is assumed to be based on one AOA only ($\theta_{k,l} = \theta_k$). As per convention, the

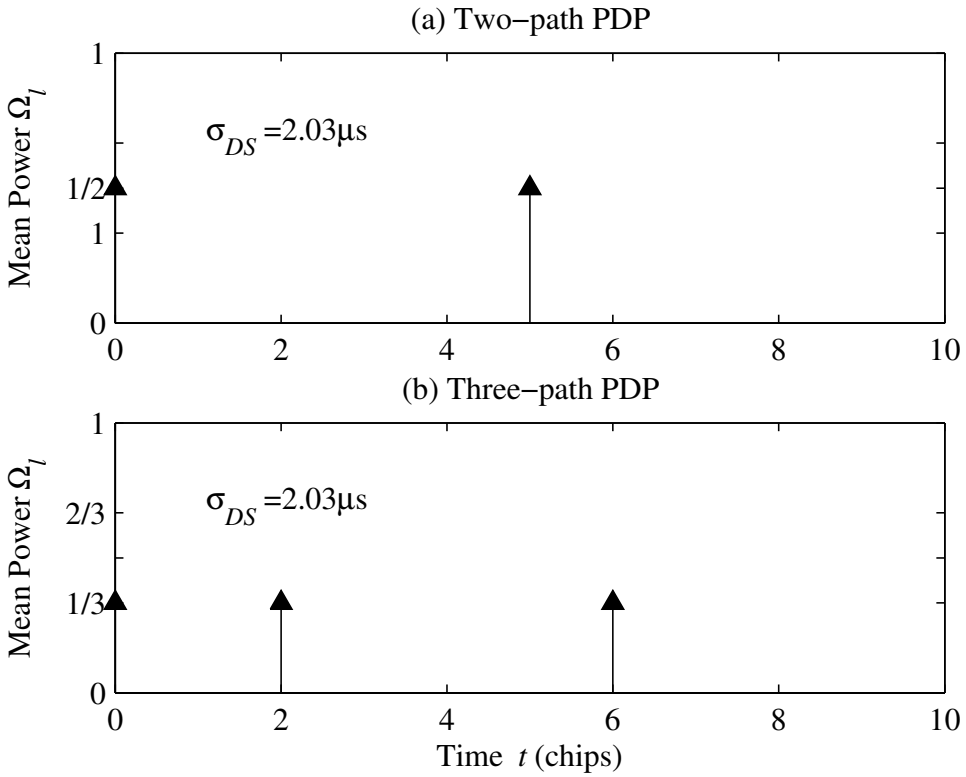

Figure 3.4: Uniform power delay profiles: (a) two-path and (b) three-path.

mean AOA θ_k is measured from the array broadside with $\theta = 0^\circ$ referred to as the broadside direction.

From Section 2.1.1, the array steering vector which models the spatial response of the ULA antenna is given as

$$\mathbf{a}(\theta) = \begin{bmatrix} 1 & e^{-j\mathcal{K}d\sin\theta} & \cdots & e^{-j\mathcal{K}d(N-1)\sin\theta} \end{bmatrix}^T \tag{3.15}$$

3.1.7 Angular Distribution of Users

The distribution of users in the cellular network is an important element of the spatial channel model. A number of approaches to the modelling of user locations have been proposed in literature. For example, a uniform MS distribution was proposed in [143] and a modified Gaussian distribution was proposed in [144]. A more general pdf that describes the user distribution and is applicable to many scenarios was proposed and discussed in [145].

Base stations are frequently split into three sectors, with 120° coverage per sector, to ac-

commodate more users per base station. In this thesis, a single 120° sector is considered for compatibility with the tri-sectored approach used by most of the current commercial systems. It is assumed that the K users in the system are uniformly distributed in $[-60^\circ, 60^\circ]$, along the arc boundary of the sector cell in the far field of the array.

3.1.8 Azimuth Field Dispersion at MS and BS

One of the most important spatial assumption relates to the probability density function (pdf) of the Angle of Departure (AOD) of the subpaths at the MS and the pdf of the Angle of Arrival (AOA) of the subpaths at the BS respectively. There is a fundamental difference between azimuthal field dispersion at an elevated BS and a MS, even though the propagation channel is assumed to be reciprocal, e.g at the elevated BS, the incoming field can be expected to be more concentrated in azimuth since the BS antenna is located well above the scatterers [57].

3.1.8.1 pdf in AOD

The pdf in the AOD at the MS describes the angular distribution of the subpaths departing the MS in azimuth. It is assumed that the azimuth field distribution at the MS can be modelled by a uniform probability density function over $[0, 2\pi]$. This corresponds to the isotropic scattering model, also known as the Clarke's model [45, 46]. Recently, it has been suggested that von Mises distribution provides a more accurate description of the angular distribution of the subpaths at the MS [146, 147].

3.1.8.2 pdf in AOA

The pdf in the AOA at the BS describes the angular distribution of the subpaths arriving at the BS in azimuth. For urban environments, a commonly used assumption for azimuth energy distribution is a uniform distribution [148], given by

$$f_{AOA}(\theta) = \frac{1}{2\Delta}, \qquad \theta_k - \Delta \leq \theta \leq \theta_k + \Delta \tag{3.16}$$

where Δ is called the scattering angle and is related to the standard deviation of the uniform distribution as $\sigma_{AOA} = \frac{\Delta}{\sqrt{3}}$ and 2Δ is the range of angles about the Mean AOA θ_k.

Another distribution that has been suggested is a Gaussian distribution in AOA, given by [149]

$$f_{AOA}(\theta) = \frac{C_g}{\sqrt{2\pi}\sigma_{AOA}} \exp\left[\frac{(\theta-\theta_k)^2}{2\sigma_{AOA}^2}\right], \qquad -\pi+\theta_k \leq \theta \leq \pi+\theta_k \tag{3.17}$$

where σ_{AOA} is the standard deviation and controls the spread of the pdf function and C_g is a constant that ensures that $f_{AOA}(\theta)$ fulfils the requirements of a pdf, given by [150]

$$C_g = \frac{1}{\text{erf}(\pi/\sqrt{2}\sigma_{AOA})} \tag{3.18}$$

where $\text{erf}(x) = 2/(\sqrt{\pi})\int_0^x e^{-t^2}dt$ is the error function. Note that when angular spread is small, C_g is almost unity. The uniform and Gaussian distributions are shown in Figures 3.5 and 3.6 respectively for various angle spreads $\sigma_{AOA} = 5^\circ, 10^\circ, 20^\circ, 60^\circ$ about the mean AOA $\theta = 0^\circ$.

In addition to the uniform and Gaussian distributions, other distributions have also been proposed, e.g. $\cos^n(\theta)$ [62] and Laplacian distributions [151, 152]. According to [57], a Gaussian pdf best matches the azimuth pdf in typical urban environments. However from the point of view of simulations, the key parameter of the system performance is the standard deviation of the pdf in AOA and not the type of pdf in AOA under investigation [115, 153, 154].

3.1.9 Spatial Correlation Coefficient

The performance of different antenna array architectures is dependant on the spatial correlation between the antenna elements, e.g. traditional beamforming techniques depend on the perfect correlation of the received signals at the array while diversity techniques depend on low correlation of the received signal between the antenna branches. Thus it is important to study the cross-correlation behaviour for different environment conditions. The cross-correlation between the waves impinging on two antenna elements depends mostly on the pdf in AOA. In this section, both uniform and Gaussian distributions are employed to model the AOA's and their impact on array spatial correlation is considered. To allow a consistent comparison, the Angle Spread (AS) is assumed equal to the standard deviation σ_{AOA} of the underlying pdf.

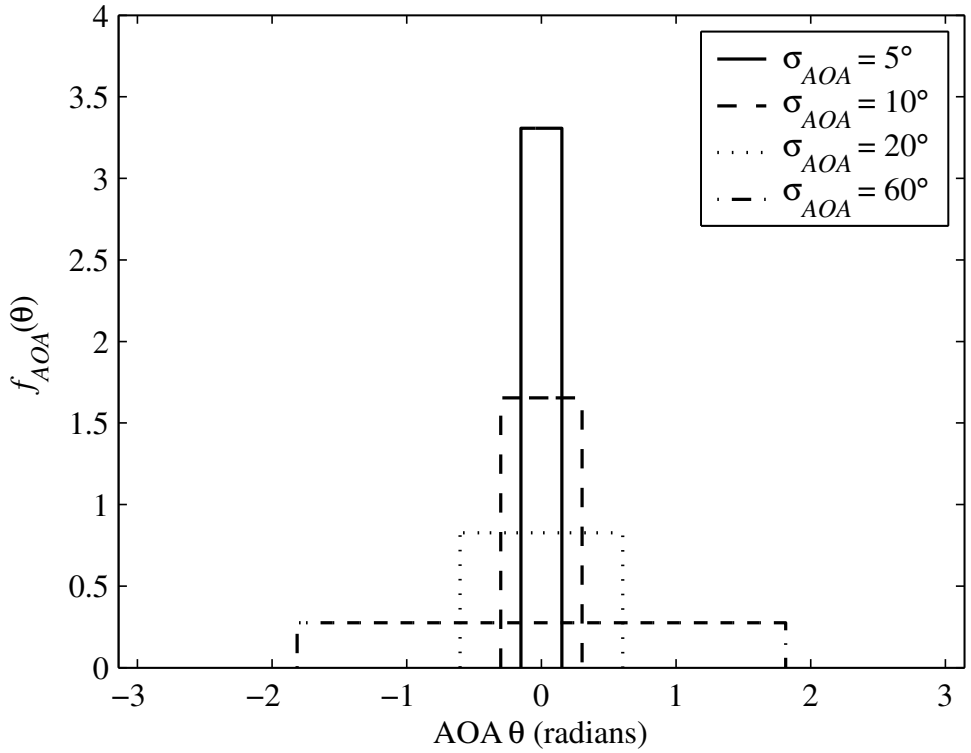

Figure 3.5: Uniform pdf's in azimuth AOA for mean AOA $\theta = 0^\circ$ and angle spreads $\sigma_{AOA} = 5^\circ, 10^\circ, 20^\circ, 60^\circ$ respectively.

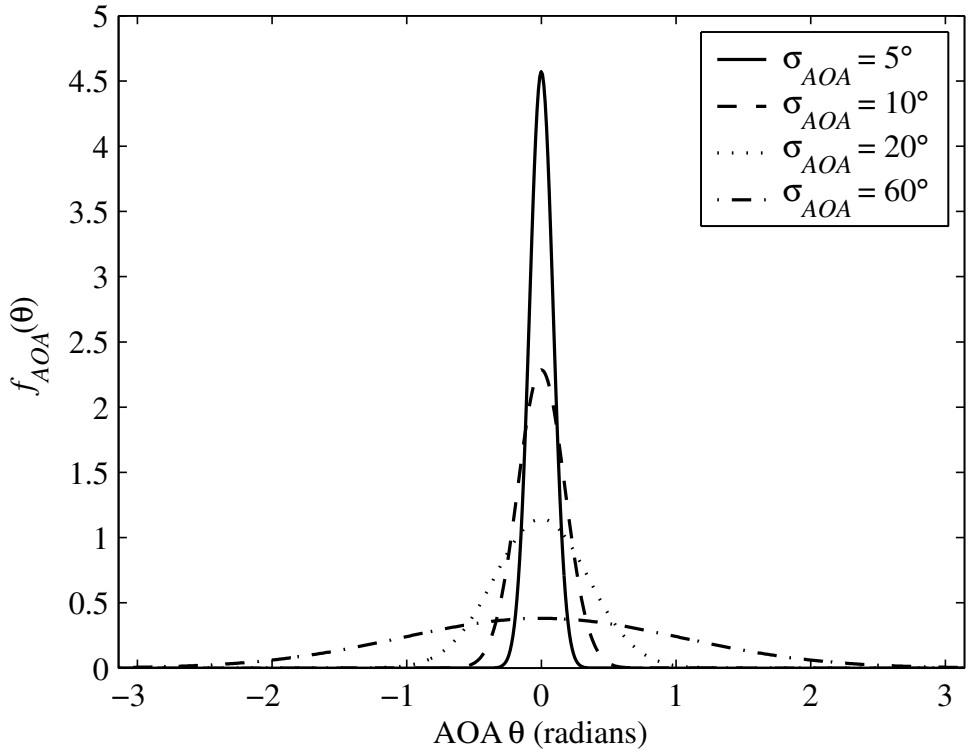

Figure 3.6: Gaussian pdf's in azimuth AOA for mean AOA $\theta = 0^\circ$ and angle spreads $\sigma_{AOA} = 5^\circ, 10^\circ, 20^\circ, 60^\circ$ respectively.

The array spatial correlation between the nth and pth antenna elements for the ULA is defined as

$$\begin{aligned}\mathbf{R}_s(n,p) &= E\{a_n(\theta)a_p^*(\theta)\} \\ &= \int_\theta a_n(\theta)a_p^*(\theta)\, f_{AOA}(\theta) \equiv \Re\{\mathbf{R}_s(n,p)\} + j\Im\{\mathbf{R}_s(n,p)\} \end{aligned} \tag{3.19}$$

where $(\cdot)^*$ denotes complex conjugate, $f_{AOA}(\theta)$ is the pdf of the AOA distribution and $a_n(\theta)$ and $a_p(\theta)$ are elements of the array steering vector from (3.15).

The spatial envelope correlation coefficient ρ_s is then defined as

$$\rho_s = |\mathbf{R}_s(n,p)|^2 = |\Re\{\mathbf{R}_s(n,p)\} + j\Im\{\mathbf{R}_s(n,p)\}|^2 \tag{3.20}$$

where $\Re\{\mathbf{R}_s(n,p)\}$ and $\Im\{\mathbf{R}_s(n,p)\}$ are the real and imaginary parts of signal correlation respectively. The required antenna separation for $\rho_s = 0.7$ is also known as the correlation distance.

Assuming a uniform distribution in AOA, the real and imaginary parts of signal correlation between the nth and pth antenna elements are given by [148, 155]

$$\Re\{\mathbf{R}_s(n,p)\} = J_0(z_{np}) + 2\sum_{v=1}^{\infty} J_{2v}(z_{np})\cos(2v\theta)\,\mathrm{sinc}(2v\Delta) \tag{3.21a}$$

$$\Im\{\mathbf{R}_s(n,p)\} = 2\sum_{v=0}^{\infty} J_{2v+1}(z_{np})\,\sin[(2v+1)\theta]\,\mathrm{sinc}[(2v+1)\Delta] \tag{3.21b}$$

where $z_{np} = 2\pi|p-n|d/\lambda$, d is the inter-element distance, λ is the wavelength, θ is the mean AOA, Δ is the scattering angle, $J_n(x)$ is the nth order Bessel function of the first kind and $\mathrm{sinc}(x) = \frac{\sin(x)}{x}$ is the sinc$(\cdot)$ function.

Assuming a Gaussian distribution in AOA, it can be shown that the real and imaginary parts of $\mathbf{R}_s(n,p)$ are given by [149, 156]

$$\begin{aligned}\Re\{\mathbf{R}_s(n,p)\} &= J_0(z_{np}) + 2C_g\sum_{v=1}^{\infty} J_{2v}(z_{np})\cos(2v\theta) \\ &\quad \exp\left(-2v^2\sigma_{AOA}^2\right)\Re\left\{\mathrm{erf}\left(\frac{\pi + j2v\sigma_{AOA}^2}{\sqrt{2}\sigma_{AOA}}\right)\right\} \end{aligned} \tag{3.22a}$$

$$\begin{aligned}\Im\{\mathbf{R}_s(n,p)\} &= 2C_g\sum_{v=0}^{\infty} J_{2v+1}(z_{np})\sin[(2v+1)\theta] \\ &\quad \exp\left[\frac{-(2v+1)^2\sigma_{AOA}^2}{2}\right]\Re\left\{\mathrm{erf}\left[\frac{\pi + j(2v+1)\sigma_{AOA}^2}{\sqrt{2}\sigma_{AOA}}\right]\right\} \end{aligned} \tag{3.22b}$$

where C_g is given in (3.18) and $\text{erf}(a+jb)$ is the complex input error function [157].

(3.21) and (3.22) can be numerically evaluated using MATLAB [126]. For the numerical evaluation, the summation of over 30 terms is enough for accuracy of six digits after the decimal point [150]. Figures 3.7 and 3.8 show the plots of ρ_s assuming uniform and Gaussian AOA's and different angle spreads respectively. The figures show that in general, the spatial correlation decreases with increasing angular spread, increasing inter-element distance and decreasing angle of arrival as measured from the array broadside. The largest correlation is achieved at $\theta = 90^\circ$ and $\sigma_{AOA} = 0^\circ$. The consequences of this correlation behaviour are two-fold [149]:-

- If the azimuth angular spread is small, the output signals of the elements of the BS antenna array are strongly correlated. Therefore the array antenna will provide beamforming gain only.
- If the azimuth angular spread is moderate or large, the output signals of the elements of the BS antenna array are not strongly correlated. Therefore in this situation, the array antenna can provide diversity gain from spatial fading in addition to the beamforming gain.

3.1.10 MS Mobility Model

Modelling of MS mobility is a crucial subject for the simulation of space-time channels. The movement of the MS influences both the spatial and temporal channel characteristics. Also for the case of adaptive beamforming, the smart antenna must track and steer its beam towards the desired user. Therefore, the performance of a smart antenna cannot be realistically evaluated without simulating MS mobility.

For implementation efficiency, the following assumptions are used to model the effects of MS mobility [67]:-

- The number of subpaths and the number of multipath components are kept constant as the mobile moves for a particular Monte Carlo simulation run.
- The subpath parameters (angles of departures, random phases and angular spread) are kept constant as the mobile moves.
- Only the mean AOA θ_k of the path is adjusted as the mobile moves.

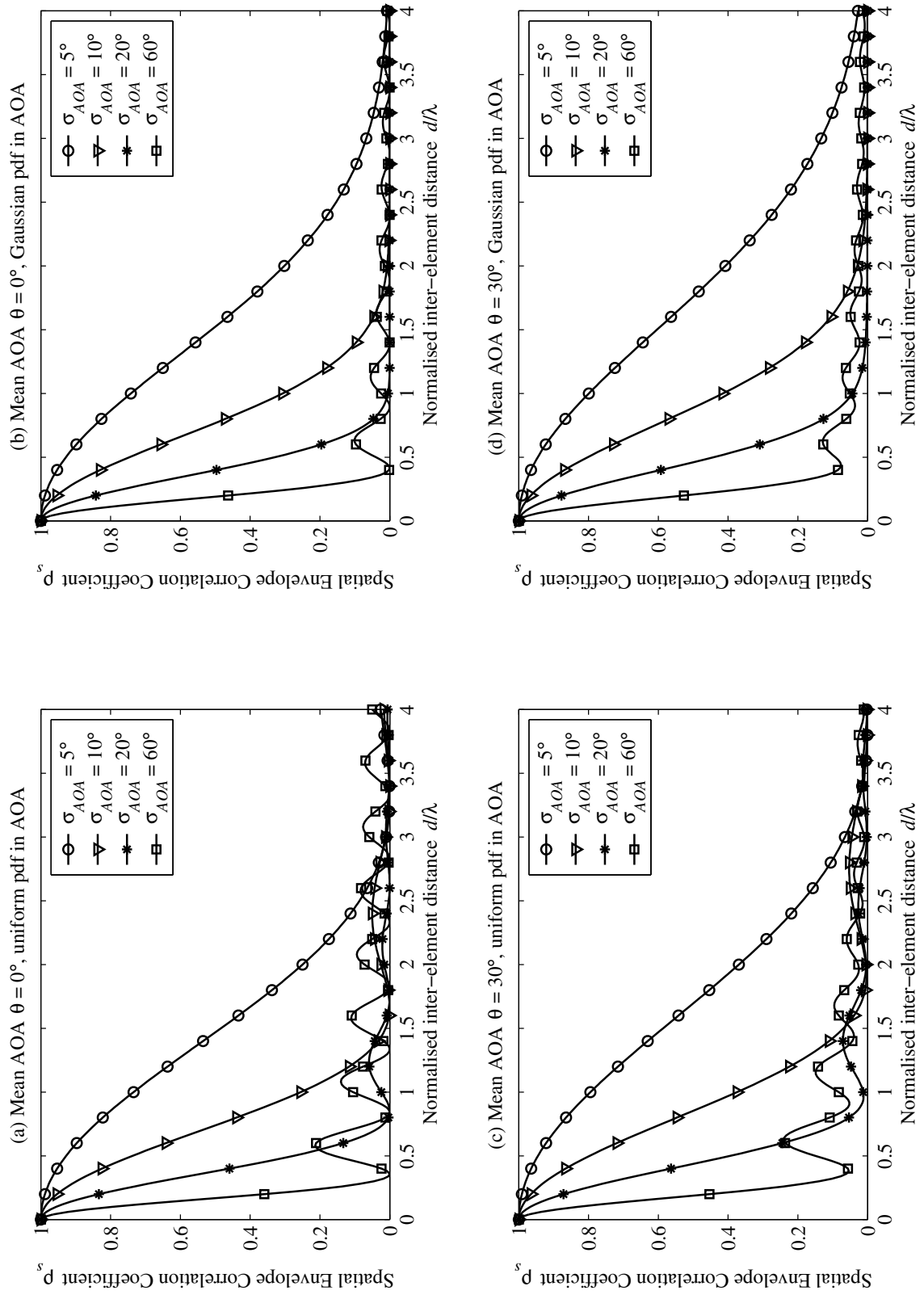

Figure 3.7: Spatial envelope correlation coefficient for mean AOA's $\theta = 0^\circ, 30^\circ$ and angle spreads $\sigma_{AOA} = 5^\circ, 10^\circ, 20^\circ, 60^\circ$ assuming uniform and Gaussian pdf's in AOA respectively.

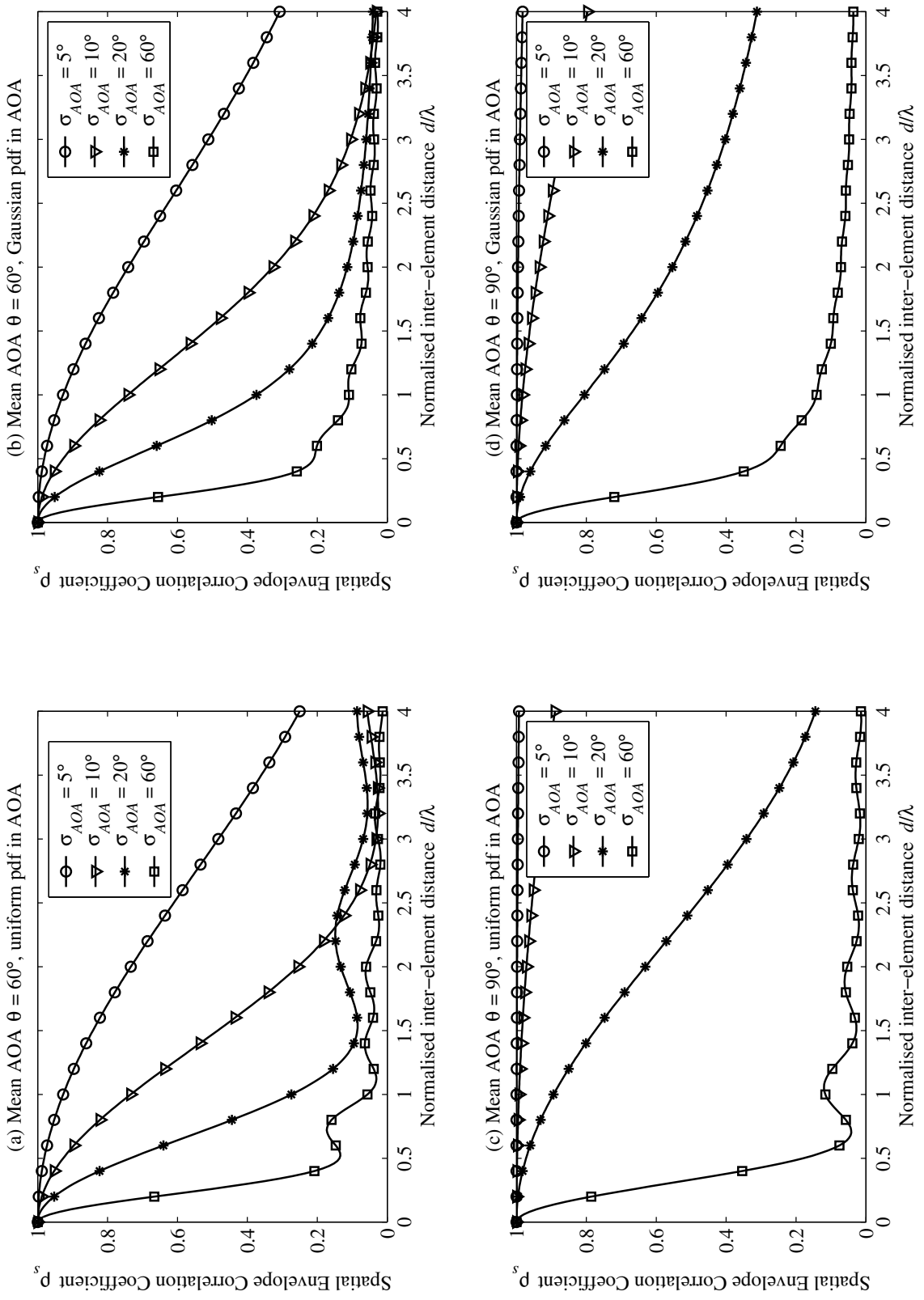

Figure 3.8: Spatial envelope correlation coefficient for mean AOA's $\theta = 60^\circ, 90^\circ$ and angle spreads $\sigma_{AOA} = 5^\circ, 10^\circ, 20^\circ, 60^\circ$ assuming uniform and Gaussian pdf's in AOA respectively.

In the simulations, the mean AOA of the desired user is varied from -60° to 60° with step size $\Delta\theta = 0.01^\circ$ per snapshot to cover the entire azimuth range. This value of the step size is widely used in the simulation studies, for instance [34, 37, 158]. It corresponds to an angular speed of 48 degree/s and provides a worst case scenario for a very fast moving MS at a very close distance to the BS, e.g. an MS travelling at velocity 300 km/hr at only 100 m from the BS. By comparison, when an MS travels at velocity 120 km/hr at a distance of 0.5 km from the BS, this corresponds to an angular speed of only 3.82 degree/s.

It must be noted that effect of mobility (Doppler frequency f_D) on temporal fading characteristics is already taken into account, as explained in Section 3.1.4.

3.2 Channel Response Vector

Following the approach of [71], the temporal and spatial parameters discussed in the previous section can be combined into a single model. As discussed in Section 3.1, it is assumed that the BS is equipped with a ULA of N receive antennas while each MS has a single transmit antenna. The signal received at the BS for the kth user consists of L time delayed multipath replicas of the transmitted signal. The individual paths are defined by their powers, delays and angles of arrival. Each path is itself a superposition of S subpaths. These subpaths arrive at the base station from a random direction $\theta_{k,l}^{(s)} = \theta_k + \vartheta_{k,l}^{(s)}$, where θ_k is the mean AOA and $\vartheta_{k,l}^{(s)}$ is a zero mean random angular deviation with standard deviation σ_{AOA}. The following two cases of Rayleigh and Rician fading are considered:-

3.2.1 Rayleigh Fading

For the case of Rayleigh fading multipaths, the total multiplicative distortion of the lth resolvable path of the kth user at the nth antenna can be given as [71, 116]

$$\begin{aligned} h_{k,l,n}(t) &= \sqrt{\frac{\Omega_{k,l}}{S}} \sum_{s=1}^{S} \left\{ \exp\left[j(\phi_{k,l}^{(s)} + 2\pi f_D t \cos\Psi_{k,l}^{(s)}) \right] \right\} \exp\left[-j\mathcal{K}d(n-1)\sin(\theta_k + \vartheta_{k,l}^{(s)}) \right] \\ &= \sum_{s=1}^{S} \alpha_{k,l}^{(s)} \exp\left[-j\mathcal{K}d(n-1)\sin\theta_{k,l}^{(s)} \right] \end{aligned} \tag{3.23}$$

where $\alpha_{k,l}^{(s)}$ denotes the complex subpath amplitude, $\Omega_{k,l}$ is the mean path power (all S

subpaths associated with the lth multipath have identical powers $\Omega_{k,l}/S$), $\mathcal{K} = 2\pi/\lambda$ is the wave number, d is the inter-element distance, $\phi_{k,l}^{(s)}$ is random phase of each subpath uniformly distributed over $[0, 2\pi]$ and $\Psi_{k,l}^{(s)}$ is the AOD for each subpath relative to the motion of the mobile and is also uniformly distributed over $[0, 2\pi]$.

In vector notation, the spatial signature or channel response vector associated with the lth multipath of the kth user can be expressed by a $N \times 1$ vector as

$$\mathbf{h}_{k,l}(t) = \left[\sum_{s=1}^{S} \alpha_{k,l}^{(s)} \sum_{s=1}^{S} \alpha_{k,l}^{(s)} e^{[-j\mathcal{K}d\sin(\theta_k + \vartheta_{k,l}^{(s)})]} \cdots \sum_{s=1}^{S} \alpha_{k,l}^{(s)} e^{[-j\mathcal{K}d(N-1)\sin(\theta_k + \vartheta_{k,l}^{(s)})]} \right]^T \quad (3.24)$$

The following two special subcases of no angle spread and small angle spread are considered:-

3.2.1.1 No Angle Spread

This subcase is applicable for the case of rural or suburban environments. It is equivalent to the point source or plane wave channel model, which is commonly used when AOA estimation algorithms are used [73]. In this case, $\theta_{k,l}^{(s)} = \theta_k$ and (3.23) can be simplified as follows

$$\begin{aligned} h_{k,l,n}(t) &= \left(\sum_{s=1}^{S} \alpha_{k,l}^{(s)} \right) [\exp(-j\mathcal{K}d(n-1)\sin\theta_k)] \\ &= \alpha_{k,l}(t) \exp[-j\mathcal{K}d(n-1)\sin\theta_k] \end{aligned} \quad (3.25)$$

where $\alpha_{k,l}(t)$ denotes the complex Rayleigh fading coefficient given by

$$\alpha_{k,l}(t) = \sum_{s=1}^{S} \alpha_{k,l}^{(s)} = \sqrt{\frac{\Omega_{k,l}}{S}} \sum_{s=1}^{S} \exp\left[j(\phi_{k,l}^{(s)} + 2\pi f_D t \cos\Psi_{k,l}^{(s)}) \right] \quad (3.26)$$

The channel vector associated with the signal transmitted by the kth user can thus be written as

$$\mathbf{h}_{k,l}(t) = \alpha_{k,l}(t)\, \mathbf{a}(\theta_k) \quad (3.27)$$

where $\mathbf{a}(\theta_k)$ is the $N \times 1$ array steering vector given by (3.15).

3.2.1.2 Moderate Angle Spread

This subcase is applicable to suburban and urban environments with angle spread in the range $5^\circ - 15^\circ$ [57]. For the case of small to moderate angle spread, a Taylor expansion of (3.23) gives [95]

$$\mathbf{h}_{k,l}(t) \approx \alpha_{k,l}\, \mathbf{a}(\theta_k) + \bar{\alpha}_{k,l}\, \mathbf{d}(\theta_k) \tag{3.28}$$

where $\mathbf{a}(\theta_k)$ is the array steering vector and $\mathbf{d}(\theta_k)$ is the gradient of the array steering vector, which for a linear array is given by

$$\begin{aligned} \mathbf{d}(\theta_k) &= \frac{d}{d\theta}\mathbf{a}(\theta_k) \\ &= \left[0 \;\; -j\mathcal{K}d\cos\theta_k\, e^{-j\mathcal{K}d\sin\theta_k} \;\; \cdots \;\; -j\mathcal{K}d(N-1)\cos\theta_k\, e^{-j\mathcal{K}d(N-1)\sin\theta_k}\right]^T \end{aligned} \tag{3.29}$$

and the constants $\alpha_{k,l}$ and $\bar{\alpha}_{k,l}$ are given by

$$\alpha_{k,l} = \sum_{s=1}^{S} \alpha_{k,l}^{(s)} \tag{3.30a}$$

$$\bar{\alpha}_{k,l} = \sum_{s=1}^{S} \alpha_{k,l}^{(s)}\, \vartheta_{k,l}^{(s)} \tag{3.30b}$$

(3.28) shows that for a particular AOA, the time variant channel vector $\mathbf{h}_{k,l}(t)$ can be represented as a linear combination of two time-invariant vectors $\mathbf{a}(\theta_k)$ and $\mathbf{d}(\theta_k)$ and two uncorrelated time-variant weights $\alpha_{k,l}$ and $\bar{\alpha}_{k,l}$. This fact can be used in estimating the channel vector for smart antenna applications [95].

3.2.2 Rician Fading

For the case of Rician fading ($L = 1$), which is relevant to urban micro-cellular areas with a direct LOS component, the channel impulse response for the kth user at the nth antenna is given as [71, 117]

$$h_{k,n}(t) = \sqrt{\frac{K_R}{1+K_R}}\, h_{k,n}^{(LOS)}(t) + \sqrt{\frac{1}{1+K_R}}\, h_{k,n}^{(NLOS)}(t) \tag{3.31}$$

where K_R is the Rician factor given in (3.5) and $h_{k,n}^{(LOS)}(t)$ and $h_{k,n}^{(NLOS)}(t)$ are the specular and scattered components given by

$$h_{k,n}^{(LOS)}(t) = \exp\left[j(\phi_k^{(LOS)} + 2\pi f_D t\cos\theta_k)\right]\exp\left[-j\mathcal{K}d(n-1)\sin\theta_k\right] \quad (3.32)$$

$$h_{k,n}^{(NLOS)}(t) = \frac{1}{\sqrt{S}}\sum_{s=1}^{S}\left\{\exp\left[j(\phi_k^{(s)} + 2\pi f_D t\cos\Psi_k^{(s)})\right]\right\} e^{[-j\mathcal{K}d(n-1)\sin\theta_k]} \quad (3.33)$$

where $\phi_k^{(LOS)}$ is the random phase of the LOS subpath. It can be observed that $h_{k,n}^{(NLOS)}(t)$ is a random process while $h_{k,n}^{(LOS)}(t)$ is deterministic.

3.3 Rayleigh Fading Channel Simulations

The results in this section are obtained by implementing (3.23), using the simulation model developed for the purpose (see Appendix B). The value of $S = 15$ subpaths is used in the simulations. The following cases are considered:-

3.3.1 Single Antenna, Zero Angle Spread

Figure 3.9 shows the magnitude (a) and phase (b) of the simulated channel response for a total time period of 100 ms, assuming a Doppler frequency $f_D = 100$ Hz. The distance covered by the mobile station during this time period is equal to 3.33 m or 10λ. It can be seen that deep fades occur with a periodicity of almost half wavelength. Also the occurrence of deep fades coincides with the rapid jumps in the phase plot.

Figure 3.9 (c) shows the probability density histogram of the channel amplitude. The statistics of the channel amplitude are collected over an extended time period of 2.5 s (corresponding to 250λ). The theoretical Rayleigh probability density function is also shown for comparison. It can be seen that there is a very good match between the simulated and theoretical values. Thus the channel coefficients follow a Rayleigh distribution. Also from Figure 3.9 (d), which shows the plot of the cumulative distribution function of the phase of the channel, it is observed that the phase is well described by a uniform distribution.

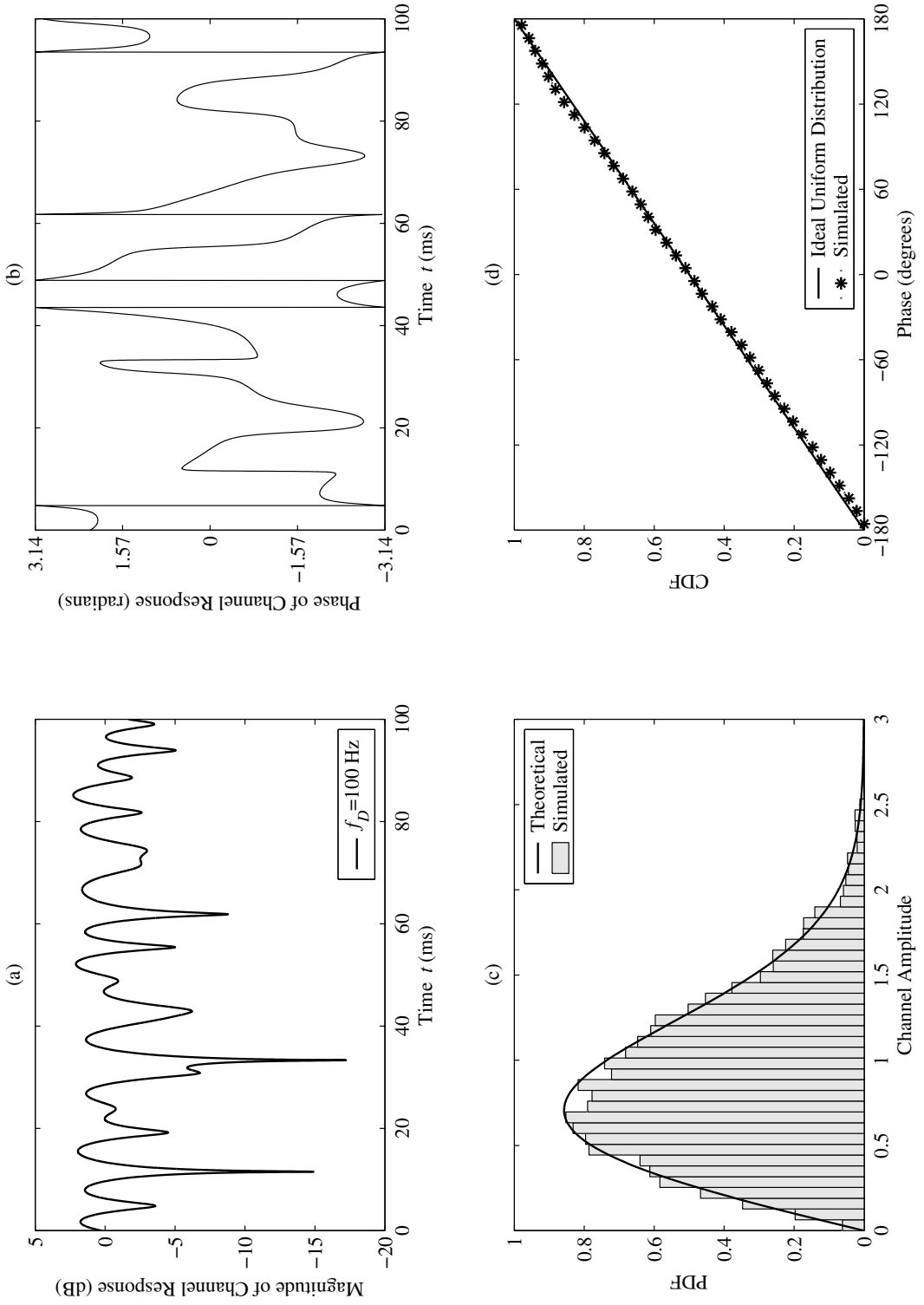

Figure 3.9: Plot of (a) magnitude of channel response (b) phase of channel response (c) probability density function of the channel amplitude and (d) the cumulative distribution function of the channel phase for single antenna assuming Rayleigh fading and Doppler frequency $f_D = 100$ Hz.

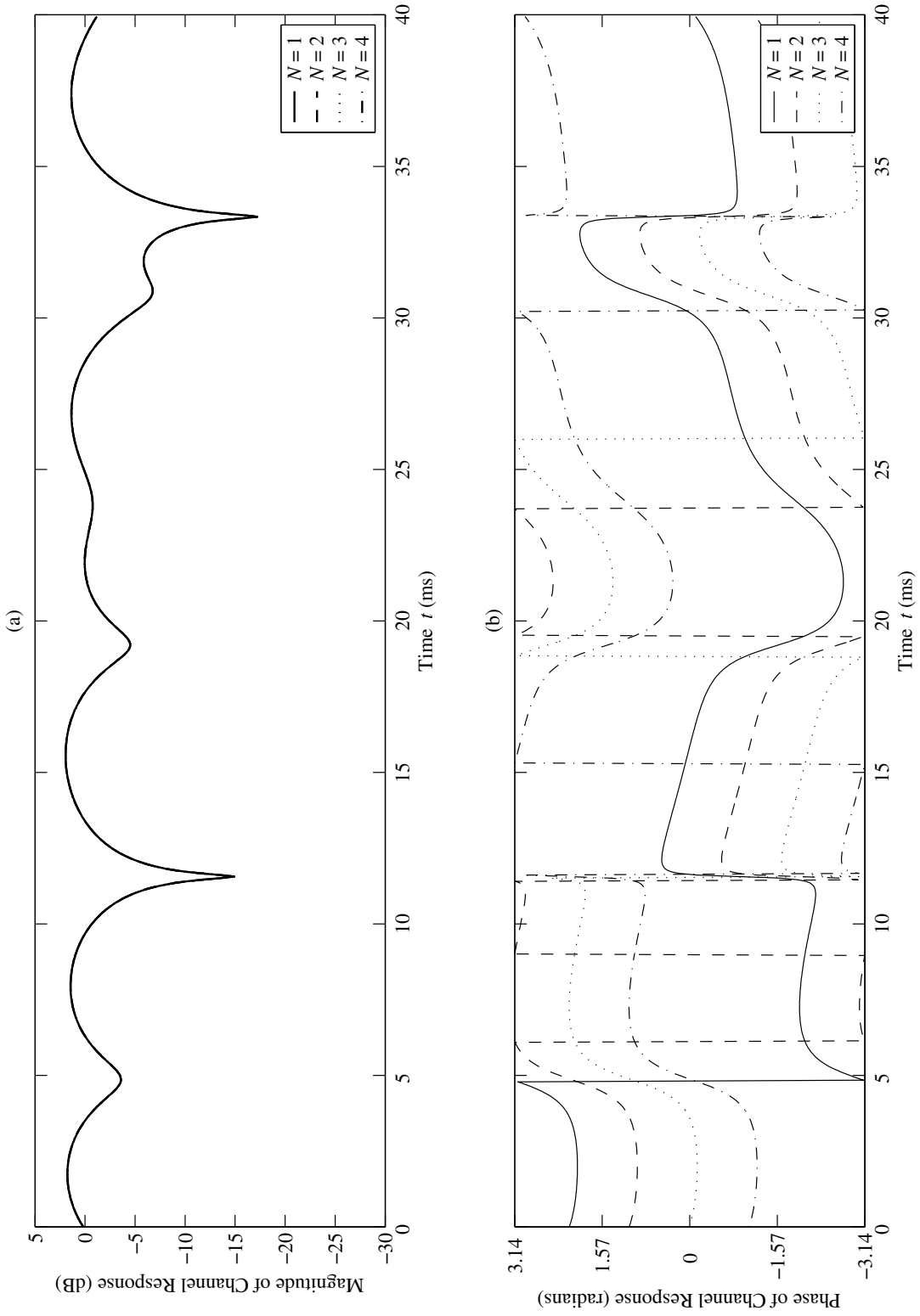

Figure 3.10: Plot of (a) magnitude and (b) phase of channel response for $N = 4$ antenna elements with inter-element spacing $d = \lambda/2$ assuming Rayleigh fading, mean AOA $\theta = 20^\circ$, Doppler frequency $f_D = 100$ Hz and no angle spread.

3.3.2 Array Antennas with Zero Angle Spread

Figures 3.10 show the plots of (a) magnitude and (b) phase respectively of channel response for $N = 4$ ULA antenna with inter-element spacing $d = \lambda/2$, AOA $\theta = 20^\circ$ and Doppler frequency $f_D = 100$ Hz. It is observed that the channel coefficients at different antennas have the same magnitude (overlapping plots) and differ only by a phase shift that is related to the angle of arrival of the plane wave relative to the array.

3.3.3 Array Antennas with Angle Spread

Next the general case of non-zero angle spread is considered. Figure 3.11 shows the magnitude of the channel response for $N = 4$ linear array antenna with uniform inter-element spacing $d = \lambda/2$, mean AOA $\theta = 0^\circ$, Doppler frequency $f_D = 100$ Hz and different angle spreads assuming Gaussian pdf in AOA respectively. From the figure it is clear that as the value of angle spread increases, there is spatial fading across the array. Thus as angle spread increases, the channel coefficients become increasingly uncorrelated.

To illustrate this further, the magnitude of the channel response is plotted as a function of both space and time. Figures 3.12 and 3.13 show the channel magnitude response across a $N = 8$ ULA with inter-element spacing $d = \lambda/2$, over a period of 40 ms with Doppler frequency $f_D = 100$ Hz and angle spread $\sigma_{AOA} = 0^\circ$ and 10° respectively. For the case of zero angle spread, it can be seen that at any particular time instant, the signal level is the same across the array. This is because with zero angle spread, all the subpaths contributing to the received signal level at the array arrive from the same direction and have the same relative phase at different points across the array and therefore all add up either constructively or destructively [87]. This produces time selective fading only. For the case of angle spread $\sigma_{AOA} = 10^\circ$, Figure 3.13 reveals that for any given time instant, the signal level across the array varies. In this case, different subpaths contributing to the received signal arrive from different directions and their relative phase shifts are different, and therefore, they add up either constructively or destructively at each point across the array depending on the relative phase relationship [87]. This produces space-time selective fading. As σ_{AOA} increases, the signal level across the array varies more rapidly.

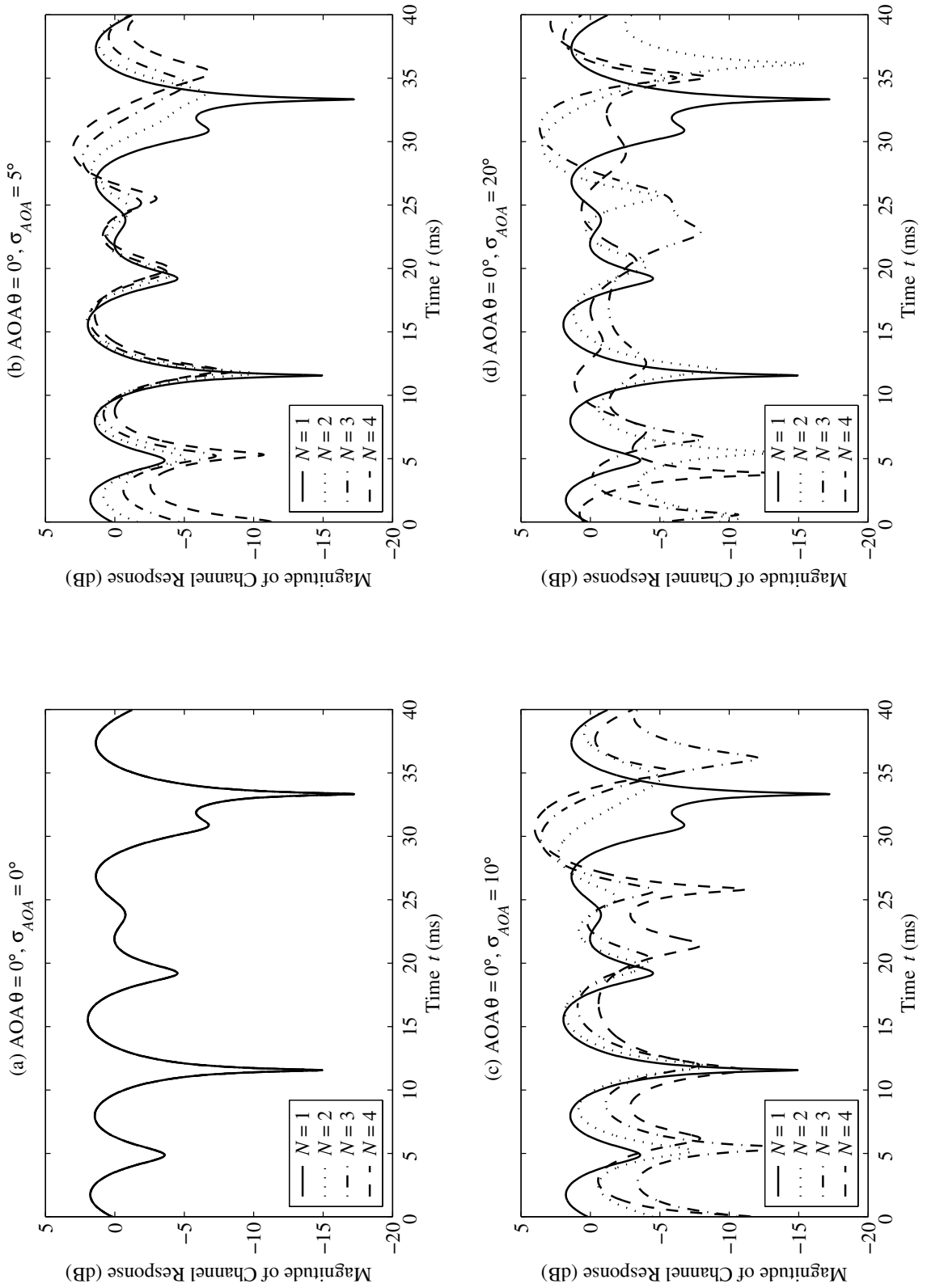

Figure 3.11: Channel magnitude response for $N = 4$ antenna elements with inter-element spacing $d = \lambda/2$ assuming Rayleigh fading, Gaussian pdf in AOA, mean AOA $\theta = 0^\circ$ and angle spreads $\sigma_{AOA} = 0^\circ, 5^\circ, 10^\circ, 20^\circ$ respectively.

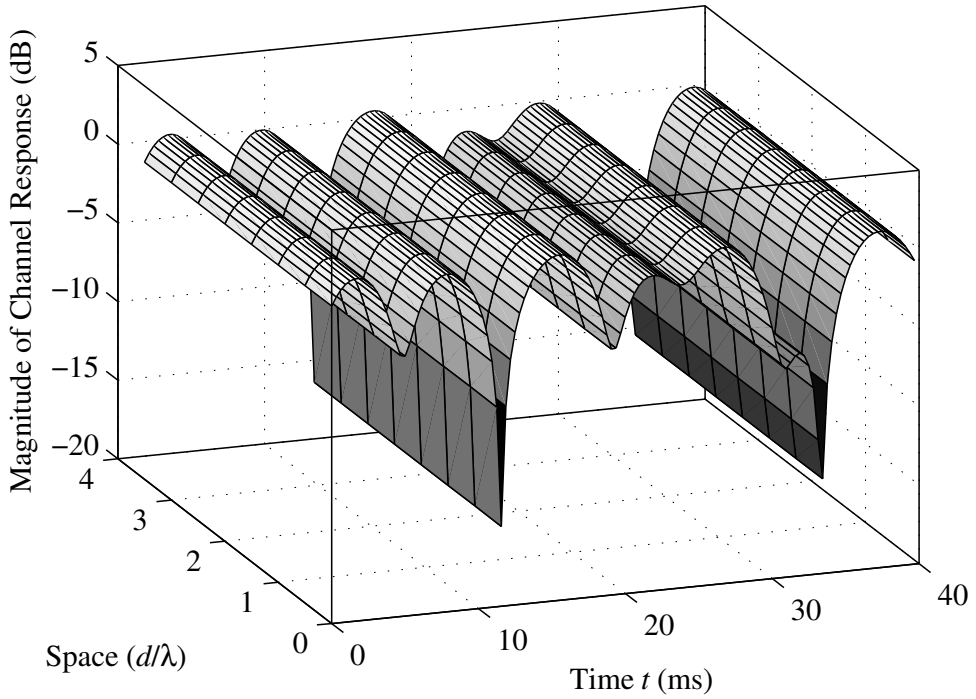

Figure 3.12: Space-time fading: $N = 8$ antenna elements, $d = \lambda/2$, Doppler frequency $f_D = 100$ Hz and angle spread $\sigma_{AOA} = 0^\circ$.

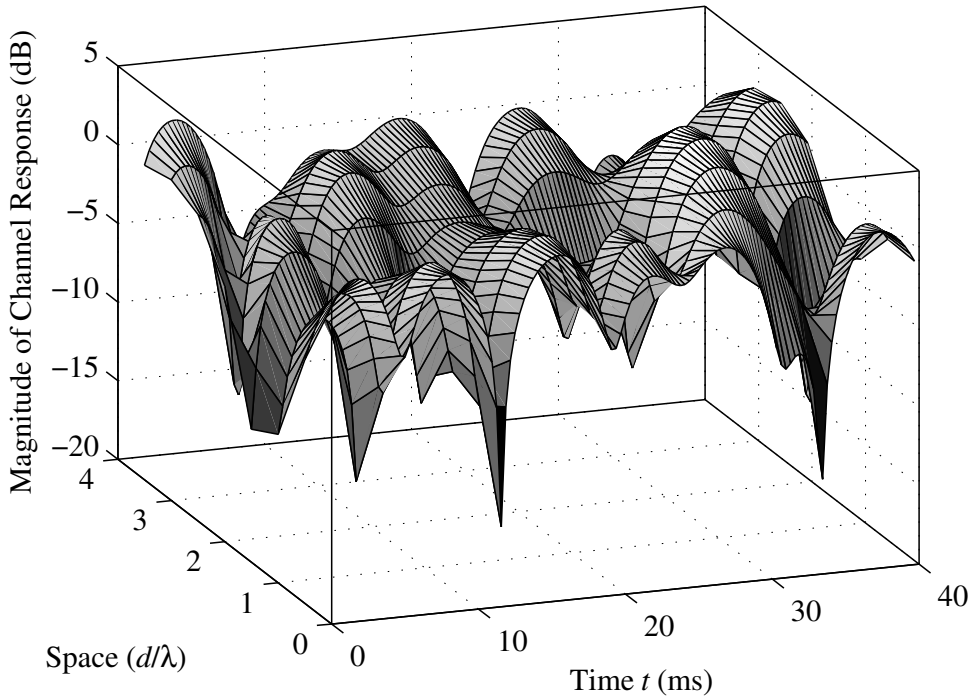

Figure 3.13: Space-time fading: $N = 8$ antenna elements, $d = \lambda/2$, Doppler frequency $f_D = 100$ Hz and angle spread $\sigma_{AOA} = 10^\circ$.

3.4 Rician Fading Channel Simulations

The results in this section are obtained by implementing (3.31), using the simulation model developed for the purpose (see Appendix B). The value of $L = 1$ path is used in the simulations. The following cases are considered:-

3.4.1 Effect of Rice Factor

Figure 3.14 shows the magnitude of the channel response with Rician fading for a total time period of $t = 200$ ms and different Rician factors $K_R = -\infty, 1, 5, 7, 10$ (dB) respectively. The curve for $K_R = 0$ ($-\infty$ dB) corresponds to the case of Rayleigh fading. From the figure, it is clear that as K_R increases, the probability of encountering deep fades is reduced. Thus a Rician channel is a more 'friendly' channel while the Rayleigh case represents a 'worst-case' mobile channel, as the signal fading is more severe with deeper and more frequent nulls.

3.4.2 Distribution of Channel Coefficients

Figure 3.15 shows the probability density histograms of the channel amplitude for $K_R = -\infty, 1, 5, 10$ dB respectively. The statistics of the channel amplitudes are collected over an extended time period of 2.5 s (corresponding to 250λ). The theoretical Rice probability density functions are also shown for comparison. It can be observed that there is a very good match between the simulated and theoretical values. This result indicates that the proposed model is able to accurately simulate Rician fading characteristics.

3.5 Summary

This chapter has presented a new parameterized physical channel model for use in performance evaluation of smart antennas. The proposed model includes the temporal and spatial propagation processes such as MS mobility, azimuth angle of arrival, angle spread and Doppler frequency which are of critical importance for smart antenna systems. A mathematical formulation of the channel model has also been presented, along with the

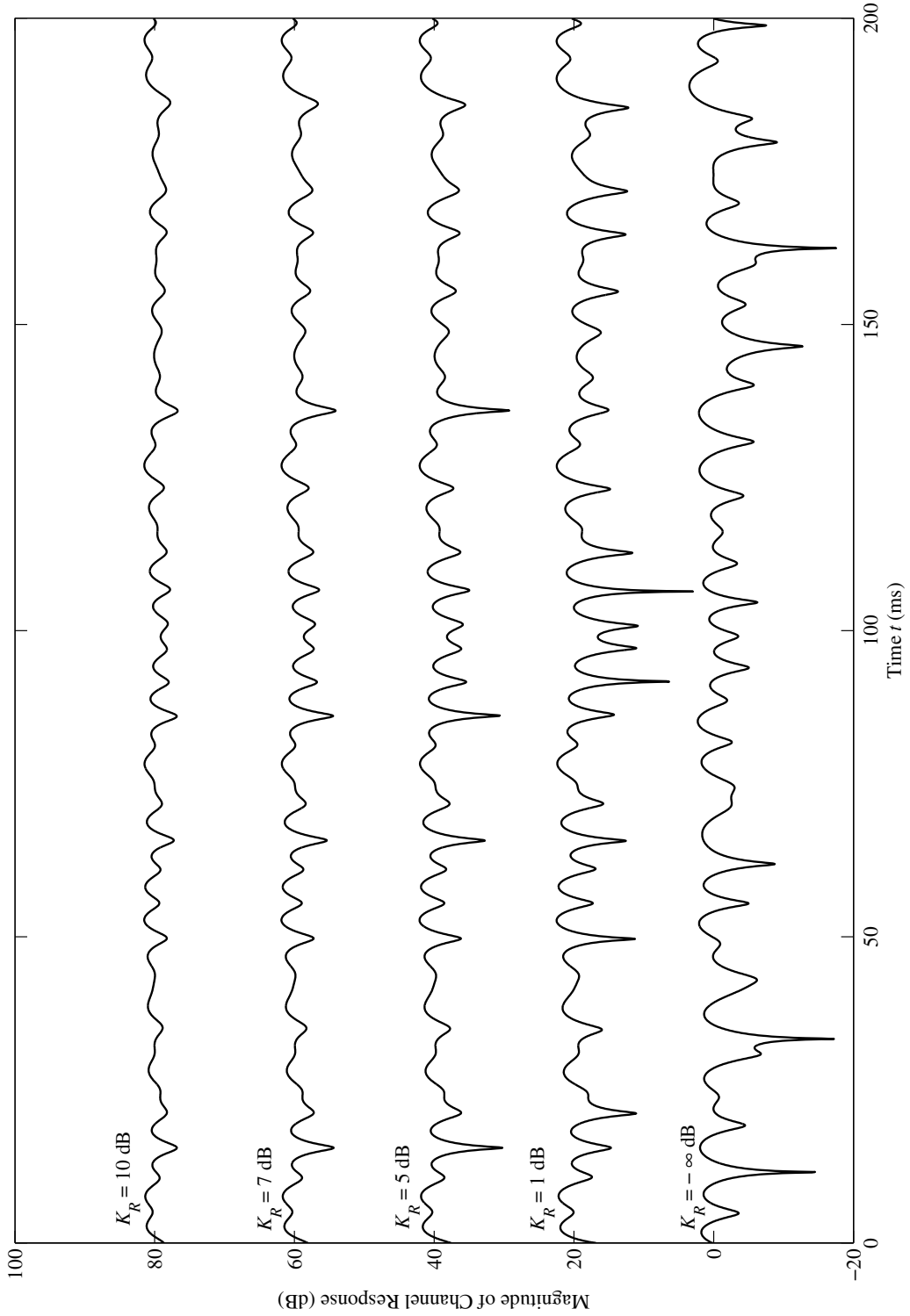

Figure 3.14: Channel magnitude response for single antenna assuming Rician fading and Rice factors $K_R = -\infty, 1, 5, 7, 10$ dB respectively. Curves are offset upwards by 20 dB for increasing K_R values for clarity.

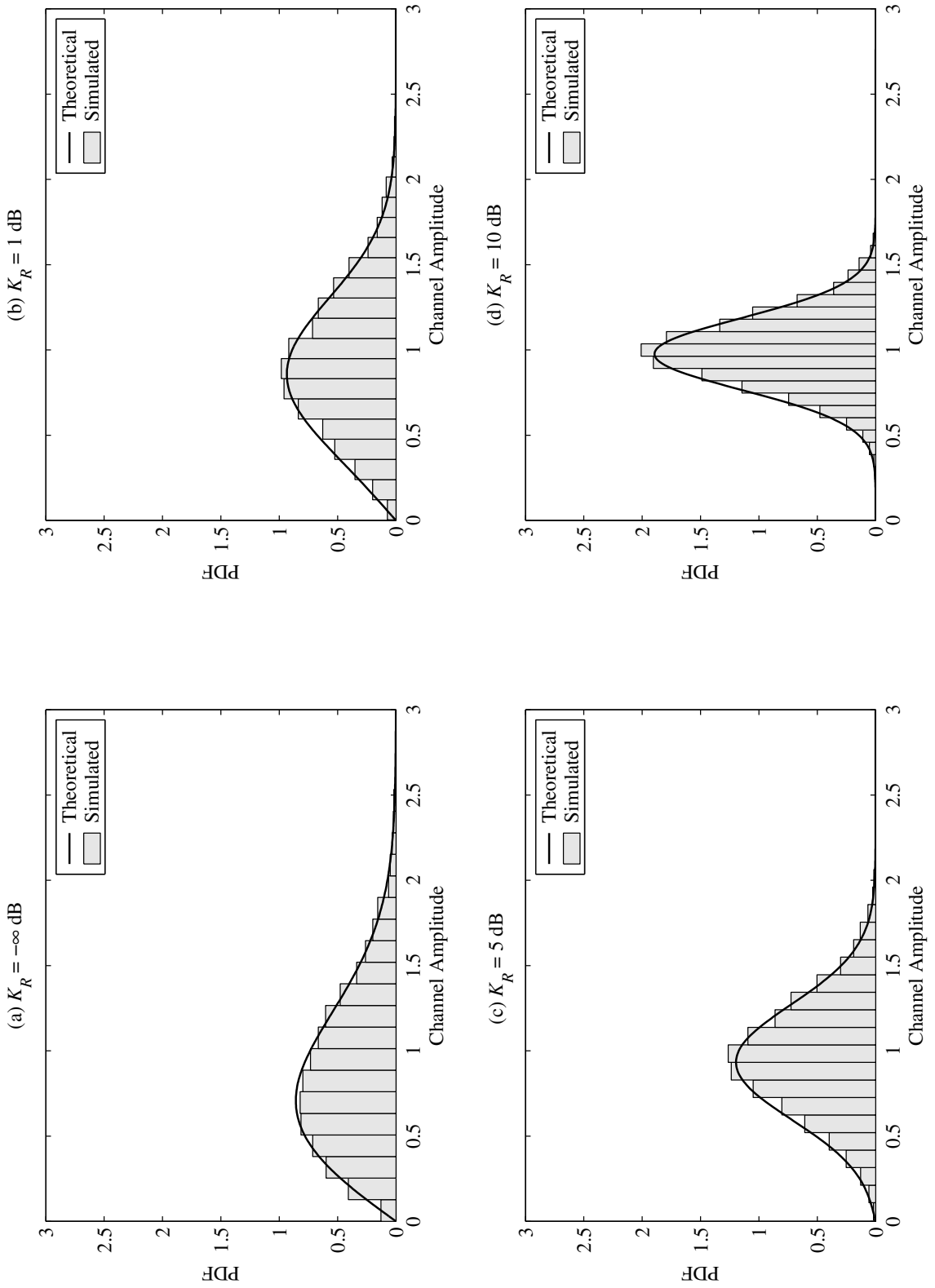

Figure 3.15: The probability density histograms of the channel amplitude assuming Rician fading and Rice factors $K_R = -\infty, 1, 5, 10$ dB respectively.

simulation results. It has been shown that the proposed channel model is able to accurately simulate various Rayleigh and Rician fading scenarios. In addition, it has been shown that angle spread produces spatial fading across the array, affording additional space diversity gain. The proposed channel model is used to analyse and simulate the performance of smart antenna systems in Chapters 4 and 5.

Chapter 4

Performance Evaluation of Smart Antennas for CDMA

In this chapter an analytical model for investigating the mean Bit Error Rate (BER) performance of a Direct Sequence Code Division Multiple Access (DS-CDMA) system employing a smart antenna is described. The DS-CDMA system is assumed to utilise M-ary orthogonal modulation. As mentioned in Chapter 1, this type of modulation has been successfully used in the reverse link of IS-95 CDMA system and is also specified in radio configurations 1 and 2 of the reverse link in cdma2000 standard. The proposed model incorporates the array and channel models developed in Chapters 2 and 3 respectively.

This chapter is organised as follows. The detailed system model is presented in Section 4.1. The smart antenna receiver structure and its different blocks are described in Section 4.2. The analysis results for noncoherent M-ary orthogonal modulation with single antenna, which form the basis of the proposed model, are outlined in Section 4.3. Following this, the analytical model is described in Section 4.4. The simulation assumptions and Monte Carlo simulation strategy employed to simulate the performance of smart antennas are discussed in Section 4.5. Finally, the analytical results are compared with simulation results in Section 4.6 to validate the proposed model.

4.1 System Model

Consider a BS serving a single 120° angular sector. Without loss of generality, it is assumed that the BS employs a Uniform Linear Array (ULA) of N identical omni-directional antenna

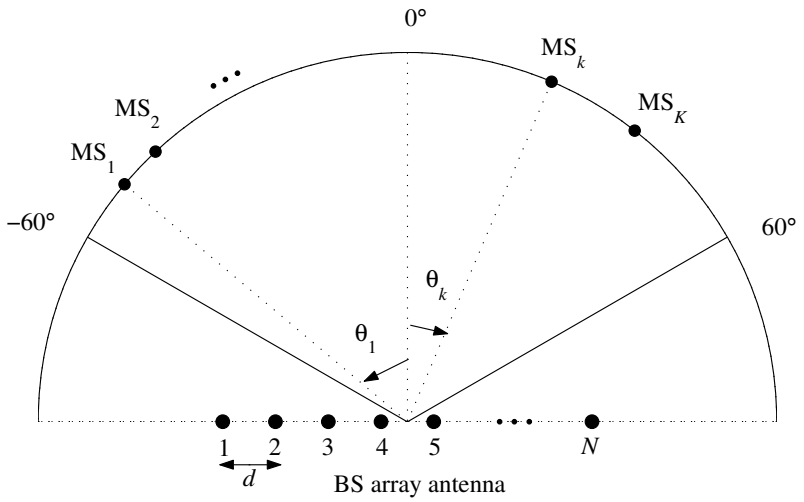

Figure 4.1: Smart antenna BS serving a single 120° angular sector of CDMA system.

elements, with inter-element spacing of $d = \lambda/2$, as shown in Figure 4.1.

Let K denote the total number of active Mobile Stations (MS) in the system, which are randomly distributed in the azimuthal direction, along the arc boundary of the sector cell in the far field of the array. It is assumed that each MS uses M-ary orthogonal modulation [159]. The $k = 1$ user is assumed to be the desired user. For simplicity, an uncoded system is considered i.e. the convolutional encoder and interleaver are ignored. This approach is widely used (see, for instance [30, 34, 82, 83]) as it allows the analysis of wireless communication systems employing multiple antennas. It has to be noted that, in practice, channel coding is an essential component of DS-CDMA wireless communication systems. The signals transmitted by the K users pass through a multipath channel and are received by the BS array antenna. The location of each MS is characterized by its Angle of Arrival (AOA) θ_k, which is conventionally measured from the array broadside.

The BS receiver consists of a two-dimensional (2-D) RAKE receiver [82] with a conventional Maximum Signal to Noise Ratio beamformer [160] followed by an L finger noncoherent RAKE combiner [161]. As mentioned in Chapter 1, the actual beamforming algorithms used to determine the weights fall outside the scope of this thesis. Hence, the ideal solution for the beamforming weight vectors is used. Also the RAKE receiver is assumed to have perfect knowledge of the multipath delays.

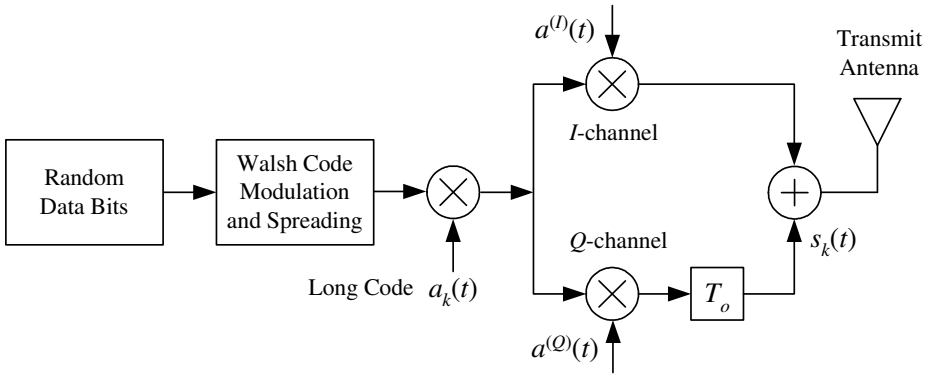

Figure 4.2: Block diagram of mobile station transmitter.

4.1.1 Transmitter Model

The block diagram of the MS transmitter is shown in Figure 4.2, which is adapted from Figure A.1 (see Appendix A). It employs Offset Quadrature Phase Shift Keying (OQPSK) M-ary orthogonal modulation and closely follows the reverse link specifications of the IS-95 CDMA [4, 159]. The transmitted signal $s_k(t)$ of the kth user can be written as [82]

$$s_k(t) = W_k^{(m)}(t)\, a_k^{(I)}(t)\cos(\omega_c t) + W_k^{(m)}(t-T_o)\, a_k^{(Q)}(t-T_o)\sin(\omega_c t) \tag{4.1}$$

where $m = 1, 2, \ldots, M$, $W_k^{(m)}(t)$ is a Hadamard-Walsh function of dimension M which represents the mth orthogonal signal of the kth user, $a_k^{(I)}(t) = a_k(t)\, a^{(I)}(t)$, $a_k^{(Q)}(t) = a_k(t)\, a^{(Q)}(t)$, $a_k(t)$ is the kth user's long code sequence, $a^{(I)}(t)$ and $a^{(Q)}(t)$ are the in-phase and quadrature channel Pseudo-Noise (PN) random sequences respectively, T_o is the half chip delay for OQPSK signals, $\omega_c = 2\pi f_c$ and f_c is the carrier frequency. The transmitted power of each user is assumed unity. This reflects the assumption of perfect power control. To simplify the analysis, the PN codes are represented by [77]

$$a_k^{(I)}(t) = \sum_{r=-\infty}^{\infty} a_{k,r}^{(I)}(t)\, p(t - T_c) \tag{4.2}$$

$$a_k^{(Q)}(t) = \sum_{r=-\infty}^{\infty} a_{k,r}^{(Q)}(t)\, p(t - T_c) \tag{4.3}$$

where $a_{k,r}^{(I)}$ and $a_{k,r}^{(Q)}$ are assumed to be independent and identically distributed (i.i.d.) random variable taking values ± 1 with equal probability and $p(t)$ is the chip pulse shape, which is assumed to be rectangular.

Re-writing the transmitted signal in (4.1), we get

$$\begin{aligned} s_k(t) &= \Re\left\{[W_k^{(m)}(t)\,a_k^{(I)}(t) + j\,W_k^{(m)}(t-T_o)\,a_k^{(Q)}(t-T_o)]\,e^{-j\omega_c t}\right\} \\ &= \Re\{\tilde{s}_k(t)\,e^{-j\omega_c t}\} \end{aligned} \tag{4.4}$$

where $\tilde{s}_k(t) = s_k^{(I)}(t) + j\,s_k^{(Q)}(t)$ is the complex low pass equivalent of the transmitted signal. The two representations are equivalent [162] and are used interchangeably in this chapter.

4.1.2 Channel Model

The *k*th user's signal propagates through a multipath fading channel with Angle of Arrival (AOA) θ_k. Using the channel model presented in Chapter 3, the complex lowpass equivalent representation of the channel impulse response between the *l*th multipath of the *k*th user and the *n*th element of the array antenna is given by

$$\begin{aligned} \tilde{h}_{k,l,n}(t) &= \beta_{k,l}\,e^{-j(\phi_{k,l}+2\pi\frac{d}{\lambda}(n-1)\sin\theta_k)}\delta(t-\overline{\tau}_{k,l}) \\ &= \beta_{k,l}\,e^{-j\varphi_{k,l,n}}\delta(t-\overline{\tau}_{k,l}) \end{aligned} \tag{4.5}$$

where $\beta_{k,l}$, $\phi_{k,l}$ and $\overline{\tau}_{k,l}$ are the path gain, phase and delay respectively, $\varphi_{k,l,n}$ is the overall phase which includes the path phase and the difference in propagation delays between the antennas and λ is the wavelength. The path gains are assumed to follow the Rayleigh or the Rician distributions respectively. It is also assumed that the multipath channel parameters $\beta_{k,l}(t)$ and $\varphi_{k,l,n}(t)$ remain constant for the duration of a Walsh symbol [77]. Therefore, $\beta_{k,l}(t) = \beta_{k,l}$ and $\varphi_{k,l,n}(t) = \varphi_{k,l,n}$ for $t \in [0, T_w]$, where T_w is Walsh symbol period.

4.1.3 Received Signal

Following [77], the total received signal at the *n*th antenna element can be written as

$$\begin{aligned} x_n(t) &= \sum_{k=1}^{K}\sum_{l=1}^{L}\Re\{[\tilde{s}_k(t-\Gamma_k) * \tilde{h}_{k,l,n}(t)]\,e^{-\omega_c t}\} + \eta(t) \\ &= \sum_{k=1}^{K}\sum_{l=1}^{L}\Big[\beta_{k,l}\,W_k^{(m)}(t-\tau_{k,l})\,a_k^{(I)}(t-\tau_{k,l})\cos(\omega_c t + \varphi_{k,l,n}) \\ &+ \beta_{k,l}\,W_k^{(m)}(t-T_o-\tau_{k,l})\,a_k^{(Q)}(t-T_o-\tau_{k,l})\sin(\omega_c t + \varphi_{k,l,n})\Big] + \eta_n(t) \end{aligned} \tag{4.6}$$

where $s_k(t)$ is the signal transmitted by kth user given in (4.1), $\tau_{k,l} = \Gamma_k + \bar{\tau}_{k,l}$, Γ_k is the random delay of the kth user due to the asynchronous nature of the CDMA system and $\eta(t)$ is the Additive White Gaussian Noise (AWGN). The noise may be represented in terms of its lowpass equivalent by

$$\eta(t) = \Re\{\tilde{\eta}(t)\, e^{-j\omega_c t}\} \tag{4.7}$$

where $\tilde{\eta}(t) = \eta^{(I)}(t) + j\eta^{(Q)}(t)$ and $\eta^{(I)}(t)$ and $\eta^{(Q)}(t)$ are the in-phase and quadrature components of $\eta(t)$.

4.2 Smart Antenna Receiver Model

The functional block diagram of the smart antenna receiver is shown in Figure 4.3, which is adapted and simplified from [82]. It has a Two-Dimensional (2-D) RAKE structure where the multipath components are tracked in both time and space. From the figure, the following main blocks can be identified (i) array antenna, (ii) PN despreading, (iii) beamforming and (iv) Walsh correlation and demodulation. The function and modelling of these blocks is explained below.

4.2.1 Extraction of Quadrature Components

The first step for the receiver is to obtain the quadrature components at each antenna. This is achieved by multiplying the received waveforms by $\cos(\omega_c t)$ and $\sin(\omega_c t)$ respectively and then lowpass filtering to remove the double frequency components that result from multiplication [159]. The output of the I-channel and Q-channel lowpass filters can be written as

$$\begin{aligned} x^{(I)}_{k,l,n}(t) &= \left[x_{k,l,n}(t)\cos(\omega_c t)\right]_{LPF} \\ &= \Big\{\beta_{k,l}\, W^{(m)}_k(t-\tau_{k,l})\, a^{(I)}_k(t-\tau_{k,l})\,\frac{\cos\varphi_{k,l,n}}{2} \\ &\quad + \beta_{k,l}\, W^{(m)}_k(t-T_o-\tau_{k,l})\, a^{(Q)}_k(t-T_o-\tau^{k,l})\,\frac{\sin\varphi_{k,l,n}}{2}\Big\} + \frac{\eta^{(I)}(t)}{2} \end{aligned} \tag{4.8}$$

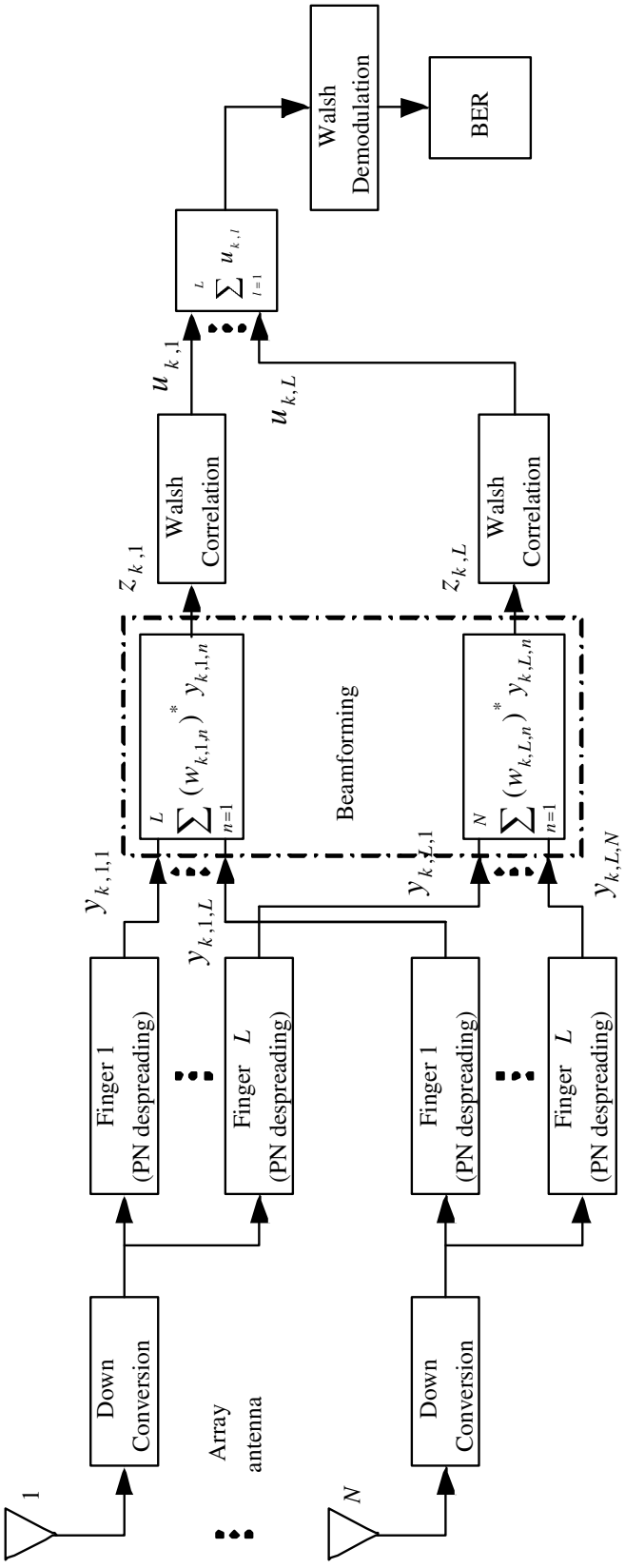

Figure 4.3: Block diagram of smart antenna receiver.

$$
\begin{aligned}
x_{k,l,n}^{(Q)}(t) &= \left[x_{k,l,n}(t)\sin(\omega_c t)\right]_{LPF} \\
&= \left\{\beta_{k,l}\, W_k^{(m)}(t-\tau_{k,l})\, a_k^{(Q)}(t-T_o-\tau_{k,l})\,\frac{\cos\varphi_{k,l,n}}{2}\right. \\
&\quad \left. -\beta_{k,l}\, W_k^{(m)}(t-T_o-\tau_{k,l})\, a_k^{(I)}(t-\tau_{k,l})\,\frac{\sin\varphi_{k,l,n}}{2}\right\} + \frac{\eta^{(Q)}(t)}{2}
\end{aligned} \tag{4.9}
$$

Using the quadrature components, the complex lowpass equivalent of the received signal can be written as

$$
\tilde{x}_{k,l,n}(t) = x_{k,l,n}^{(I)}(t) + j\, x_{k,l,n}^{(Q)}(t) \tag{4.10}
$$

4.2.2 Despreading for Noncoherent Detection

After filtering, each resolvable path is then detected by one of the RAKE fingers immediately following the radio-frequency stages. To detect the lth path, the signal is despread using the sequence of the respective mobile and synchronized to the delay of the lth path. Additionally, the cross-correlation of the I and Q channels is found in order to noncoherently combine the signals. Thus the in-phase signal is also correlated with the quadrature arm and an equivalent operation performed for the quadrature signal, as shown in Figure 4.4 [159]. This process can be mathematically represented as follows.

Let the complex lowpass equivalent of the post PN-despread signal $\tilde{y}_{k,l,n}(t)$ be given as

$$
\tilde{y}_{k,l,n}(t) = y_{k,l,n}^{(I)}(t) + j\, y_{k,l,n}^{(Q)}(t) \tag{4.11}
$$

Denoting the despreading sequences as $\tilde{a}(t) = [a_k^{(I)}(t-\tau_{k,l}) + j\, a_k^{(Q)}(t-T_o-\tau_{k,l})]$ [107, 163], the quadrature components of $\tilde{y}_{k,l,n}$ can be written as

$$
\begin{aligned}
y_{k,l,n}^{(I)}(t) &= \Re\left\{\left(\tilde{a}(t), \tilde{x}_{k,l,n}(t)\right)\right\} \\
&= x_{k,l,n}^{(I)}(t)\, a_k^{(I)}(t-\tau_{k,l}) + x_{k,l,n}^{(Q)}(t)\, a_k^{(Q)}(t-T_o-\tau_{k,l}) \qquad (4.12) \\
y_{k,l,n}^{(Q)}(t) &= \Im\left\{\left(\tilde{a}(t), \tilde{x}^{k,l,n}(t)\right)\right\} \\
&= x_{k,l,n}^{(I)}(t)\, a_k^{(Q)}(t-T_o-\tau_{k,l}) - x_{k,l,n}^{(Q)}(t)\, a_k^{(I)}(t-\tau_{k,l}) \qquad (4.13)
\end{aligned}
$$

where $(a,b) = a \cdot b^*$ denotes the dot product between the complex numbers.

The post PN-despread signals can be written in vector notation as

$$
\mathbf{y}_{k,l} = \left[\, y_{k,l,1}\ y_{k,l,2}\ \cdots\ y_{k,l,N}\,\right]^T \tag{4.14}
$$

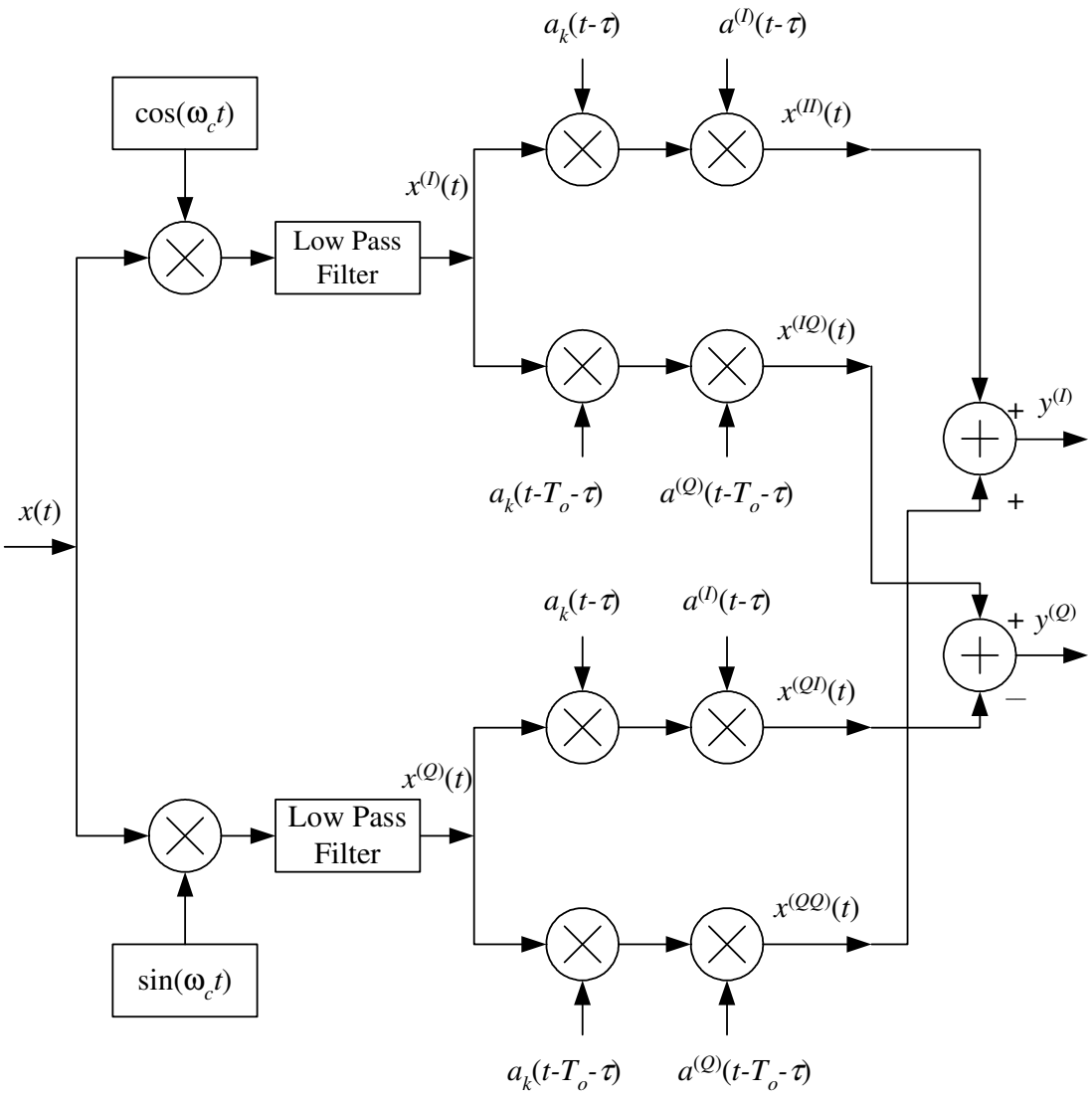

Figure 4.4: Despreading for noncoherent detection of M-ary orthogonal modulation.

4.2.3 Beamforming

A beamformer is then constructed for each resolvable multipath and the signal after PN despreading is combined by the beamformer. In the beamforming operation, the signals received by the antenna elements are weighted by complex weights and then summed up. The smart antenna output is given by

$$\tilde{z}_{k,l}(t) = (\mathbf{w}_{k,l})^H \mathbf{y}_{k,l}(t) \quad (4.15)$$

$$= z_{k,l}^{(I)} + j z_{k,l}^{(Q)} \quad (4.16)$$

where $\mathbf{w}_{k,l}$ is the beamforming weight vector given by

$$\mathbf{w}_{k,l} = \left[w_{k,l,1} \;\; w_{k,l,2} \;\; \cdots \;\; w_{k,l,N} \right]^T \quad (4.17)$$

It is assumed that the weights are determined using the Maximum Signal to Noise Ratio (SNR) beamforming criteria [160]. As mentioned in Chapter 1, the actual mechanisms used to determine the weights fall outside the scope of the thesis. Thus the weights are set as $\mathbf{w}_{k,l} = \mathbf{h}_{k,l}$ and these vector channel coefficients are assumed to be perfectly known. This provides the best case system performance.

4.2.4 Walsh Correlation and Demodulation

The next step is the correlation of the smart antenna output with stored replicas of the Walsh functions. This is required to form the decision variable for demodulation. The output of the qth Walsh correlator ($q = 1, 2, \cdots, M$) is given by

$$Z_{k,l}^{(I)}(q) = \frac{1}{T_w} \int_{\tau_{k,l}}^{T_w+\tau_{k,l}} [z_{k,l}^{(I)} W^{(q)}(t - \tau^{k,l}) + z_{k,l}^{(I)} W^{(q)}(t - T_o - \tau_{k,l})]\, dt \quad (4.18)$$

$$Z_{k,l}^{(Q)}(q) = \frac{1}{T_w} \int_{\tau_{k,l}}^{T_w+\tau_{k,l}} [z_{k,l}^{(Q)} W^{(q)}(t - \tau^{k,l}) + z_{k,l}^{(Q)} W^{(q)}(t - T_o - \tau_{k,l})]\, dt \quad (4.19)$$

The decision variable for the lth multipath of the kth user is obtained from the Walsh correlated values as

$$u_{k,l}(q) = \left(Z_{k,l}^{(I)}\right)^2 + \left(Z_{k,l}^{(Q)}\right)^2 \quad (4.20)$$

The overall decision variable is obtained by Equal Gain Combining (EGC) of all the decision variables from the L multipaths as [79]

$$u_k(q) = \sum_{l=1}^{L} u_{k,l}(q) = \sum_{l=1}^{L} \left[\left(Z_{k,l}^{(I)} \right)^2 + \left(Z_{k,l}^{(Q)} \right)^2 \right] \tag{4.21}$$

Finally, the receiver makes a hard decision on the mth symbol of the kth user by using the Maximum Likelihood Criteria rule as

$$\hat{m} = \arg \max_{q=1,\ldots,M} \{u_k(q)\} \tag{4.22}$$

4.3 Probability of Error Analysis for Single Antenna

Before considering the performance of the smart antenna system, discussed in the previous section, the Mean BER performance of the conventional single antenna receiver (i.e. $N = 1$) is examined. The results in this section form the basis of the proposed analytical model, which is presented in the next section.

4.3.1 Variances

Following [77, 79], it can be shown that for a single antenna, the output of the qth Walsh correlator ($q = 1, 2, \cdots, M$) can be written as

$$Z_{k,l}^{(I)}(q) = \begin{cases} \beta_{k,l} \cos \varphi_{k,l} + I_{k,l}^{(I)} + M_{k,l}^{(I)} + N_{k,l}^{(I)} & ;\text{if } q = m \\ I_{k,l}^{(I)} + M_{k,l}^{(I)} + N_{k,l}^{(I)} & ;\text{else} \end{cases} \tag{4.23}$$

$$Z_{k,l}^{(Q)}(q) = \begin{cases} \beta_{k,l} \sin \varphi_{k,l} + I_{k,l}^{(Q)} + M_{k,l}^{(Q)} + N_{k,l}^{(Q)} & ;\text{if } q = m \\ I_{k,l}^{(Q)} + M_{k,l}^{(Q)} + N_{k,l}^{(Q)} & ;\text{else} \end{cases} \tag{4.24}$$

where $N_{k,l}^{(I)}$ and $N_{k,l}^{(Q)}$ denote the noise terms, $M_{k,l}^{(I)}$ and $M_{k,l}^{(Q)}$ denote the MAI terms and $I_{k,l}^{(I)}$ and $I_{k,l}^{(Q)}$ denote the self interference terms.

The Gaussian approximation is used for the noise and interference terms [80]. The Gaussian approximation does not always hold for CDMA analyses. However for large N_c, this approximation has been shown to give reasonable results [164]. Using this approximation, it can be shown that the multiple access interferences terms $M_{k,l}^{(I)}$ and $M_{k,l}^{(Q)}$ can be

modelled as zero mean Gaussian random processes with variance [79]

$$\sigma_M^2 = \frac{E_s}{3N_c} \sum_{k=1}^{K-1} \sum_{l=1}^{L} E[(\beta_{k,l})^2] \tag{4.25}$$

where $E_s = E_b \log_2(M)$ is the symbol energy, E_b is the bit energy and $N_c = T_w/T_c$ is the spreading factor.

$I_{k,l}^{(I)}$ and $I_{k,l}^{(Q)}$ are the respective self interferences due to the desired users own multipaths and can be modelled as zero mean Gaussian random processes with variance [79]

$$\sigma_I^2 = \frac{E_s}{3N_c} \sum_{l=1}^{L-1} E[(\beta_{k,l})^2] \tag{4.26}$$

The noise terms $N_{k,l}^{(I)}$ and $N_{k,l}^{(Q)}$ are mutually independent zero mean Gaussian random processes with variance

$$\sigma_N^2 = \frac{N_o}{2} \tag{4.27}$$

where N_o is the noise PSD.

The decision variable in (4.21) is a sum of squares of two Gaussian random variables, each with variance

$$\begin{aligned} \sigma_T^2 &= \sigma_N^2 + \sigma_I^2 + \sigma_M^2 \\ &= \frac{N_o}{2} + \frac{E_s}{3N_c} \left\{ \sum_{l=1}^{L-1} E[(\beta_{k,l})^2] + \sum_{k=1}^{K-1} \sum_{l=1}^{L} E[(\beta_{k,l})^2] \right\} \end{aligned} \tag{4.28}$$

It is assumed that uniform power delay profile is used to characterize the multipath fading channel and that all users have the same average signal power at the receiver due to perfect power control, i.e. $\Omega_{k,1} = \Omega_{k,2} = \cdots = \Omega_{k,L} = \Omega/L$. Therefore, (4.28) becomes

$$\begin{aligned} \sigma_T^2 &= \frac{N_o}{2} + \frac{E_s}{3N_c} \frac{\Omega}{L} (L-1) + \frac{E_s}{3N_c} \frac{\Omega}{L} (K-1)L \\ &= \frac{N_o}{2} + \frac{E_s}{3N_c} \frac{\Omega}{L} (KL-1) \end{aligned} \tag{4.29}$$

The SINR can thus be written as

$$\rho = \frac{\Omega}{L} \frac{E_s}{2\sigma_T^2} = \frac{\gamma}{1 + \frac{2}{3N_c}\gamma(KL-1)} \tag{4.30}$$

where $\gamma = \frac{\Omega}{L}\frac{E_s}{N_o} = \frac{\Omega}{L}\frac{E_b}{N_o}\log_2(M)$.

4.3.2 Decision Statistics and Error Probability

Using the SINR in (4.30), the BER of the single antenna system can be derived. Following [79], it can be shown that when the desired signal is not present (i.e. $q \neq m$), the decision variable $u_k(q)$ in (4.21) has a chi-square distribution with $2L$ degrees of freedom and its probability density function (pdf) is given by

$$f_{u_k(q)}(z) = \frac{1}{(2\sigma_T^2)^L\,(L-1)!} z^{L-1} \exp\left(-\frac{z}{2\sigma_T^2}\right) \tag{4.31}$$

When the desired signal is present (i.e. $q = m$), the decision variable $u_k(q)$ has a noncentral chi-square distribution with $2L$ degrees of freedom and noncentrality parameter

$$c = E_s \sum_{l=1}^{L} (\beta_{k,l})^2 \tag{4.32}$$

Therefore given the path gains $\beta_{k,l}$, the conditional probability density function of the decision variable $u_k(q)$ is given by

$$f_{u_k(q)}(z|c) = \frac{1}{2\sigma_T^2} \left(\frac{z}{c}\right)^{\frac{L-1}{2}} \exp\left(-\frac{z+c}{2\sigma_T^2}\right) I_{L-1}\left(\frac{\sqrt{zc}}{\sigma_T^2}\right) \tag{4.33}$$

where σ_T^2 is given in (4.29) and $I_{L-1}(\cdot)$ is the modified Bessel function of order $L-1$. The conditioning in (4.33) may be removed using

$$f_{u_k(q)}(z) = \int_0^\infty f_{u_k(q)}(z|c)\; f(c)\, dc \tag{4.34}$$

where $f(c)$ is the pdf of c.

The receiver uses maximum likelihood decision rule and chooses the largest among the decision variables. We assume without loss of generality that $m = 1$, i.e. the first Walsh symbol $W^{(1)}(t)$ is transmitted. Then the probability of symbol error is

$$\begin{aligned} P_M &= 1 - P_c \\ &= 1 - P(u_k(2) < u_k(1), u_k(3) < u_k(1), \ldots, u_k(M) < u_k(1)) \\ &= 1 - \int_0^\infty [P(u_k(2) < z_1 \,|\, u_k(1) = z_1)]^{M-1}\; f_{u_k(1)}(z_1)\, dz_1 \end{aligned} \tag{4.35}$$

where P_c is the probability of correct decision. Finally the corresponding BER can easily be obtained using the relationship [159]

$$P_b^{(\text{1-D})} = \frac{2^{K-1}}{2^K - 1} P_M = \frac{M/2}{M-1} P_M \tag{4.36}$$

The results, obtained by evaluating and simplifying (4.35) for the commonly used Rayleigh and Rician fading distributions, are given below:-

4.3.2.1 Rayleigh Fading

For the case of Rayleigh fading, it can be shown that the mean BER for a conventional one-dimensional (1-D) RAKE receiver (i.e. single antenna without beamforming) with L-fold multipath diversity and Equal Gain Combining (EGC) is given by [159]

$$P_b^{(1\text{-D})} = \frac{M/2}{M-1}\sum_{m=1}^{M-1}\binom{M-1}{m}\frac{(-1)^{m+1}}{(1+m+m\rho)^L}\sum_{l=0}^{m(L-1)}\mathcal{C}_l(m)\binom{L+l-1}{l}\left(\frac{1+\rho}{1+m+m\rho}\right)^l \tag{4.37}$$

where ρ is given in (4.30) and the coefficients $\mathcal{C}_l(m)$ can be computed recursively using [159]

$$\mathcal{C}_l(m) = \begin{cases} \frac{1}{l}\sum\limits_{q=1}^{l}\binom{l}{q}[(m+1)q-l]\,\mathcal{C}_{l-q}(m) & ;\, l \le L-1, \\ \frac{1}{l}\sum\limits_{q=1}^{L-1}\binom{l}{q}[(m+1)q-l]\,\mathcal{C}_{l-q}(m) & ;\, l \ge L-1. \end{cases} \tag{4.38}$$

with $\mathcal{C}_0(m) = 1$ for all m.

For the special case of no multipath diversity (i.e. $L = 1$), (4.37) reduces to

$$P_b^{(1\text{-D})} = \frac{M/2}{M-1}\sum_{m=1}^{M-1}\binom{M-1}{m}\frac{(-1)^{m+1}}{1+m+m\rho}$$

where ρ is given by substituting $L = 1$ in (4.30) and its value is $\rho = \frac{\gamma}{1+\frac{2}{3N_C}\gamma(K-1)}$.

4.3.2.2 Rician Fading

For the case of Rician fading with $L = 1$, it can be shown that the mean BER for a conventional 1-D RAKE receiver (i.e. single antenna without beamforming) is given by [165]

$$P_b^{(1\text{-D})} = \frac{M/2}{M-1}\sum_{m=1}^{M-1}\binom{M-1}{m}\frac{(-1)^{m+1}}{(1+m+m\delta_1)}\exp\left(\frac{-\delta_1}{1+m+m\delta_2}\right) \tag{4.39}$$

where the variables δ_1 and δ_2 are given by

$$\delta_1 = \frac{\rho}{1+\frac{1}{K_R}} \tag{4.40}$$

$$\delta_2 = \frac{\rho}{1+K_R} \tag{4.41}$$

and ρ is given by substituting $L = 1$ in (4.30) and K_R is the Rice factor given in (3.5).

4.4 Probability of Error Analysis for Array Antennas

The performance analysis of CDMA systems with smart antennas can be carried out by following the same approach as outlined in the previous section for the case of the conventional receiver. However, the inclusion of the complex beamformer weights in (4.15) significantly complicates the mathematical analysis. As discussed in Section 1.4.3, various BER approximation techniques have been proposed in order to analyse the mean BER of the CDMA system with smart antennas. In this thesis the BER approximation procedure for generic 2-D RAKE receivers described in [85] is followed.

4.4.1 BER Approximation Procedure

The BER approximation proposes to adapt the single antenna performance bounds (which have been presented in Section 4.3) to array antenna systems. This is achieved by manipulating those terms in the error probability formulas for single antenna receivers that account for the noise and MAI. The following assumptions are made [85, 86, 166]:-

- The interferers are uniformly distributed in the coverage area comprising an angular sector of 120°.
- The interferers are partitioned into two spatial equivalence classes [167] $-$ in-beam and out-of-beam $-$ based on whether their Angles of Arrivals lie inside or outside the beam formed toward the desired user.
- A piece-wise beampattern is used to approximate the actual ULA beampattern. In the pass band (or in-beam) the beampattern is modelled by a triangular function while in the stop-band (or out-of-beam) the beampattern is approximated by a constant attenuation factor representing an average side-lobe level.
- Because of the piece-line approximation, the energy of each in-beam interferer is a random variable uniformly distributed within $[\frac{1}{2}, 1]$ (half power beamwidth region). Hence a correction factor of $\upsilon = 3/4$ (average value) is applied for in-beam interferers.

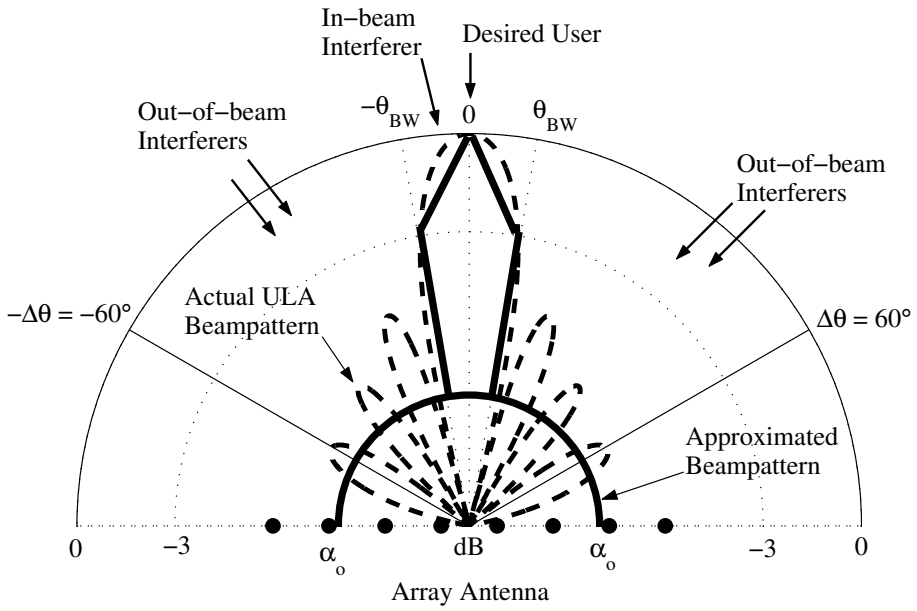

Figure 4.5: Illustration of the beampattern approximation and partitioning of interferers.

- For the purpose of evaluation of the error probability, the in-beam interferers are counted as interference while the out-of-beam users increase the additive noise level.

The beampattern assumption and the partitioning of interferers is illustrated in Figure 4.5.

4.4.1.1 Mathematical Expression for Mean BER

Using the above model, it can be shown that the average bit error probability of a generic 2-D RAKE receiver is given by [85]

$$P_b^{(2\text{-D})} = \sum_{\kappa=0}^{K-1} \chi \xi^{\kappa} \binom{K-1}{\kappa} P_b^{(1\text{-D})} \tag{4.42}$$

where κ denotes the number of in-beam interferers, $(K-\kappa-1)$ is the number of out-of-beam interferer, $P_b^{(1\text{-D})}$ is the probability of bit error for the scalar (single) antenna receiver and χ and the probability of an in-beam interferer ξ, are defined as [85]

$$\xi = \frac{(2\theta_{BW})}{\Delta\theta} \tag{4.43}$$

$$\chi = (1-\xi)^{K-\kappa-1} \tag{4.44}$$

Table 4.1: Equivalent beamforming parameters

Number of antenna elements N	4	6	8
Attenuation α_o (dB)	-12	-14	-16
Beamwidth $2\theta_{BW}$ (degs.)	30°	20°	15°

where $\Delta\theta = 120^\circ$ is the total coverage angle of the sector and $2\theta_{BW}$ is the total beamwidth towards the desired user. The optimized values of equivalent beamforming parameters $2\theta_{BW}$ and α_o used in this work are given in Table 4.1 [85].

(4.42) can be adapted to different receivers depending on the probability of bit error of the scalar receiver. In the next section, this approximation is applied and extended to the case of a 2-D RAKE receiver for CDMA with noncoherent M-ary orthogonal modulation.

4.4.2 Modified Variances

Let the modified variances of the noise, self interference and MAI be denoted as $\bar{\sigma}_N^2$, $\bar{\sigma}_I^2$ and $\bar{\sigma}_M^2$ respectively.

Partitioning the interferers into in-beam and out-of-beam categories, we have

$$\bar{\sigma}_M^2 = \overbrace{\left\{\alpha_o \frac{E_s}{3N_c}\frac{\Omega}{L}(K-\kappa-1)L\right\}}^{\text{out-of-beam}} + \overbrace{\left\{\upsilon\frac{E_s}{3N_c}\frac{\Omega}{L}\kappa L\right\}}^{\text{in-beam}} \tag{4.45}$$

where α_o is the attenuation factor for out-of-beam interferers and $\upsilon = 3/4$ is a correction factor for in-beam interferers.

Since the spatial channel in (4.5) is based on one AOA only, the self interference due to desired user's multipaths cannot be reduced by beamforming. Hence we have $\bar{\sigma}_I^2 = \sigma_I^2$, where σ_I^2 is given in (4.26).

In comparison with the power of the desired signal, the noise power at the output of the antenna array is reduced by N times [37], where N is the number of antenna elements. Hence,

$$\bar{\sigma}_N^2 = \frac{\sigma_N^2}{N} = \frac{\frac{N_o}{2}}{N} \tag{4.46}$$

The modified SINR at the output of the 2-D RAKE receiver is thus given by $\rho = \frac{E_s}{2\bar{\sigma}_T^2}$, where $\bar{\sigma}_T^2 = \bar{\sigma}_N^2 + \bar{\sigma}_I^2 + \bar{\sigma}_M^2$ is the total variance. Substituting the values and simplifying, we get

$$\rho = \frac{\gamma}{\frac{1}{N} + \frac{2\gamma}{3N_c}\left[(L-1) + \alpha_o\,(K-\kappa-1)\,L + \upsilon\,\kappa L\right]} \tag{4.47}$$

where average E_b/N_o of each multipath is $\gamma = \frac{\Omega}{L}\frac{E_s}{N_o} = \log_2(M)\frac{\Omega}{L}\frac{E_b}{N_o}$.

4.4.3 Mean BER

The mean BER of the smart antenna system is given by [85]

$$P_b^{(2\text{-D})} = \sum_{\kappa=0}^{K-1} \chi\,\xi^{\kappa}\binom{K-1}{\kappa} P_b^{(1\text{-D})} \tag{4.48}$$

where $P_b^{(1\text{-D})}$ is given by (4.37) for Rayleigh fading and (4.39) for Rician fading respectively, ρ is given in (4.47), χ and ξ are given in (4.43) and the equivalent beamforming parameters $2\theta_{BW}$ and α_o are given in Table 4.1 [85].

4.5 General Simulation Assumptions

Monte Carlo simulations [168, 169], based on the system model presented in Sections 4.1 and 4.2, are performed to confirm the validity and accuracy of the analytical model presented in Section 4.4. It has to be noted that the analytical model is applicable to both 2G IS-95 CDMA system and 3G cdma2000 system (radio configurations 1 and 2) respectively. However for the purpose of simulations, an uncoded IS-95 CDMA system with alphabet size $M = 64$ and spreading gain $N_c = 256$ is considered for simplicity to reduce the simulation times (see Appendix B). The following assumptions are made with respect to the system parameters:-

- **Cell layout**

  A single 120° angular sector is considered for compatibility with the tri-sectored approach used by most of the current wireless communication systems.

- **Number of users**

  The number of active users K is varied in the range $1-20$. User $K = 1$ is assumed to be the desired user.

- **Frame length**

  A frame length of 576 bits is used. This frame size is consistent with specifications of IS-95 maximum data rate of 9600 bps at the output of the convolutional encoder.

- **Asynchronous user delay**

  The random asynchronous user delay for each interferer is assumed to be uniformly distributed over the interval $[0, T_c]$, where T_c is the chip period. An over-sampling factor of $Q = 4$ is used (i.e. there are 4 samples/chip).

- **Spreading sequences**

  The spreading sequences used are PN random sequences. The characteristic polynomials used for generating the long code PN sequence and the in-phase and the quadrature short code PN sequences are [4]

$$\begin{aligned} a(x) &= x^{42}+x^{35}+x^{31}+x^{27}+x^{26}+x^{25}+x^{22}+x^{21}+x^{19} \\ &+ x^{18}+x^{17}+x^{16}+x^{10}+x^{6}+x^{5}+x^{3}+x^{2}+x+1 \end{aligned} \tag{4.49}$$

$$a^{(I)}(x) = x^{15}+x^{13}+x^{9}+x^{8}+x^{7}+x^{5}+1 \tag{4.50}$$

$$a^{(Q)}(x) = x^{15}+x^{12}+x^{11}+x^{10}+x^{6}+x^{5}+x^{4}+x^{3}+1 \tag{4.51}$$

  The total processing gain of the system is equal to $N_c = 256$.

- **Channel environments**

  The following two distinct operating environments are considered:-

  1. Rician fading with $L = 1$ path. This situation can occur in the case of urban micro cell with LOS propagation.
  2. Rayleigh fading with $L = 1, 2, 3$ multipaths respectively. This situation corresponds to the case of urban or sub-urban macro cell with NLOS propagation. It is assumed that all multipaths fade independently i.e. the effect of correlated fading is not considered.

- **Power delay profile**

  A uniform power delay profile is assumed. The two- and three-ray power delay profiles used in the simulations have been discussed in Section 3.1.5 and are shown specifically in Figure 3.4. The total average multipath power is normalized to one for each user.

- **Doppler frequency**

  The maximum Doppler frequency considered is $f_D = 100$ Hz in all cases. This corresponds to a fast vehicular channel.

- **User locations**

  The desired user is assumed to be located at -60° at the start of the simulation. The desired user then moves with angle change $\Delta\theta = 0.01^\circ$ per snapshot to cover the entire azimuth range $[-60^\circ, 60^\circ]$. The interferers are assumed to be uniformly distributed in angle throughout the sector.

- **User mobility**

  To simulate MS mobility, the snapshot rate is assumed equal to the Walsh symbol rate and the angle change between snapshots is $\Delta\theta = 0.01^\circ$ per snapshot. This value corresponds to a worst case scenario e.g., a fast moving MS at very close distance to the BS and is widely used in the simulation studies, as discussed in Section 3.1.10.

- **Power control**

  All the signals from the K users are assumed to arrive at the BS with the same power level i.e. an ideal power control scenario is assumed.

- **RAKE fingers**

  It is assumed that the 2-D RAKE receiver employs three fingers, i.e. all multipath energy is assumed to be captured by the receiver. Also the multipath delays are assumed to be perfectly estimated by the 2-D RAKE receiver.

- **Adaptive array antenna**

  BS employs a Uniform Linear Array (ULA) of N identical omni-directional antenna elements, with inter-element spacing of $d = \lambda/2$, to receive the signals.

- **Weight vector adaptation**

  The smart antenna weight vector adaptation rate (snapshot rate) is assumed equal to Walsh symbol rate. Also the weight vector is assumed to match perfectly with the channel response vector i.e. the effect of imperfect adaptation is not considered.

The main simulation parameter values, as discussed above, are summarized in Table 4.2.

Table 4.2: Main parameters for smart antenna simulations

Category	Parameter	Description or value
Monte Carlo	Number of drops	$50-100$
	Minimum number of bit errors	100
General	Cellular layout	Single 120° angular sector
	Power control	Ideal
	Channel coding	No
	Oversampling factor	$Q=4$
	Pulse shaping	No
	Detection	Noncoherent
IS-95 CDMA	Chip time	$T_c=\frac{1}{1228800}$ s
	Modulation	OQPSK
	Frame length	20 ms
	Bits/frame	576
	Base station synchronisation	Asynchronous operation
	Spreading codes	Long code and I and Q channel sequences
	Number of users	$K=1-20$
Smart Antenna	Antenna geometry	Uniform linear array
	Number of antenna elements	$N=1,4,6,8$
	Inter-element distance	$d=\lambda/2$
	Element pattern	Omnidirectional
	Angle of Arrival	$-\pi/3\leq\theta\leq\pi/3$
	User motion	0.01° per snapshot
	Smart antenna adaptation	perfect
Multipath Fading Channel	Fading distributions	Rayleigh or Rician
	Number of subpaths	$S=15$
	pdf in AOD	Uniform
	Number of multipaths	$L=1,2,3$
	Power Delay Profile	Uniform (two- and three-path)
	Noise	AWGN
	Doppler frequency	$f_D=100$ Hz

4.5.1 Simulation Strategy

In order to generate performance results that represent an average measure of the cellular system's performance, the following Monte Carlo simulation strategy is adopted:-

- A simulation 'drop' [71] is defined as the transmission and reception of 125 frames, which corresponds to the time required by the desired user to traverse the entire azimuth range $[-60^\circ, 60^\circ]$ with angle change $\Delta\theta = 0.01^\circ$ per snapshot.
- In each simulation run over the variable of interest (e.g. E_b/N_o or K or N), the number of bit errors is collected over a minimum of 50 drops. If the number of bit errors exceeds the specified minimum number of bit errors (i.e. 100 [169]), then the simulation is terminated and the mean BER is calculated. Otherwise, the simulations are continued until at least 100 bit errors have been detected or the number of drops reaches a maximum of $M_c = 100$. This upper limit on the number of drops is imposed to limit the overall simulation time.
- At the beginning of each drop, the desired user's AOA is set to -60°, while the AOA's of the interferers are uniformly randomly distributed over the azimuth sector range. Also the fading parameters for the multipaths are appropriately initialised as discussed in Section 3.1.
- During a drop, the MS's AOA increases or decreases linearly with angle change $\Delta\theta$. Also the channel undergoes fast fading according to the motion of the MS's.

This procedure ensures that the BER performance of the system is averaged over the ensemble of channel parameters and AOA of the multiple users and is not conditioned on a particular spatial or temporal state of the system.

4.6 Results

The analytical results in this section are generated using (4.48) while the simulation results are obtained by using the simulation model developed for the purpose (for details, see Appendix B).

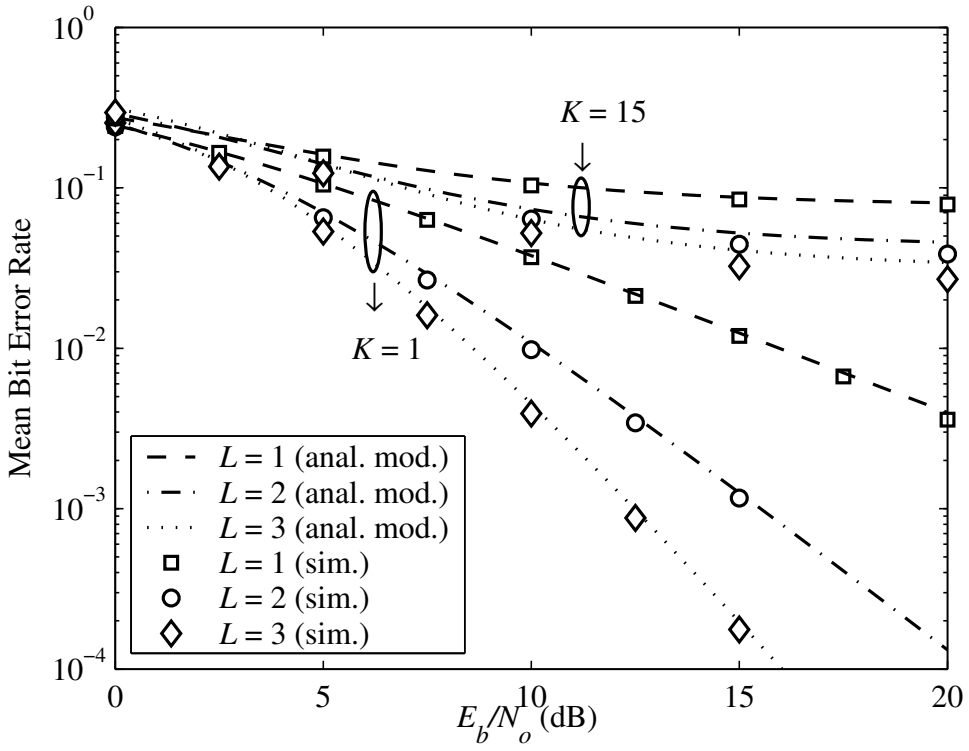

Figure 4.6: Mean BER vs. E_b/N_o for $N = 1$ antenna, assuming $K = 1, 15$ users, $L = 1, 2, 3$ Rayleigh fading paths/user respectively (lines: analytical model, markers: simulations).

4.6.1 Single Antenna

First we take a look at the results for the case of a conventional single antenna receiver. Figure 4.6 shows a plot of Mean BER vs. E_b/N_o for $N = 1$ antenna, assuming $K = 1, 15$ users and $L = 1, 2, 3$ Rayleigh fading paths/user respectively. It can be seen that the simulation results (markers) show good agreement with analytical results (lines). The single antenna results serve as a reference for assessing the impact of smart antennas.

4.6.2 Rician Fading

The next case considered is the performance of smart antenna system, with parameters specified in Table 4.2, operating in a Rician fading environment with $L = 1$.

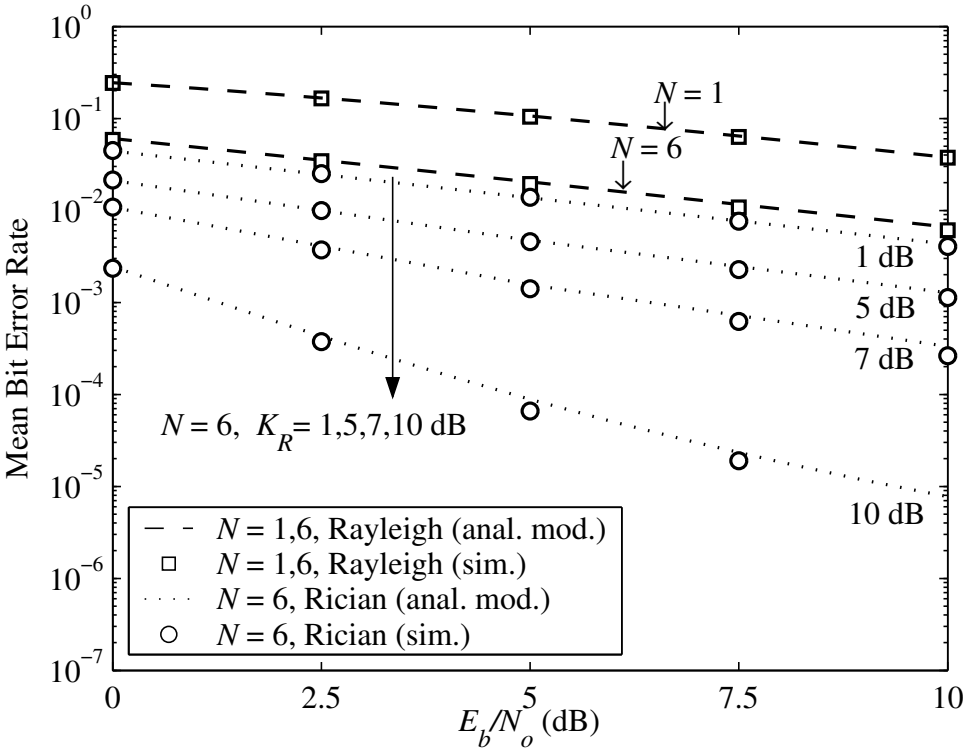

Figure 4.7: Mean BER vs. E_b/N_o (dB) for $N = 6$ antennas, $K = 1$ user, $L = 1$ path/user, assuming Rayleigh and Rician fading channels respectively (lines: analytical model, markers: simulations).

4.6.2.1 Effect of of varying the noise level for single user

Figure 4.7 shows the Mean BER vs. E_b/N_o (dB) for $N = 6$ antennas, $K = 1$ user with single path assuming Rician fading with Rice factor $K_R = 1, 5, 7, 10$ dB respectively. The performance in Rayleigh fading (corresponding to $K_R = -\infty$ dB) and the performance of conventional receiver (i.e. $N = 1$ with no beamforming) are also shown as reference. From this figure, it can be seen that beamforming improves the performance of the system. For low values of Rice factor, the performance is very close to the performance in Rayleigh fading. However for larger Rice factors, there is a tremendous improvement in the Mean BER, e.g. for $E_b/N_o = 5$ dB, a Rician factor of $K_R = 5$ dB improves the BER by a factor of approximately 4 as compared to the case of Rayleigh fading. The simulation results (markers) show excellent agreement with analytical results (lines) for the different combinations of E_b/N_o and Rician factors K_R.

4.6.2.2 Effect of of varying the number of users

Figure 4.8 shows the Mean BER vs. Number of users K for $E_b/N_o = 10$ dB, $N = 6$ antennas, $L = 1$ path/user, assuming Rician fading with different Rice factors. The reference curves for single antenna and Rayleigh fading are also shown in the figure. The figure shows that as the number of users increases, the performance of the system gradually deteriorates. This is to be expected as CDMA systems are interference limited systems. However, as for the case of a single user, there is an improvement in performance with the increase in K_R, e.g. for $K = 15$ users, a Rician factor of $K_R = 5$ dB improves the BER by a factor of approximately 4 over the Rayleigh fading case.The figure shows that the analytical model provides a good match with simulation results for multi-user scenarios as well.

4.6.2.3 Effect of varying the number of antennas in multiple user scenario

Figure 4.9 shows the Mean BER vs. Number of antennas N, for $E_b/N_o = 10$ dB, $K = 15$ users assuming Rician fading with different Rice factors. The figure shows that doubling the number of antennas from 4 to 8 improves the BER by a factor of approximately two only, for values of Rician factor up to 5 dB (e.g. 1.9 for $K_R = -\infty$ dB, 1.9 for $K_R = 1$ dB and 2.2 for $K_R = 5$ dB). However, for higher values of Rician factors the order of BER improvement is greater than two, depending upon the value of K_R (e.g. 2.9 for $K_R = 7$ dB and 5.4 for $K_R = 10$ dB). This observation is of value in the planning of smart antenna structures for urban micro cellular areas. It can also be seen again that the simulation results show excellent agreement with the analytical results for the different combinations of number of antennas N and Rician factors K_R.

4.6.3 Rayleigh Fading

Finally, the performance of the smart antenna system in Rayleigh fading multipath environment is examined.

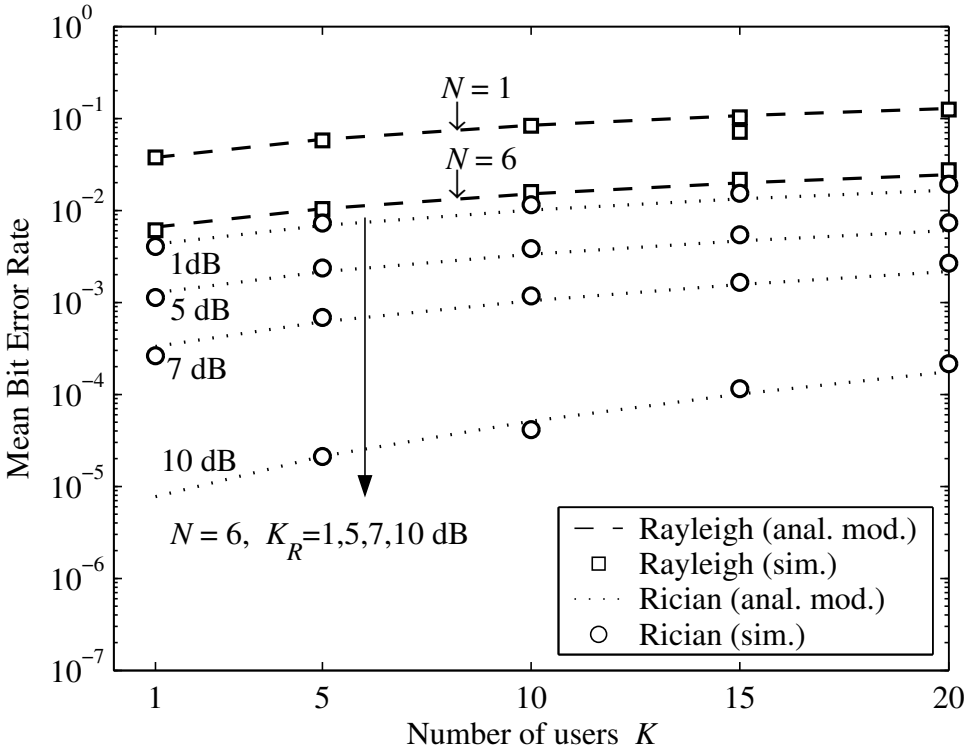

Figure 4.8: Mean BER vs. Number of users K for $E_b/N_o = 10$ dB, $N = 6$ antennas, $L = 1$ path/user, assuming Rayleigh and Rician fading channels respectively (lines: analytical model, markers: simulations).

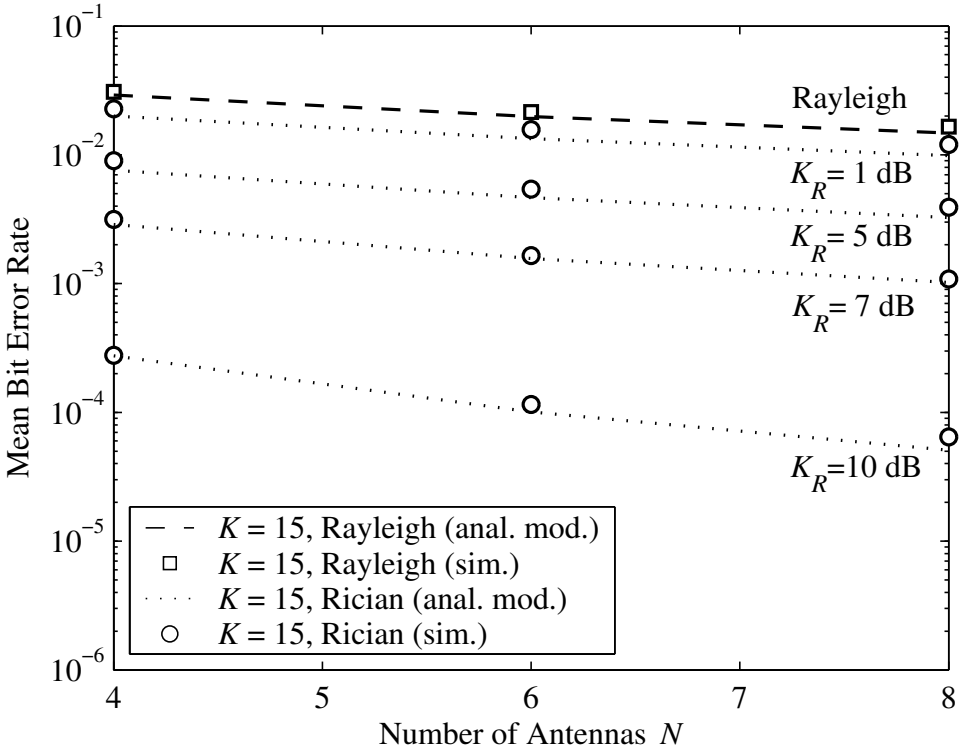

Figure 4.9: Mean BER vs. Number of antennas N, for $E_b/N_o = 10$ dB, $K = 15$ users, $L = 1$ path/user, assuming Rayleigh and Rician fading channels respectively (lines: analytical model, markers: simulations).

4.6.3.1 Effect of varying the number of users

Figure 4.10 shows the Mean BER vs. Number of users K for $E_b/N_o = 10$ dB, assuming $L = 1,2$ Rayleigh fading multipaths and $N = 1,4,6,8$ antennas respectively. Comparing with the reference curves for single antenna ($N = 1$), it is clear that beamforming improves the performance of the system considerably, e.g. for $K = 20$ users and $L = 2$ paths/user, a $N = 4$ element smart antenna system improves the BER by a factor of approximately 8 as compared to the performance of a conventional receiver. It can be seen from the figure that as the number of users increases, the analytical model provides a closer match with simulation results, especially for the case of $L = 2$ paths/user. This behaviour is further illustrated in the next figure.

4.6.3.2 Effect of varying the noise level in a multiple user scenario

Figure 4.11 shows the mean BER versus E_b/N_o (dB) with $N = 8$ antennas, $K = 5,20$ users and $L = 2,3$ paths/user respectively. It can be seen that for $K = 5$ users the simulation results (markers) are close to the analytical results (lines). However for $K = 20$ users, which represents a more realistic mobile communications scenario, the simulation results provide an even better agreement with the results obtained by the analytical model. This is because the average BER performance predicted by the analytical model in (4.48) is highly sensitive to the number of in-beam interferers. Consequently, as the number of users and hence the probability of in-beam interferers increases, the prediction matches more closely with the simulations.

4.6.3.3 Effect of varying the number of antennas

Figure 4.12 shows the Mean BER vs. Number of antennas N, for $E_b/N_o = 10$ dB, $K = 15$ users, assuming $L = 1,2,3$ Rayleigh fading multipaths. The figure shows that doubling the number of antennas from 4 to 8 improves the BER by a factor that increases as L increases, e.g. (approximately) 1.9 for $L = 1$, 3.0 for $L = 2$ and 3.7 for $L = 3$. Thus the number of multipaths has a significant effect on the performance of the smart antenna system. It can be seen again that the simulation results agree well with the analytical results.

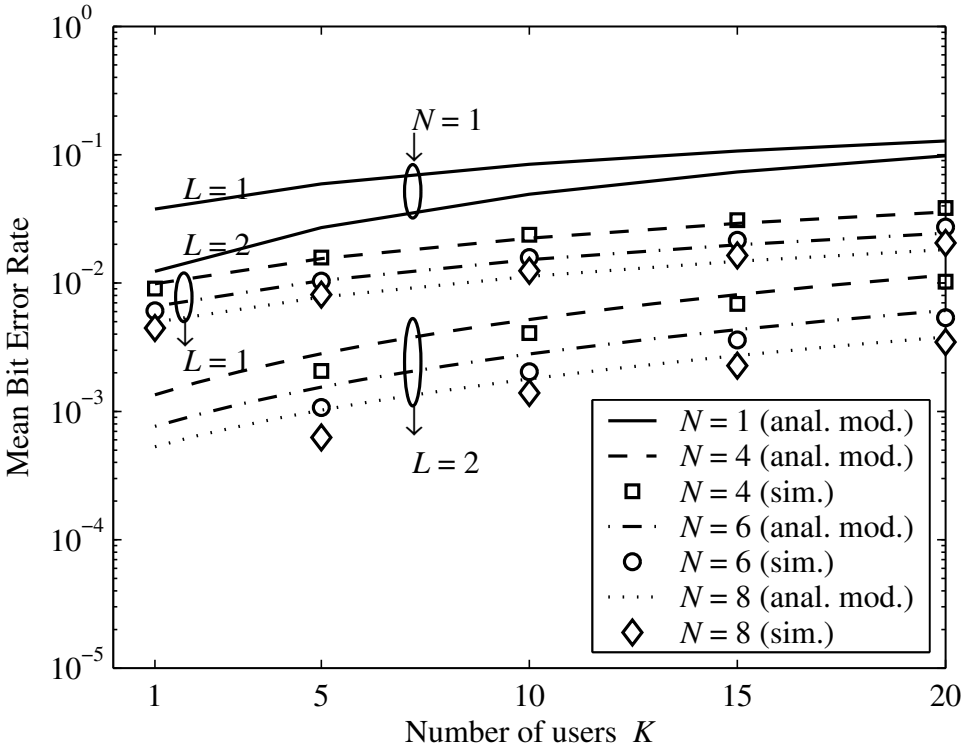

Figure 4.10: Mean BER vs. Number of users K for $E_b/N_o = 10$ dB, assuming $L = 1,2$ Rayleigh fading paths/user and $N = 1,4,6,8$ antennas respectively (lines: analytical model, markers: simulations).

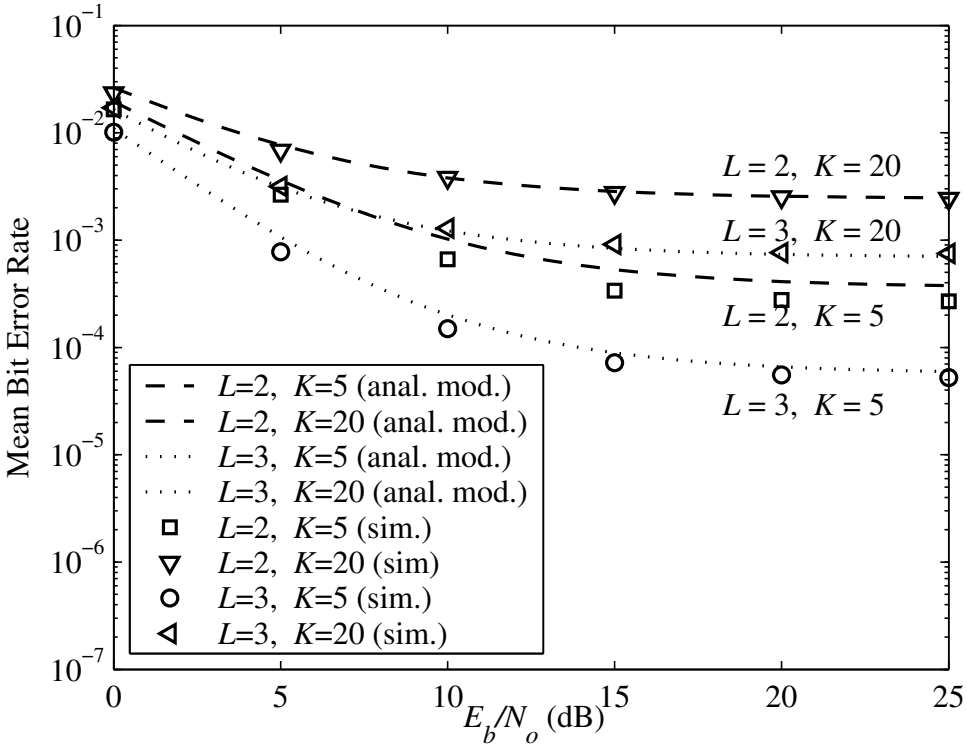

Figure 4.11: Mean BER vs. E_b/N_o for $N = 8$ antennas, assuming $K = 5,20$ users and $L = 2,3$ Rayleigh fading paths/user respectively (lines: analytical model, markers: simulations).

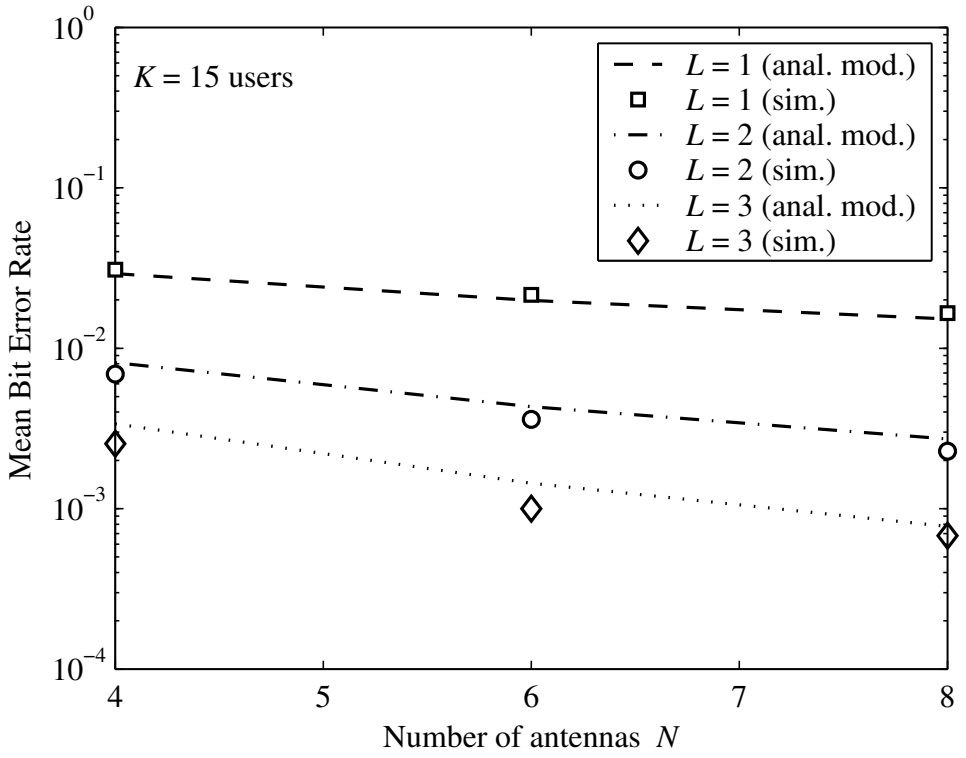

Figure 4.12: Mean BER vs. Number of antennas N, for $E_b/N_o = 10$ dB, $K = 15$ users, assuming $L = 1,2,3$ Rayleigh fading paths/user respectively (lines: analytical model, markers: simulations).

4.7 Summary

In this chapter, the performance of smart antennas for CDMA with noncoherent M-ary orthogonal modulation in Rayleigh and Rician fading environments has been analysed. A simple analytical model has been proposed which permits the BER to be readily evaluated using a closed-form expression. The results obtained using this analytical model show good agreement with the (computationally intensive) Monte Carlo simulation results. Thus the analytical model can be used to rapidly calculate the smart antenna system performance under a variety of user and channel scenarios and is of value in the planning of smart antenna systems for urban and suburban areas.

Chapter 5

Performance of Hierarchical Beamforming for CDMA

In the last chapter, it has been shown that a smart antenna can mitigate Multiple Access Interference (MAI) by beamforming or spatial filtering operation i.e. a smart antenna enhances the signal from the desired user (array gain in the direction of the desired user) and discriminates against interferers located outside the main beam (beamforming gain). As mentioned in Chapter 1, the performance of a CDMA system is limited by MAI and fast fading. Traditionally, widely separated diversity antennas have been used to mitigate fading. In this chapter a hybrid scheme of diversity and smart antennas called Hierarchical Beamforming (HBF) is investigated for an IS-95 CDMA system, to jointly combat fading and MAI.

This chapter is organised as follows. In Section 5.1, the system model for the mathematical characterisation of HBF is presented. The HBF receiver model is described in Section 5.2. The simulation strategy employed to simulate the performance of HBF is discussed in Section 5.3. Finally, in Section 5.4 the simulation results are presented and the performance of HBF is compared with Conventional Beamforming (CBF).

5.1 System Model

Consider a BS serving a single 120° angular sector. It is assumed that the BS is equipped with F co-linear sub-beamforming arrays. The number of array elements in each sub-array is B. Thus the total number of array elements is $N = F \times B$. Each sub-array has an

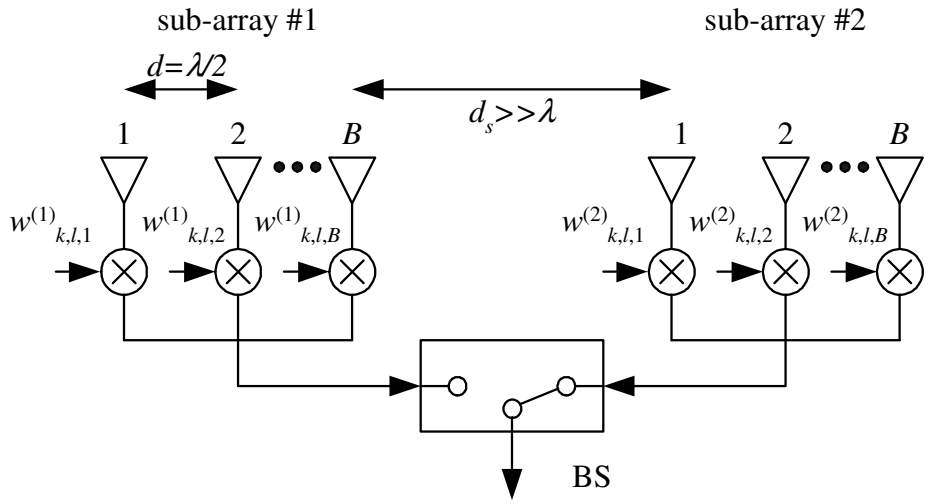

Figure 5.1: Hierarchical beamforming array geometry.

inter-element spacing of $d = \lambda/2$, while the spacing between the adjacent sub-arrays (d_s) is assumed large enough (e.g. 20λ or more) to ensure uncorrelated fading. This model is also applicable to CBF. Specifically, the extreme case of $F = 1$ and $B = N$ corresponds to CBF. The array geometry is illustrated in Figure 5.1 for the case of $F = 2$.

The total number of Mobile Stations (MS) in the system is denoted by K. It is assumed that the MS's follow specifications of the IS-95 CDMA reverse link [159] and are randomly distributed in the azimuthal direction, along the arc boundary of the sector cell in the far field of the array. The $k = 1$ user is assumed to be the desired user.

The kth user's signal propagates through a multipath fading channel with Angle of Arrival (AOA) θ_k, as measured from the array broadside. As the required spacing between sub-arrays for space diversity is much smaller than the sector radius, this AOA is assumed to be the same at each sub-array [110].

A hierarchical beamforming receiver is implemented at the BS. Each sub-array employs a two-dimensional (2-D) RAKE receiver with a Maximum Signal to Noise Ratio beamformer followed by an L finger noncoherent RAKE combiner, which has been discussed in Section 4.2. The ideal solution for the weight vectors is used in the beamformer. The decision variable is obtained by selecting the signal from the sub-array branch with the best channel state [110].

5.1.1 Expression of Transmitted Signal

The transmitted signal $s_k(t)$ of the kth user can be written as [82]

$$s_k(t) = W_k^{(m)}(t)\, a_k(t)\, a^{(I)}(t) \cos(\omega_c t) + W_k^{(m)}(t - T_o)\, a_k(t - T_o)\, a^{(Q)}(t - T_o) \sin(\omega_c t) \quad (5.1)$$

where $W_k^{(m)}(t)$ is the mth M-ary Walsh Symbol $(m = 1, 2, \ldots, M = 64)$ of the kth user, $a^{(I)}(t)$ is the In-phase (I) channel spreading sequence, $a^{(Q)}(t) =$ Quadrature (Q) channel spreading sequence, $a_k(t)$ is the kth user long code sequence, T_o is the half chip delay for OQPSK signals, $\omega_c = 2\pi f_c$ and f_c is the carrier frequency.

5.1.2 Channel Model

The transmitted signal is assumed to propagate over a Rayleigh fading multipath channel. Using the channel model presented in Chapter 3, the complex lowpass equivalent representation of the channel impulse response between the lth multipath of the kth user and the bth antenna in the fth sub-array is given as

$$\tilde{h}_{k,l,b}^{(f)}(t) = \beta_{k,l}^{(f)}\, e^{-j\varphi_{k,l,b}^{(f)}}\, \delta(t - \overline{\tau}_{k,l}) \quad (5.2)$$

where $\beta_{k,l}^{(f)}$ is the path amplitude, $\varphi_{k,l,b}^{(f)}$ is the overall path phase and $\overline{\tau}_{k,l}$ is the path delay respectively.

In vector notation, the spatial signature or channel response vector $\mathbf{h}_{k,l}^{(f)}(t)$ is given as

$$\mathbf{h}_{k,l}^{(f)}(t) \;=\; \left[h_{k,l,1}^{(f)} \;\; h_{k,l,2}^{(f)} \;\; \cdots \;\; h_{k,l,B}^{(f)} \right]^T \quad (5.3)$$

5.1.3 Received Signal

Under the above assumptions, the total received signal for the fth sub-array can be written in vector notation as

$$\mathbf{x}^{(f)}(t) = \sum_{k=1}^{K} \sum_{l=1}^{L} s_k(t - \tau_{k,l})\, \mathbf{h}_{k,l}^{(f)}(t) + \boldsymbol{\eta}^{(f)}(t) \quad (5.4)$$

where $\tau_{k,l} = \Gamma_k + \overline{\tau}_{k,l}$, Γ_k is the random delay of the kth user due to the asynchronous nature of the CDMA system, $\boldsymbol{\eta}$ is the noise which is assumed to be Additive White Gaussian Noise (AWGN) and $\mathbf{h}_{k,l}^{(f)}(t)$ the channel response vector given in (5.3).

5.2 Receiver Model

A block diagram of the receiver incorporating HBF array is shown in Figure 5.2, which is adapted and modified from Figure 4.3. The received signal at each sub-array antenna is first down-converted. Each resolvable path is then detected by one of the RAKE fingers immediately following the radio-frequency stages. To detect the lth path, the signal at the different sensors is despread using the sequence of the respective mobile and synchronized to the delay of the lth path. The post PN-despread signal vector is

$$\mathbf{y}_{k,l}^{(f)} = \left[y_{k,l,1}^{(f)} \; y_{k,l,2}^{(f)} \; \cdots \; y_{k,l,B}^{(f)} \right]^T \tag{5.5}$$

Next a beamformer is constructed for each resolvable multipath and the signal after PN despreading is combined by the beamforming process. The beamforming output is given by

$$z_{k,l}^{(f)} = (\mathbf{w}_{k,l}^{(f)})^H \, \mathbf{y}_{k,l}^{(f)} \tag{5.6}$$

where $\mathbf{w}_{k,l}^{(f)}$ is the Maximum SNR beamforming weight vector given by

$$\mathbf{w}_{k,l}^{(f)} = \left[w_{k,l,1}^{(f)} \; w_{k,l,2}^{(f)} \; \cdots \; w_{k,l,B}^{(f)} \right]^T \tag{5.7}$$

As discussed in Section 4.2.3, the weights are set equal to the channel response vector for the desired user. This provides a lower bound on the system performance.

Finally, all the outputs of the beamformers are Walsh correlated and then processed by the conventional RAKE Receiver to combine the various multipath signals and produce the decision variable by equal gain combining for Walsh demodulation for the fth sub-array. The overall decision is then made by selecting the decision outcomes from the respective sub-beamforming array with the best channel state [110].

5.3 General Simulation Assumptions

The general simulation assumptions and the simulation strategy are similar to the one described in Section 4.5 in the previous chapter. For clarity of investigations, the main simula-

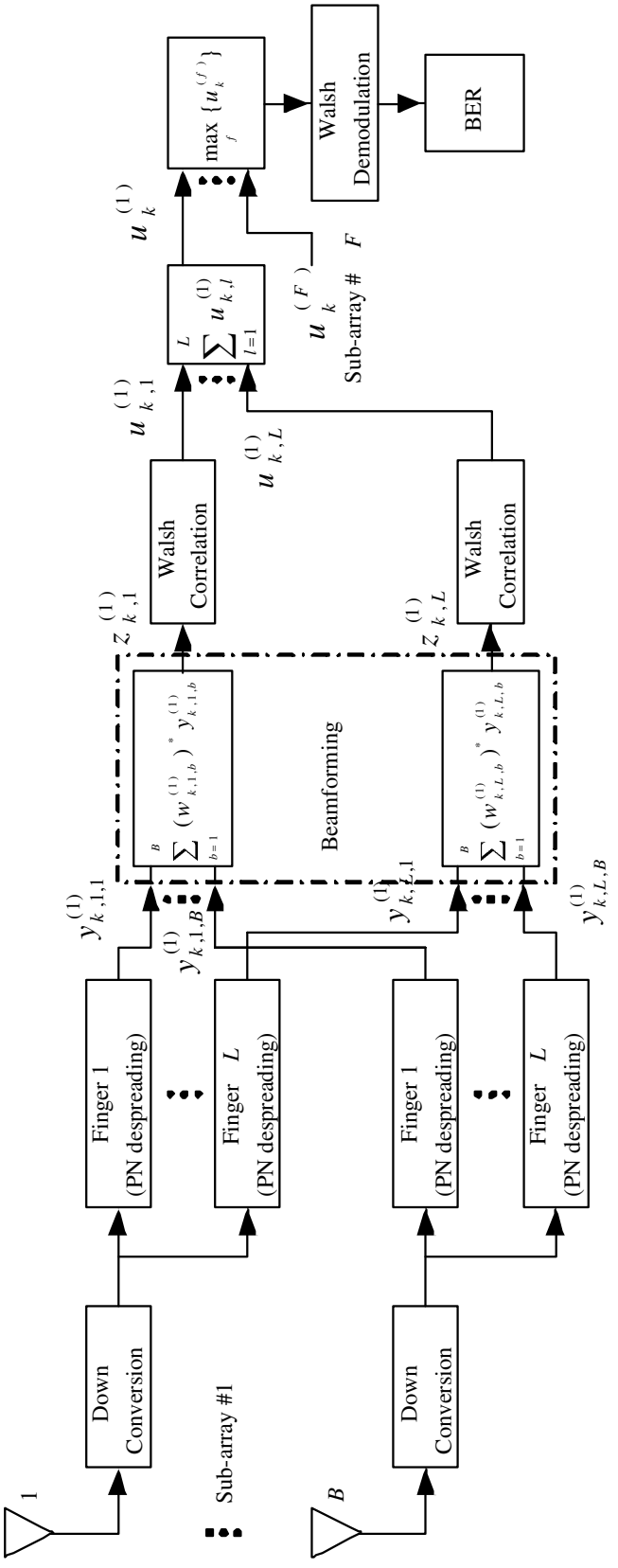

Figure 5.2: Receiver block diagram for hierarchical beamforming.

tion assumptions are summarized in Table 5.1 and the additional assumptions with respect to the system parameters are discussed below:-

- **Number of antenna elements**

  To make a fair comparison, the total number of antenna elements N is assumed to be the same for both HBF and CBF.

- **Number of HBF branches**

  It is assumed that the BS is equipped with $F = 2$ co-linear sub-beamforming arrays. This choice of the number of sub-arrays is motivated by practical array size considerations.

- **Channel**

  The channel considered is Rayleigh fading with $L = 1, 2$ paths/user respectively.

- **pdf in AOA**

  The angular distribution of the waves arriving at the BS in azimuth is described by the pdf in the AOA. A Gaussian PDF in AOA is assumed, which has been shown to best match the azimuth pdf in typical urban environments [57].

- **Angle spread**

  According to measurements [57], the median angle spread σ_{AOA} in urban macrocellular areas lies between $5^\circ - 15^\circ$, depending on the height of the BS. The values of angle spread used in the simulations, therefore, lie in the above range.

5.4 Results

The performance of HBF is jointly determined by the interaction of a number of factors. These include beamforming gain via closely spaced antenna elements within each sub-array, space diversity gain via widely separated sub-arrays, additional space diversity gain via angle spread and temporal diversity gain via the multipaths [119]. To investigate the impact of these gains on the performance of HBF and CBF, the effect of varying the noise level E_b/N_o, angle spread σ_{AOA}, number of antennas N, number of multipaths L and number of users K is studied. The results are generated by using the simulation model developed for the purpose (for details, see Appendix B).

Table 5.1: Main parameters for hierarchical beamforming simulations

Parameter	Value/Description
Chip time	$T_c = \frac{1}{1228800}$ s
Bits/frame	576
Frame length	20 ms
Oversampling factor	$Q = 4$
Base station synchronisation	Asynchronous operation
Channel estimation	perfect
Power control	ideal
RAKE receiver synchronization	perfect
Detection	Non-coherent
Sectorization angle	120° (3 sectors/cell)
Antenna geometry	Uniform Linear Array
Number of antenna elements	$N = 4, 6, 8$
Number of sub-arrays	$F = 2$
Inter-element distance	$d = \lambda/2$
Angle of Arrival	$-60^\circ \leq \theta \leq 60^\circ$
User mobility	0.01° per snapshot
Number of sub-paths	$S = 15$
Doppler frequency	$f_D = 100$ Hz
Power Delay Profile	$L = 2$ equal strength paths ($\tau_d = 5T_c$)
pdf in AOD	Uniform
pdf in AOA	Gaussian
Angle spread	$\sigma_{AOA} = 0^\circ, 5^\circ, 10^\circ, 15^\circ$

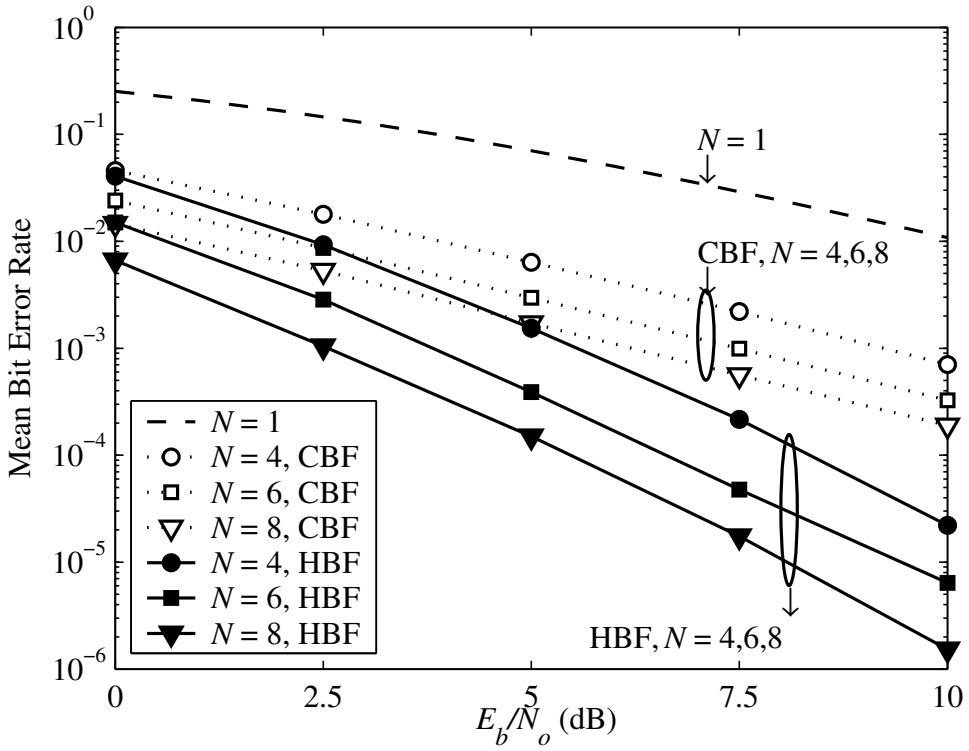

Figure 5.3: Mean BER vs. E_b/N_o (dB) for $K = 1$ user, $L = 2$ Rayleigh fading paths/user, angle spread $\sigma_{AOA} = 0^\circ$ and $N = 4, 6, 8$ antennas respectively.

5.4.1 Effect of Noise Level

To begin with, the performance of HBF and CBF is examined for the case of a single user. It is apparent that there is no MAI in this case. Figure 5.3 shows the plot of mean BER vs. E_b/N_o (dB) for $K = 1$ user, $L = 2$ paths/user, zero angle spread and $N = 4, 6, 8$ antennas respectively. The reference curve in the figure is the theoretical performance of conventional receiver with a single antenna element in (4.37). It can be seen that both CBF and HBF show a big improvement in mean BER compared to the conventional receiver and the improvement increases with increasing E_b/N_o. The performance of HBF is superior to CBF, e.g. for a BER threshold of 10^{-3} and $N = 8$, an E_b/N_o of about 6.2 dB is required for CBF but only 2.5 dB is required for HBF. This performance improvement can be attributed to the space diversity gain offered by the widely separated sub-arrays, which is the dominant factor (in the absence of MAI) for the case of a single user.

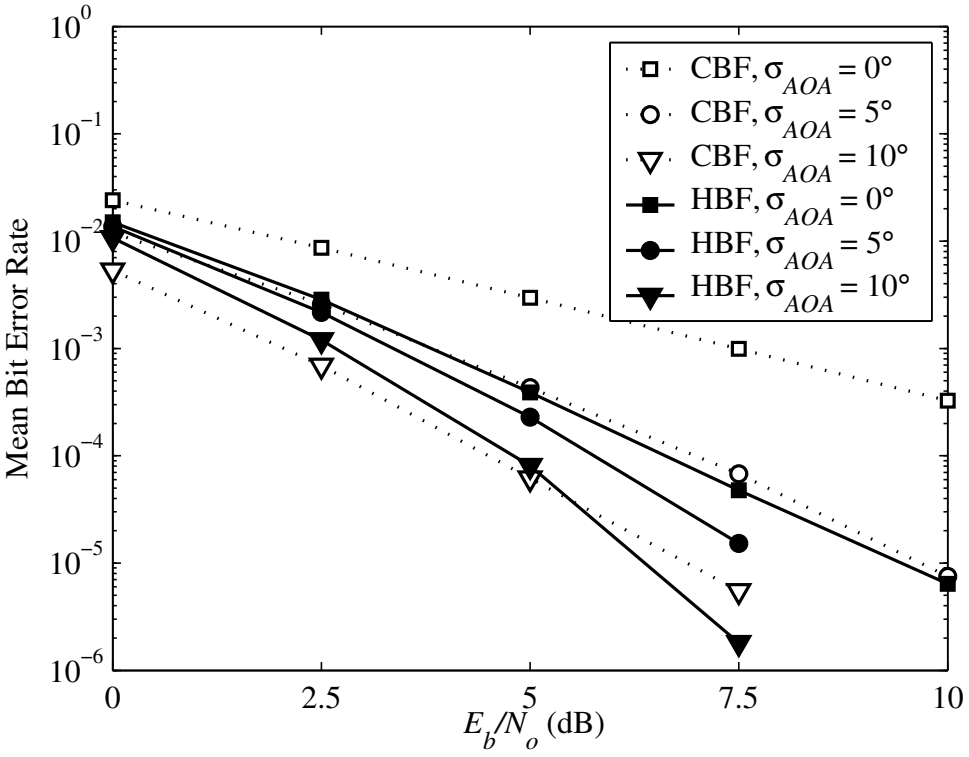

Figure 5.4: Mean BER vs. E_b/N_o (dB) for $N = 6$ antennas, $K = 1$ user, $L = 2$ Rayleigh fading paths/user and angle spreads $\sigma_{AOA} = 0^\circ, 5^\circ, 10^\circ$ respectively.

5.4.2 Effect of Angle Spread

Figure 5.4 shows the performance of HBF and CBF for $N = 6$ antennas, $K = 1$ user, $L = 2$ paths/user and angle spreads $\sigma_{AOA} = 0^\circ, 5^\circ, 10^\circ$ respectively. The inclusion of angle spread produces spatial fading across the array which results in additional spatial diversity gain and improves the performance of both CBF and HBF. Consequently, the performance further improves as the angle spread σ_{AOA} increases from 5° to 10°. Comparing CBF and HBF in the presence of angle spread, it can be seen that for low E_b/N_o CBF is slightly better, but as E_b/N_o gets higher diversity gain becomes dominant and HBF becomes better.

5.4.3 Effect of Number of Antennas

Figure 5.5 shows the plot of mean BER vs. Number of antennas N for $E_b/N_o = 10$ dB, $K = 15$ users, $L = 1$ path/user and angle spreads $\sigma_{AOA} = 0^\circ, 5^\circ, 10^\circ, 15^\circ$ respectively. From

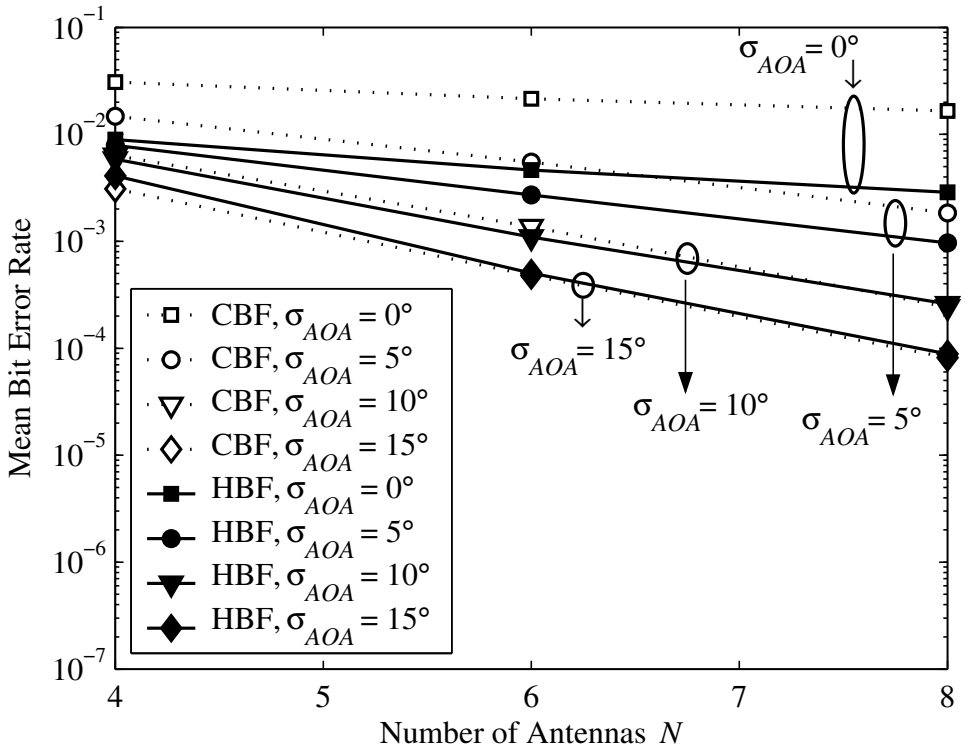

Figure 5.5: Mean BER vs. Number of antennas N for $E_b/N_o = 10$ dB, $K = 15$ users, $L = 1$ Rayleigh fading path/user and angle spreads $\sigma_{AOA} = 0^\circ, 5^\circ, 10^\circ, 15^\circ$ respectively.

the figure, it can be observed that for zero angle spread, HBF is again better than CBF due to diversity gain afforded by the array architecture. However for both CBF and HBF, there is not much improvement in performance by doubling the number of antennas N from 4 to 8. This finding is important from the point of view of planning of antenna systems. By comparison in angle spread scenario, the performance of both schemes improves by increasing the number of antennas. It can be seen that for $\sigma_{AOA} = 5^\circ$, HBF is better than CBF. For larger angle spreads of $\sigma_{AOA} = 10^\circ$ and 15°, both array architectures show a similar performance since all antenna elements in HBF and CBF arrays respectively are nearly uncorrelated.

5.4.4 Effect of Number of Multipaths

Figure 5.6 shows the mean BER vs. Number of antennas N for $E_b/N_o = 10$ dB, $K = 15$ users, $L = 2$ paths/user and angle spreads $\sigma_{AOA} = 0^\circ, 5^\circ, 10^\circ, 15^\circ$ respectively. From the

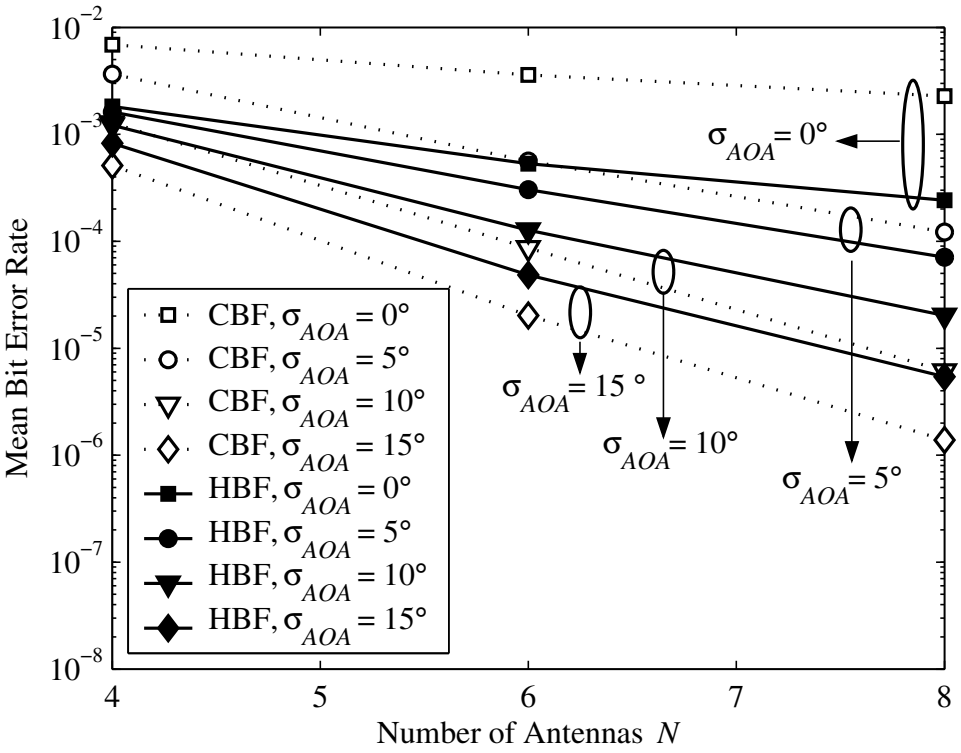

Figure 5.6: Mean BER vs. Number of antennas N for $E_b/N_o = 10$ dB, $K = 15$ users, $L = 2$ Rayleigh fading paths/user and angle spreads $\sigma_{AOA} = 0^\circ, 5^\circ, 10^\circ, 15^\circ$ respectively.

figure, it can be observed that for the case of zero angle spread, HBF is again much better than CBF. For $\sigma_{AOA} = 5^\circ$, HBF is still better than CBF. However for $\sigma_{AOA} = 10^\circ$ and 15°, we see that CBF outperforms HBF. This is because at these angle spreads all the antenna elements in HBF and CBF arrays respectively are nearly uncorrelated and, in the presence of path diversity, the MAI becomes the dominant factor.

5.4.5 Effect of Number of Users

Finally, the performance of HBF and CBF with varying number of users is examined. Figure 5.7 shows the plot of mean BER vs. Number of users K with $E_b/N_o = 10$ dB, $N = 6$, $L = 2$, and $\sigma_{AOA} = 0^\circ, 5^\circ, 10^\circ$ respectively. The trends identified in Figures 5.3, 5.4 and 5.5 are re-confirmed from this figure. It can be seen that for $\sigma_{AOA} = 0^\circ$ and 5°, HBF is superior to CBF. For $\sigma_{AOA} = 10^\circ$ and small number of users, HBF is better than CBF. However for larger number of users when MAI becomes the dominant factor, beamforming gain helps to combat interference and it is better to utilise all available elements for CBF.

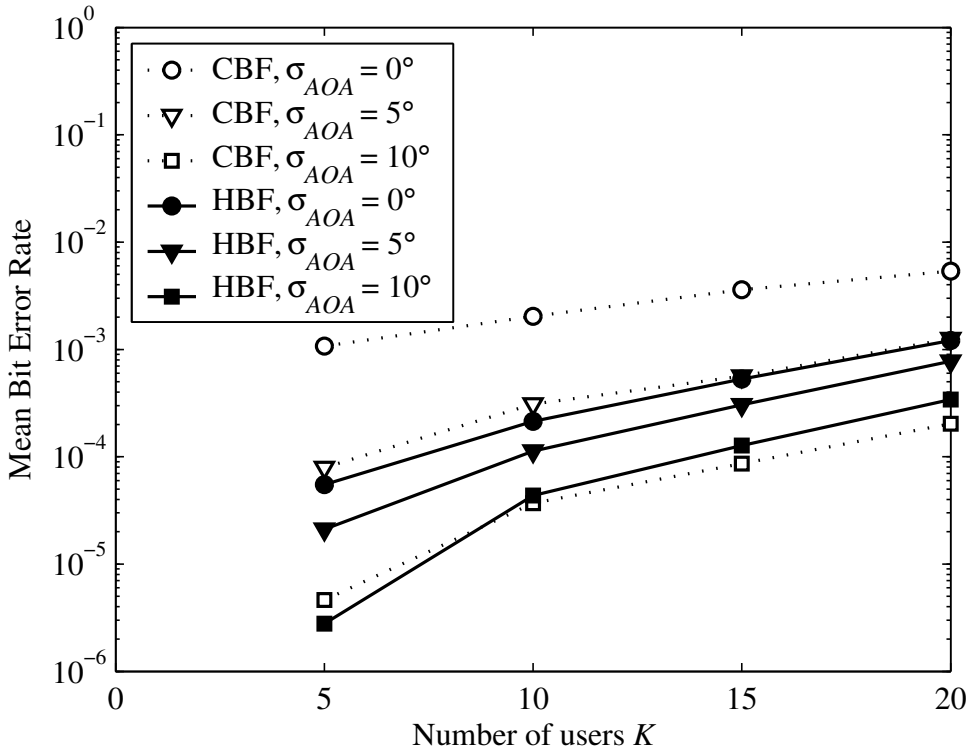

Figure 5.7: Mean BER vs. Number of users K for $E_b/N_o = 10$ dB, $N = 6$ antennas, $L = 2$ Rayleigh fading paths/user and angle spreads $\sigma_{AOA} = 0^\circ, 5^\circ, 10^\circ$ respectively.

5.5 Summary

In this chapter, a hybrid scheme of diversity and beamforming called hierarchical beamforming has been investigated. The application of this scheme to the reverse link of IS-95 CDMA system has been discussed. Furthermore, its performance has been compared with conventional beamforming and the effect of varying the system parameters such as angle spread, number of antennas, number of multipaths and number of users has been studied. It has been shown that the performance of hierarchical beamforming is superior to conventional beamforming while assuming zero angle spread. However for the case of moderate or large angle spread, when path diversity is exploitable and the system is heavily loaded, conventional beamforming yields better mean Bit Error Rate results than hierarchical beamforming. Thus the choice of the optimum receiver architecture is dependant on the channel conditions.

Chapter 6

Conclusions and Future Work

The previous chapters of this thesis have reported on the work concerning the four main thesis aims, which have been outlined in Section 1.3. This included the performance analysis and comparison of linear and circular arrays with respect to their interference rejection capabilities, an introduction of a suitable channel model incorporating user mobility for smart antennas, proposal of an analytical model for evaluating the mean BER of a CDMA system employing a smart antenna and assessment of a hybrid antenna system with diversity and beamforming capabilities.

This chapter provides a summary of the main findings resulting from the undertaken work and is organised as follows. Section 6.1 provides a discussion of individual findings of each chapter. Section 6.2 presents suggestions for future investigations.

6.1 Summary of Thesis Conclusions

In Chapter 2 a unified approach has been proposed for analysing and comparing the interference rejection capabilities of linear and circular arrays of half-wavelength spaced dipoles, which can be part of a base station of a CDMA cellular communication system. It has been shown that there is an improvement in the interference rejection, in terms of the Signal to Interference Ratio (SIR) at the array output, as the number of antenna elements N increases. For a linear array the interference rejection is maximum in the array broadside direction and deteriorates in the array end-fire direction. The range of angles (measured from array broadside) over which the most significant improvement occurs is limited to approximately

$\pm 59^{\circ}$. This occurs when about 12 antenna elements are used. Increasing N further results in diminishing returns. In comparison, for a full angular range surrounding a base station, a circular array provides a more uniform SIR improvement than a linear array. The effect of mutual coupling on these interference rejection capabilities has also been assessed. The obtained results have shown that mutual coupling degrades the SIR improvement capability of the linear array, particularly in the broad-side direction. In contrast mutual coupling has little effect on the SIR improvement capability of the circular array, for the assumed element spacing of half-wavelength. This can be attributed to the inherent symmetry of the circular array. However it has been shown that when the performance is averaged over all angles of arrival and mutual coupling is negligible, linear arrays show similar performance to circular arrays. The above findings are useful in determining the optimum number of antenna elements for base station antennas.

In Chapter 3, a parameterized physical channel model incorporating mobile station mobility has been proposed for use in performance evaluation of smart antennas. The modelling of the various temporal and spatial parameters of the channel model has been detailed. It has been shown that the proposed model is able to accurately simulate Rayleigh and Rician fading environments. In addition, it has been indicated that when azimuth angle spread is very small (e.g. a few degrees) the received signal across the antenna elements is highly correlated. As the angle spread increases, there is spatial fading across the array and the channel coefficients become increasingly uncorrelated. This affords additional space diversity gain, which can be exploited to improve the performance of the system. The proposed model is convenient and easy to use and enables realistic performance evaluation of smart antennas for wireless communication systems.

In Chapter 4 an analytical model for evaluating the mean BER of a Direct Sequence Code Division Multiple Access (DS-CDMA) system, with noncoherent M-ary orthogonal modulation, employing an array antenna and operating in Rayleigh and Rician fading environments has been proposed. The proposed model incorporates the array and channel models developed in Chapters 2 and 3 respectively. It has been shown that the assumption of Rayleigh (NLOS) fading, which is commonly used, gives the worst case performance

of the system. Under the Ricean (LOS) fading assumption, which can occur frequently in urban micro-cellular systems, the system performance is improved depending on the power of the LOS component. The proposed model has been shown to predict the performance of the complex smart antenna system in Rayleigh as well as Rician fading under different conditions with reasonable degree of accuracy. The analytical model can be used to rapidly calculate the smart antenna system performance and is of value in the planning of smart antennas for urban and suburban areas.

In Chapter 5 the performance of Hierarchical Beamforming (HBF), which is a hybrid scheme of diversity and smart antennas, has been investigated. A signal model has been presented for a HBF receiver applied to the reverse link of IS-95 CDMA, including the channel model presented earlier in Chapter 3. Simulation results have been presented comparing the performance of HBF with conventional beamforming (i.e. smart antennas which have been analysed in Chapter 4) while taking into account moderate values of angle spread. This assumption is valid for urban and suburban scenarios. It has been shown that while assuming zero angle spread, the performance of HBF is superior to Conventional Beamforming (CBF) due to space diversity gain afforded by the well separated sub-arrays. The inclusion of angle spread produces spatial fading across the array, which results in additional diversity gain and improves the performance of both CBF and HBF. For small angle spreads (e.g. $< 5^{\circ}$), the performance of HBF is still better than CBF. However for larger angle spreads (e.g. 10° or 15°), when path diversity is exploitable and the system is heavily loaded, CBF yields better mean BER results than HBF. This is because all antenna elements in HBF and CBF array are nearly uncorrelated and it is better to utilise the available antennas for beamforming to combat multiple access interference. These findings are based on the assumption of perfect channel estimation and provide an estimate of the best case system performance. The findings are of value in selecting the appropriate array architecture for a particular channel environment.

Finally, the reverse link of IS-95 CDMA is briefly described in Appendix A and the simulation model, which is used to generate the simulation results in this thesis, is discussed in Appendix B. The developed model is versatile and easily customizable for future

investigations involving multiple antennas for CDMA system.

6.2 Future Work

Although this thesis has answered a number of important questions regarding smart antennas for CDMA systems, several issues remain for possible future work:-

- The analytical model proposed in Chapter 4 can be modified for the case of enhanced radio configurations (3 and higher) of cdma2000 which use additional reverse link channels, variable length Walsh codes and complex Walsh codes to enable higher data rates. The model can also be extended for the case of coded CDMA systems, utilising error correcting codes and interleavers.
- Ideal beamforming weight vectors have been used in this thesis work. In practice, the weights are determined using an adaptive beamforming algorithm. Due to limitations of actual beamforming algorithms, errors are introduced in the beamforming weights. In this context, the performance of different beamforming algorithms can be explored with regard to their sensitivity to the operating channel and user conditions.
- The interference model considered in this thesis work assumed a perfect power control scenario. In future mobile radio systems with multi-rate wireless services, conditions with high data rate interferers and low data rate desired users are likely to occur. Thus suitable combinations of smart antennas and interference cancellation techniques is an important and interesting future research topic.
- Importance sampling technique [170] can be used in the Monte Carlo simulations to further reduce the simulation runtimes.

Appendix A

Reverse Link of IS-95 CDMA

This appendix describes the reverse link (mobile to base station) of the IS-95 CDMA air interface, which is used in the analytical model developed in Chapter 4 and the simulation model discussed in Appendix B. The IS-95 CDMA standard was first published by the US Telecommunications Industry Association (TIA) in 1993. More detailed information on this standard can be found in [2, 4, 171].

The block diagram of the reverse link transmitter in IS-95 CDMA is shown in Figure A.1 [2]. The source data is assumed to consist of sequences of random bits (1's and 0's) representing voice signals. Data transmitted on the reverse link is grouped into 20 ms frames. For maximum data rate of 9600 bps, there are 192 bits per frame. The reverse link transmitter uses a combination of convolutional coding and $M = 64$-ary orthogonal modulation to form a concatenated coding scheme. The data bits are first passed through a rate $r = 1/3$, constraint length $K_c = 9$ convolutional encoder. This produces 576 encoded bits per frame. The next stage involves interleaving the encoded bits using a 32×18 block interleaver. Bits are written column-wise in the matrix and output is read row-wise. These bits are then fed to the Walsh modulator. For each 6 bits in the input, Walsh modulator outputs 1 Walsh symbol consisting of 64 chips. Thus we get $(576/6) \times 64 = 96 \times 64 = 6144$ Walsh chips per frame at the output. Next long code PN sequence is used to spread the signal by a factor of 4. The final stage in generating the baseband reverse link signal is the Quadrature spreading operation. The long code spread stream is mapped onto both in-phase and quadrature branches with each branch being further encoded by the I-channel and Q-channel PN sequences respectively. The signal is sampled and the Q-channel is then

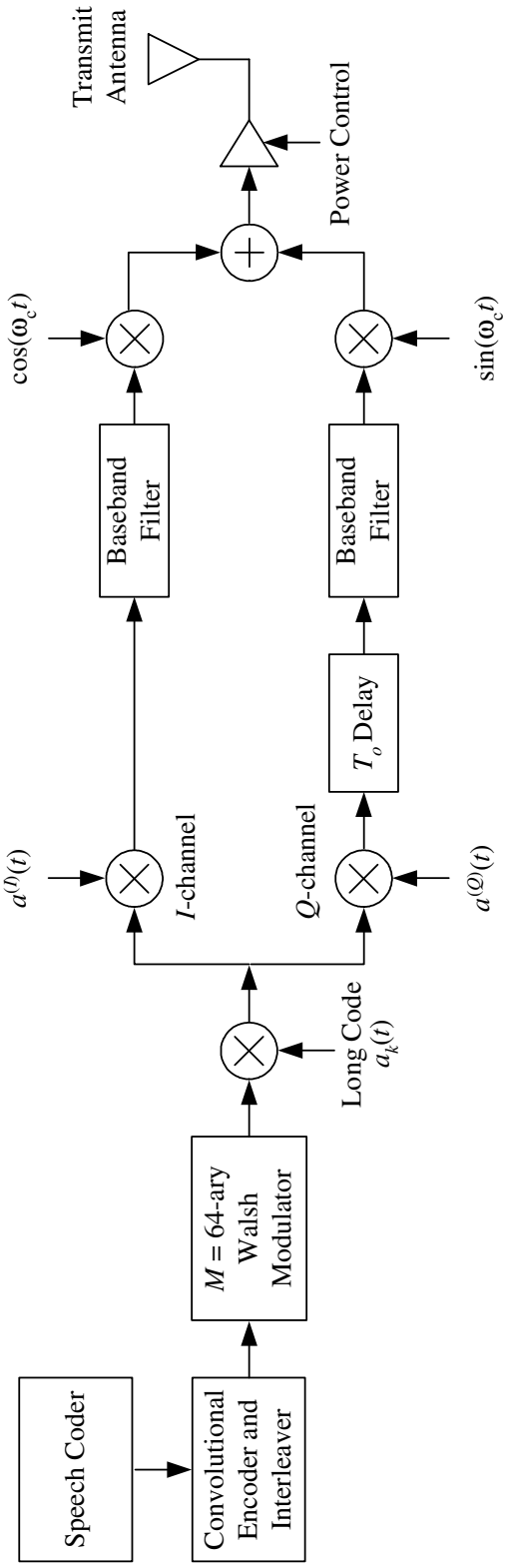

Figure A.1: Block diagram of reverse link IS-95 CDMA transmitter for a single user.

delayed by $T_o = T_c/2$ chips to achieve Offset Quadrature Phase Shift Keying (OQPSK) modulation.

The BS uses a noncoherent RAKE receiver to take advantage of multipath delays greater than T_c. Noncoherent demodulation is used because IS-95 CDMA reverse link does not have a pilot signal transmitted on the reverse link to maintain a coherent reference. Such an approach leads to reduced complexity implementation as it does not require the estimation of phase of the received signal. It also minimizes the power consumption at the MS. However noncoherent demodulation has a higher BER compared with coherent demodulation. Also since the users operate asynchronously, the system must tolerate cochannel interference generated by other users within the reference cell and in neighbouring cells. The output of the noncoherent RAKE is then decoded using hard or soft decision Viterbi decoding.

Appendix B

Simulation Model for CDMA Smart Antenna Systems

This appendix provides a brief description of the simulation model which has been developed and used to generate the simulation results presented in Sections 3.3, 3.4, 4.6 and 5.4 respectively. The appendix consists of three sections. Section B.1 describes the software platform and overall simulation environment and capabilities of the model. Section B.2 describes, with the help of an example, the general program flow to illustrate the simulation algorithm used in the model. Section B.3 provides details of the average time taken to simulate a typical smart antenna system.

B.1 Simulation Software

The simulation software is based on the reverse link of the IS-95 CDMA system (described in Appendix A). It consists of a large library of over a hundred customized MATLAB functions (m-files), which have been developed to implement the analytical models, presented in Sections 2.2, 3.2, 4.1, 4.2, 5.1 and 5.2, in this thesis. These include random signal generators, PN sequence generators, modulators and demodulators for IS-95 CDMA reverse link, Rayleigh and Rician fading multipath channels, linear and circular array antenna models, RAKE combiners, smart antenna beamformer, hierarchical beamformer and error analysis functions. The various functions can be conveniently grouped into Transmitter (TX), Channel and Receiver (RX) blocks, as illustrated in Figure B.1.

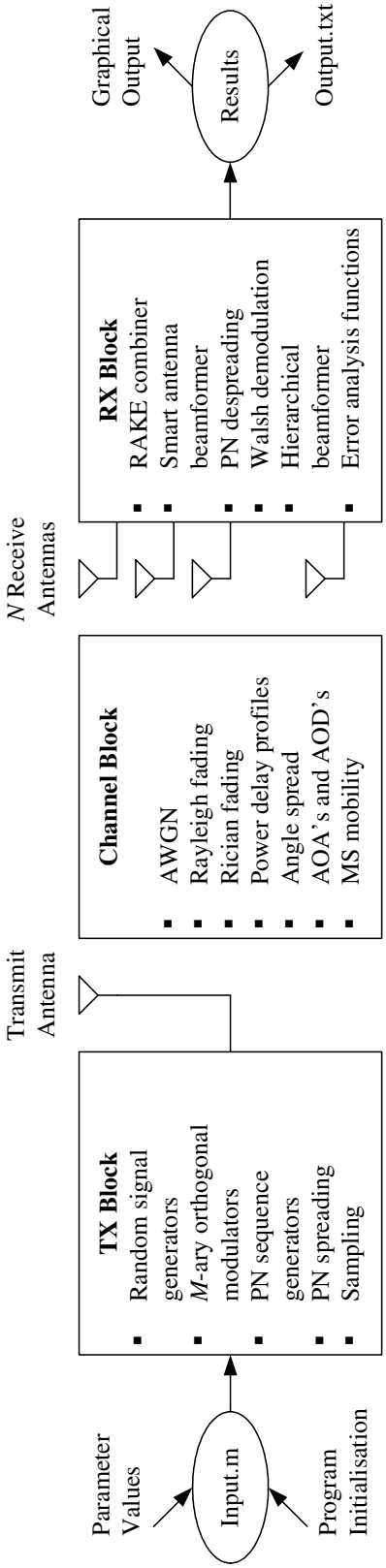

Figure B.1: Block diagram highlighting simulation program capabilities.

B.1.1 Program Environment

The simulation program has been written and tested in MATLAB 6.5 [126]. The software is implemented as a complete system in MATLAB. This means that additional MATLAB Toolboxes, such as the Communications and Signal Processing Toolboxes, are not necessary for running the program.

The open MATLAB programming language has been used to write most of the functions, enabling their easy customisation. A modular approach has been used in the design of overall software environment so that new functions can easily be written and integrated into the main program. Also frame-based data processing is used by all the functions, i.e. data is processed and propagated through the program using blocks of consecutive samples rather than individual samples. This mimics the real-time operation of communications and signal processing applications [126, 168].

To provide an efficient computational engine and to overcome MATLAB's inherent weakness in dealing with algorithms requiring nested `for` loops, vectorized MATLAB coding has been used. In addition, some of the computationally intensive functions e.g. PN sequence generators and the complex channel coefficient generators have been implemented as C language MEX (Matlab EXecutable) files for faster execution.

B.1.2 Program Operation

As illustrated in Figure B.1, the input data parameters (discussed in Sections 4.5 and 5.3) are fed to the main program through a separate "Input.m" m-file, which is read by the main program upon execution. As part of the program initialisation, the seeds for MATLAB's uniform (`rand`) and Gaussian (`randn`) random number generator functions, which determine the sequence of numbers generated, are reset to a known value. The `rand` and `randn` functions are used in the TX data generator and channel functions and resetting their seeds ensures repeatability of results. Also the arrays that store output results are preallocated. This helps to reduce memory fragmentation and consequently improves the code execution time. At the completion of the simulation, the mean BER results are displayed in graphical format. A simulation report, including the simulation time and BER results, is

also generated and saved in an “output.txt” text-file.

B.2 Example

To illustrate the structure and operation of the simulation program the simulation result shown in Figure 4.11, concerning the performance of the smart antenna (Mean BER vs. E_b/N_o for $N = 8$ antennas, assuming $K = 5$ users and $L = 3$ paths/user respectively), is used as an example. These results are obtained by implementing the Monte Carlo simulation technique, discussed in Section 4.5.1, using the following algorithm:-

1. `Initialise transmitter parameters`
   - Number of users $K = 5$
   - Number of bits/frame = 576
   - $E_b/N_o = [0 : 5 : 20]$ (using MATLAB notation)
2. `Initialise channel parameters`
   - Channel type: Rayleigh fading channel
   - Number of mutipaths/user $L = 3$
   - Number of subpaths $S = 15$
   - Doppler frequency f_D = 100 Hz
3. `Initialise receiver parameters`
   - Receiver type: smart antenna receiver with Maximum SNR beamforming
   - Number of antenna elements $N = 8$
   - Number of RAKE fingers $= 3$
4. `Initialise Monte Carlo simulation parameters`
   - Number of drops $M_c = 50 - 100$
   - Minimum number of bit errors $= 100$
   - Number of data frames/drop $= 125$
   - Oversampling factor $Q = 4$
5. `Reset MATLAB random number generator seeds and preallocate output arrays in memory`

6. `for EbNo =[0:5:25]` (using MATLAB notation)

   `while(((biterrors <= 100) & Mc <= 100) | Mc <= 50)`

   (a) Generate the random transmit data for each user

   (b) Generate channel coefficients for each user's multipath signal

   (c) Generate the total received signal

   (d) Generate the decoded data for the desired (i.e. first) user

   (e) Store the number of bit errors for each drop

   `end`

   Calculate and store the overall BER

   `end`

7. `Plot the simulation results and compare with analytical model prediction` (using (4.48))
8. `Generate and save the simulation report`

The simulation report, generated for the case considered, is shown in Table B.1.

Table B.1: Format of output file for simulation example in Section B.2

```
Mean BER vs. EbNo:-
N = 8 antennas
K = 5 users
L = 3 paths/user

Computer = PIII 1266 MHz

Simulation Time (hours) =   388.42

EbNo(dB) SNR(dB)  Drops   Tot. bits  Tot. Err.  Mean BER
0       -22.321    50     3.6e+006   36359      1.0100e-002
5       -17.321    50     3.6e+006   2805       7.7917e-004
10      -12.321    50     3.6e+006   466        1.2944e-004
15      -7.3215    50     3.6e+006   260        7.2222e-005
20      -2.3215    50     3.6e+006   199        5.5278e-005
25      +2.6785    50     3.6e+006   188        5.2222e-005
```

B.3 Simulation Timings

Table B.2 illustrates the time taken to complete a Monte Carlo simulation for a single E_b/N_o value for different combinations of input parameters (Number of antenna elements N, Number of users K, Number of paths/user L, Type of fading and No. of Drops[†]). The simulation times are indicated for the following different computers:-

- Pentium III, CPU 1.0 GHz, 256 MB of RAM.
- Pentium IV, CPU 2.5 GHz, 512 MB of RAM.
- Pentium IV, CPU 3.2 GHz, 2 GB of RAM.

It can be seen from Table B.2 that the typical simulation time for a single E_b/N_o value is of the order of a couple of days. This computationally intensive nature of the Monte Carlo simulations illustrates the advantage of the analytical model developed in this thesis.

Table B.2: Illustration of execution timings for smart antenna simulations

N	K	L	Fading	Drops	Computer Speed	Time (hours)
4	15	1	Rayleigh	100	1.0 GHz	39.4
6	15	1	Rayleigh	100	1.0 GHz	56.4
8	15	1	Rayleigh	100	1.0 GHz	74.1
4	15	1	Rician	50	2.5 GHz	17.7
6	15	1	Rician	50	2.5 GHz	26.6
8	15	1	Rician	50	2.5 GHz	35.7
4	15	2	Rayleigh	100	2.5 GHz	66.0
6	15	2	Rayleigh	100	2.5 GHz	82.6
8	15	2	Rayleigh	100	2.5 GHz	109.5
6	15	3	Rayleigh	100	3.2 GHz	79.9
8	20	3	Rayleigh	50	3.2 GHz	67.9

[†]1 Drop = 125 data frames = $125 \times 576 = 72000$ data bits (see Section 4.5).

Bibliography

[1] D. P. Agrawal and Q.-A. Zeng, *Introduction to Wireless and Mobile Systems*. Thomson Brooks/Cole, 2003.

[2] T. S. Rappaport, *Wireless Communications: Principles and Practice*, 2nd ed. Prentice Hall, 2002.

[3] CDMA Development Group. (2004). [Online]. Available: http://www.cdg.org

[4] V. K. Garg, *IS-95 CDMA and Cdma2000, Cellular/PCS System Implementation*. Prentice Hall PTR, 2000.

[5] GSM Association. (2004). [Online]. Available: http://www.gsmworld.com/index.shtml

[6] V. K. Garg and J. E. Wilkes, *Principles and Applications of GSM*. Prentice Hall, 2003.

[7] G. V. Tsoulos, "Smart antennas for mobile communication systems: Benefits and challenges," *Electronics and Communication Engineering Journal*, vol. 11, no. 2, pp. 84–94, Feb. 1999.

[8] "Adaptive antennas concepts and key technical aspects," International Telecommunications Union," Draft New Report ITU-R M [adapt] [Doc. 8/10], Dec. 2003.

[9] R. Prasad and T. Ojanpera, "An overview of CDMA evolution towards wideband CDMA," *IEEE Communications Survey*, vol. 1, no. 1, pp. 2–29, Fourth Quarter 1998.

[10] M. Landrigan and K. Ong, "Whither 3G?: Regulatory settings and investment incentives – an international perspective," *Telecommunications Journal of Australia*, vol. 53, no. 3, pp. 67–77, Spring 2002.

[11] T. S. Rappaport, Ed., *Smart Antennas: Adaptive Arrays, Algorithms & Wireless Position Location*. IEEE Press, 1998.

[12] G. V. Tsoulos, Ed., *Adaptive Antennas for Wireless Communications*. IEEE Press, 2001.

[13] R. D. Murch and K. B. Lataief, "Antenna systems for broadband wireless access," *IEEE Communications Magazine*, pp. 76–83, Apr. 2002.

[14] R. Janaswamy, *Radiowave Propagation and Smart Antennas for Wireless Communications*. Kluwer Academic Publishers, 2001.

[15] International Engineering Consortium. (2003) Smart antenna systems. [Online]. Available: http://www.iec.org/online/tutorials/smart_ant/index.html

[16] ArrayComm, Inc. (2003). [Online]. Available: http://www.arraycomm.com/prods/ic.htm

[17] A. O. Boukalov and S. G. Haggman, "System aspects of smart-antenna technology in cellular wireless communications – an overview," *IEEE Transactions on Microwave Theory and Techniques*, vol. 48, no. 6, pp. 919–929, June 2000.

[18] P. H. Lehne and M. Pettersen, "An overview of smart antenna technology for mobile communication systems," *IEEE Communications Survey*, vol. 2, no. 4, Fourth Quarter 1999.

[19] J. L. Butler, "Digital, matrix and intermediate frequency scanning," in *Microwave Scanning Antennas*, R. C. Hansen, Ed. Academic Press, 1966, vol. 3, ch. 3.

[20] B. Pattan, *Robust Modulations Methods and Smart Antennas in Wireless Communications*. Prentice Hall PTR, 2000.

[21] I. Stevanovic, A. Skrivervik, and J. R. Mosig, “Smart antenna systems for mobile communications,” Ecole Polytechnique Federale De Lausanne, Tech. Rep., Jan. 2003.

[22] J. H. Winters and M. J. Gans, “The range increase of adaptive versus phased arrays in mobile radio systems,” *IEEE Transactions on Vehicular Technology*, vol. 48, no. 2, pp. 353–362, Mar. 1999.

[23] W. Schuttengruber, A. F. Molisch, and E. Bonek. (2004) Smart antennas for mobile communications - tutorial. [Online]. Available: http://www.nt.tuwien.ac.at/mobile/research/smart_antennas_tutorial/

[24] A. Jacobsen, “Smart antennas for dummies,” Telenor,” R&D Report, Nov. 2001.

[25] R. Y. Miyamoto and T. Itoh, “Retrodirective arrays for wireless communications,” *IEEE Microwave Magazine*, vol. 3, no. 1, pp. 71–79, Mar. 2002.

[26] R. T. Derryberry, S. D. Gray, D. M. Ionescu, G. Mandyam, and B. Roghothaman, “Transmit diversity in 3G CDMA systems,” *IEEE Communications Magazine*, pp. 68–75, Apr. 2002.

[27] S. M. Alamouti, “A simple transmit diversity technique for wireless communication,” *IEEE Journal on Selected Areas in Communications*, vol. 16, pp. 1451–1458, Oct. 1998.

[28] Third Generation Partnership Project (3GPP), “Technical specification group radio access network, physical layer procedures (FDD) (release 1999), 3GPP TS25.214 v3.7.0,” 2003.

[29] M. Sandell, “Analytical analysis of transmit diversity in WCDMA on fading multipath channels,” in *Proc. IEEE International Symposium on Personal, Indoor and Mobile Radio Communications (PIMRC)*, 1999.

[30] B. A. Bjerke, Z. Zvonar, and J. G. Proakis, "Antenna diversity combining aspects for WCDMA systems in fading multipath channels," *IEEE Transactions on Wireless Communications*, vol. 3, no. 1, pp. 97–106, Jan. 2004.

[31] R. Giuliano, F. Mazzenga, and F. Vatalaro, "Smart cell sectorization for third generation CDMA systems," *Wireless Communications and Mobile Computing*, vol. 2, pp. 253–267, 2002.

[32] C. A. Balanis, *Antenna Theory: Analysis and Design*, 2nd ed. John Wiley, 1997.

[33] Y. S. Song and H. M. Kwon, "Analysis of a simple smart antenna for CDMA wireless communications," in *Proc. IEEE Vehicular Technology Conference (VTC)*, San Antonio, Texas, May 16-20, 1999, pp. 254–258.

[34] Y. S. Song, H. M. Kwon, and B. J. Min, "Computationally efficient smart antennas for CDMA wireless communications," *IEEE Transactions on Vehicular Technology*, vol. 50, no. 6, pp. 1613–1628, Nov. 2001.

[35] A. M. Wyglinski and S. D. Blostein, "Mutual coupling and scattering effects on cellular CDMA systems using smart antennas," in *Proc. IEEE Vehicular Technology Conference (VTC)*, vol. 4, Boston, MA, Sept. 2000, pp. 1656 –1662.

[36] ——, "On uplink CDMA cell capacity: Mutual coupling and scattering effects on beamforming," *IEEE Transactions on Vehicular Technology*, vol. 52, no. 2, pp. 289–304, Mar. 2003.

[37] S. Choi and D. Yun, "Design of adaptive antenna array for tracking the source of maximum power and its application to CDMA mobile communications," *IEEE Transactions on Antennas and Propagation*, vol. 45, no. 9, pp. 1393–1404, Sept. 1997.

[38] G. W. K. Colman and S. D. Blostein, "Improved power and capacity predictions of a CDMA system with base-station antenna arrays and digital beamforming," in *Proc. 19th Biennial Symposium on Communications*, Kingston, June 1998, pp. 280–284.

[39] *FEKO User's Manual*, EM Software & Systems Inc., July 2001.

[40] T. Svantesson and A. Ranheim, "Mutual coupling effects on the capacity of multielement antenna systems," in *Proc. IEEE International Conference on Speech, Acoustics, and Signal Processing (ICASSP)*, vol. 4, Salt Lake City, Utah, May 2001, pp. 2485 –2488.

[41] J. D. Parsons, *The Mobile Radio Prpagation Channel*. Halsted, 1992.

[42] M. K. Simon and M.-S. Alouini, *Digital Communication over Fading Channels*. John Wiley & Sons, 2000.

[43] J. K. Cavers, *Mobile Channel Characteristics*. Kluwer Academic Publishers, 2000.

[44] M. Patzold, *Mobile Fading Channels*. John Wiley, 2002.

[45] R. H. Clark, "A statistical theory of mobile radio reception," *Bell Labs Syst. Tech. J.*, vol. 47, pp. 957–1000, July-Aug. 1968.

[46] W. C. Jakes, *Microwave Mobile Communications*. John Wiley, 1974.

[47] B. Sklar, "Rayleigh fading channels in mobile digital communications part I: Charaterization," *IEEE Communications Magazine*, pp. 90–100, July 1997.

[48] ——, "Rayleigh fading channels in mobile digital communications part II: Mitigation," *IEEE Communications Magazine*, pp. 102–109, July 1997.

[49] R. Ertel, P. Cardieri, K. W. Sowerby, T. S. Rappaport, and J. H. Reed, "Overview of spatial channel models for antenna array communication systems," *IEEE Personal Communications Magazine*, vol. 5, no. 1, pp. 10–22, Feb. 1998.

[50] K. Yu and B. Ottersten, "Models for MIMO propagation channels: A review," *Wireless Communications and Mobile Communications*, vol. 2, no. 7, pp. 653–666, Nov. 2002.

[51] T. Aulin, "A modified model for the fading signal at a mobile radio channel," *IEEE Transactions on Vehicular Technology*, vol. 29, pp. 182–203, Aug. 1979.

[52] J. D. Parsons and M. D. Turkmani, "Characterization of mobile radio signals: Model description," *Proc. Inst. Elect. Eng.*, vol. 138, pp. 459–556, Dec. 1991.

[53] Y. Z. Mohassed and M. P. Fritz, "A 3-D spatio-temporal simulation model for wireless channels," *IEEE Journal on Selected Areas in Communications*, vol. 20, no. 6, pp. 1193–1203, Aug. 2002.

[54] G. E. Athanasiadou and A. R. Nix, "A novel 3-D indoor ray-tracing propagation model: The path generator and evaluation of narrow-band and wide-band predictions," *IEEE Transactions on Vehicular Technology*, vol. 49, no. 4, pp. 1152–1168, July 2000.

[55] P. Eggers, "Angular dispersive mobile radio environments sensed by highly directive base station antennas," in *Proc. IEEE International Symposium on Personal, Indoor and Mobile Radio Communications (PIMRC)*, Sept. 1995, pp. 522–526.

[56] L. J. Greenstein, V. Erceg, Y. S. Yeh, and M. V. Clark, "A new path-gain/delay-spread propagation model for digital cellular channels," *IEEE Transactions on Vehicular Technology*, vol. 46, no. 2, pp. 477–485, May 1997.

[57] K. I. Pedersen and P. E. Mogensen, "A stochastic model of the temporal and azimuth dispersion seen at the base sation in outdoor propagation environments," *IEEE Transactions on Vehicular Technology*, vol. 49, no. 2, pp. 437–447, Mar. 2000.

[58] D. Mavrakis, "Measurement and prediction of the indoor radio and infrared wideband channels," Ph.D. dissertation, University of Surrey, UK, Oct. 2002.

[59] G. Liang and H. L. Bertoni, "Review of ray modeling techniques for site specific propagation prediction," in *Wireless Communications: TDMA versus CDMA*, S. G. Glisic and P. A. Leppanen, Eds. Kluwer Academic Publishers, 1999, pp. 323–343.

[60] K. Rizk, J.-F. Wagen, and F. Gardiol, "Two-dimensional ray-tracing modeling for propagation prediction in microcellular environments," *IEEE Transactions on Vehicular Technology*, vol. 46, no. 2, pp. 508–518, May 1997.

[61] G. E. Athanasiadou, A. R. Nix, and J. P. McGeehan, "A microcellular ray-tracing propagation model and evaluation of its narrow-band and wide-band predictions," *IEEE Journal on Selected Areas in Communications*, vol. 18, no. 3, pp. 322–335, Mar. 2000.

[62] W. C. Y. Lee, "Effects of correlation between two mobile radio base-station antennas," *IEEE Transactions on Communications*, vol. 21, no. 11, pp. 1214–1224, 1973.

[63] H. Suzuki, "A statistical model for urban radio propagation," *IEEE Transactions on Communications*, vol. 25, pp. 673–680, July 1977.

[64] R. B. Ertel and J. H. Reed, "Angle and time of arrival statistics for circular and elliptical scattering models," *IEEE Journal on Selected Areas in Communications*, vol. 17, pp. 1829–1840, Nov. 1999.

[65] P. Petrus, J. H. Reed, and T. S. Rappaport, "Geometrically based statistical channel model for macrocellular mobile environments," in *Proc. IEEE Global Telecommunications Conference (GLOBECOM)*, London, UK, Nov. 1996, pp. 1197–1201.

[66] R. Janaswamy, "Angle and time of arrival statistics for the gaussian scatter density model," *IEEE Transactions on Wireless Communications*, vol. 1, no. 3, pp. 488 –497, July 2002.

[67] J. Jelitto, M. Stege, M. Lohning, M. Bronzel, and G. Fettweis, "A vector channel model with stochastic fading simulation," in *Proc. IEEE International Symposium on Personal, Indoor and Mobile Radio Communications (PIMRC)*, Osaka, Japan, Sept. 1999.

[68] M. P. Lotter and P. V. Rooyen, "Cellular channel modelling and the performance of DS-CDMA systems with antenna arrays," *IEEE Journal on Selected Areas in Communications*, vol. 17, no. 12, pp. 2181–2196, Dec. 1999.

[69] M. P. Lotter, "Numerical analysis of spatial/temporal cellular CDMA," Ph.D. dissertation, University of Pretoria, South Africa, July 1999.

[70] A. F. Molisch, "A generic model for MIMO wireless propagation channels in macro- and microcells," *IEEE Transactions on Signal Processing*, vol. 52, no. 1, pp. 61–71, Jan. 2004.

[71] Third Generation Partnership Project Two (3GPP2), "Spatial Channel Model Text Description (SCM Text v2.3)," Jan. 30, 2003.

[72] L. C. Godara, "Applications of antenna arrays to mobile communications, part I: Performance improvement, feasibility, and system considerations," *Proceedings of the IEEE*, vol. 85, no. 7, pp. 1031–1060, July 1997.

[73] ——, "Application of antenna arrays to mobile communications, part II: Beamforming and direction-of-arrival consideration," *Proceedings of the IEEE*, vol. 85, no. 8, pp. 1195–1245, August 1997.

[74] Q. Bi, "Performance analysis of a cellular CDMA system," in *Proc. IEEE Vehicular Technology Conference (VTC)*, Denver, CO, May10-13, 1992, pp. 43–46.

[75] K. I. Kim, "On the error probability of a DS/SSMA system with a noncoherent *M*-ary orthogonal modulation," in *Proc. IEEE Vehicular Technology Conference (VTC)*, vol. 1, Denver, CO, May 1992, pp. 482–485.

[76] Q. Bi, "Performance analysis of a CDMA system in the multipath fading environment," in *Proc. IEEE International Symposium on Personal, Indoor and Mobile Radio Communications (PIMRC)*, Boston, MA, 1992, pp. 108–111.

[77] L. M. Jalloul and J. M. Holtzman, "Performance analysis of DS/CDMA with noncoherent *M*-ary orthogonal modulation in multipath fading channels," *IEEE Journal on Selected Areas in Communications*, vol. 12, no. 5, pp. 862–870, June 1994.

[78] P. Patel and J. Holtzman, "Analysis of simple successive interference cancellation scheme in a DS/CDMA system," *IEEE Journal on Selected Areas in Communications*, vol. 12, no. 5, pp. 796–807, June 1994.

[79] V. Aalo, O. Ugweje, and R. Sudhakar, "Performance analysis of a DS/CDMA system with noncoherent *M*-ary orthogonal modulation in nakagami fading," *IEEE Transactions on Vehicular Technology*, vol. 47, no. 1, pp. 20–29, Feb. 1998.

[80] J. M. Holtzman, "A simple accurate method to calculate spread-spectrum multiple-access probabilities," *IEEE Transactions on Communications*, vol. 40, no. 3, pp. 461–464, Mar. 1992.

[81] C.-D. Iskander and P. T. Mathiopoulos, "Performance of multicode DS/CDMA with *M*-ary orthogonal modulation in multipath fading channels," *IEEE Transactions on Wireless Communications*, vol. 3, no. 1, pp. 209–223, Jan. 2004.

[82] A. F. Naguib and A. Paulraj, "Performance of wireless CDMA with *M*-ary orthogonal modulation and cell site antenna arrays," *IEEE Journal on Selected Areas in Communications*, vol. 14, no. 9, pp. 1770–1783, Dec. 1996.

[83] M. D. Anna and A. H. Aghvami, "Performance of optimum and suboptimum combining at the antenna array of a W-CDMA system," *IEEE Journal on Selected Areas in Communications*, vol. 17, no. 12, pp. 2123–2137, Dec. 1999.

[84] Y. S. Song, "Smart antenna algorithms and PN code tracking," Ph.D. dissertation, Wichita State University, Fall 2001.

[85] U. Spagnolini, "A simplified model to evaluate the probability of error in DS-CDMA systems with adaptive antenna arrays," *IEEE Transactions on Wireless Communications*, vol. 3, no. 2, pp. 578–587, Mar. 2004.

[86] ——, "A simplified model for probability in error in DS-CDMA systems with adaptive antenna arrays," in *Proc. IEEE International Conference on Communications (ICC)*, June 2001, pp. 2271–2275.

[87] A. F. Naguib, "Adaptive antennas for CDMA wireless networks," Ph.D. dissertation, Stanford University, Aug. 1996.

[88] J. S. Thompson, P. M. Grant, and B. Mulgrew, "Performance of antenna array receiver algorithms for CDMA," in *Proc. IEEE Global Telecommunications Conference (GLOBECOM)*, vol. 1, Nov. 1996, pp. 18–22.

[89] P. M. Grant, J. S. Thompson, and B. Mulgrew, "Adaptive arrays for narrowband CDMA base stations," *Electronics & Communication Engineering Journal*, vol. 10, no. 4, pp. 156 – 166, Aug. 1998.

[90] J. S. Thompson, P. M. Grant, and B. Mulgrew, "Smart antenna arrays for CDMA systems," *IEEE Personal Communications*, vol. 3, no. 5, pp. 16–25, Oct. 1996.

[91] G. V. Tsoulos, G. E. Athanasiadou, and R. J. Piechocki, "Low-complexity smart antenna methods for third-generation W-CDMA systems," *IEEE Transactions on Vehicular Technology*, vol. 49, no. 6, pp. 2382–2396, Nov. 2000.

[92] J. Choi, "Pilot channel-aided techniques to compute the beamforming vector in CDMA system with antenna array," *IEEE Transactions on Vehicular Technology*, vol. 49, no. 5, pp. 1760–1775, Sept. 2000.

[93] S. Choi, J. Choi, H.-J. Im, and B. Choi, "A novel adaptive beamforming algorithm for antenna array CDMA systems with strong interferers," *IEEE Transactions on Vehicular Technology*, vol. 51, no. 5, pp. 808–816, Sept. 2002.

[94] H. J. Li and T. Y. Liu, "Comparison of beamforming techniques for W-CDMA communication systems," *IEEE Transactions on Vehicular Technology*, vol. 52, no. 4, pp. 752–760, July 2003.

[95] J. Choi and S. Choi, “Diversity gain for CDMA systems equipped with antenna arrays,” *IEEE Transactions on Vehicular Technology*, vol. 52, no. 3, pp. 720–725, May 2003.

[96] S. Choi and D. Shim, “A novel adaptive beamforming algorithm for a smart antenna system in a CDMA mobile communication environment,” *IEEE Transactions on Antennas and Propagation*, vol. 49, no. 5, pp. 1793–1806, Sept. 2000.

[97] W.-C. Lee, S. Choi, J. Choi, and M. Suk, “An adaptive beamforming technique for smart antennas in WCDMA system,” *IEICE Transaction on Communications*, vol. E86-B, no. 9, pp. 2838–2843, Sept. 2003.

[98] S. N. Nazar, M. Ahmad, M. N. S. Swamy, and W.-P. Zhu, “An adaptive parallel interference canceler using adaptive blind arrays,” in *Proc. IEEE Vehicular Technology Conference (VTC)*, vol. 1, Sept. 24-28, 2002, pp. 425 – 429.

[99] D. Dahlhaus and C. Zhenlan, “Smart antenna concepts with interference cancellation for joint demodulation in the WCDMA UTRA uplink,” in *Proc. IEEE International Symposium on Spread Spectrum Techniques and Applications ISSSTA*, vol. 1, Sept. 2000, pp. 244 – 248.

[100] N. A. Mohamed and J. G. Dunham, “A low-complexity combined antenna array and interference cancellation DS-CDMA receiver in multipath fading channels,” *IEEE Journal on Selected Areas in Communications*, vol. 20, no. 2, pp. 248–256, Feb. 2002.

[101] B. Wang and H. M. Kwon, “PN code acquisition using smart antenna for spread-spectrum wireless communications – part I,” *IEEE Transactions on Vehicular Technology*, vol. 52, no. 1, pp. 142–149, Jan. 2003.

[102] ——, “PN code acquisition for DS-CDMA systems employing smart antennas – part II,” *IEEE Transactions on Wireless Communications*, vol. 2, no. 1, pp. 108–117, Jan. 2003.

[103] R. Knopp and G. Caire, “Power control and beamforming for systems with multiple transmit and receive antennas,” *IEEE Transactions on Wireless Communications*, vol. 1, no. 4, pp. 638–648, Oct. 2002.

[104] A. Mercado and K. J. R. Liu, “Adaptive QoS for wireless multimedia networks using power control and smart antennas,” *IEEE Transactions on Vehicular Technology*, vol. 51, no. 5, pp. 1223–1233, Sept. 2002.

[105] J. G. Proakis, *Digital Communications*, 3rd ed. McGraw-Hill, 1995.

[106] T. Eng, N. Kong, and L. B. Milstein, “Comparison of diversity combining techniques for rayleigh fading channels,” *IEEE Transactions on Communications*, vol. 44, no. 9, pp. 1117–1129, Sept. 1996.

[107] G. L. Stuber, *Principles of Mobile Communication*, 2nd ed. Kluwer Academic Publishers, 2001.

[108] P. V. Rooyen, M. Lotter, and D. V. Wyk, *Space-Time processing for CDMA Mobile Communications*. Kluwer Academic Publishers, 2000.

[109] Third Generation Partnership Project (3GPP), “Tx diversity solutions for multiple antennas (release 5), TR25.869 v1.0.0(2002-2),” in TSG-RAN Meeting #15, Jeju, Korea, Mar. 5-8, 2002.

[110] Y. Zhou, F. Chin, Y. C. Liang, and C. C. Ko, “A novel beam selection transmit diversity scheme for DS-CDMA system,” *IEICE Trans. Commun.*, vol. E84-B, no. 8, pp. 2178–2185, Aug. 2001.

[111] ——, “Performance comparison of transmit diversity and beamforming for downlink of DS-CDMA system,” *IEEE Transactions on Wireless Communications*, vol. 2, no. 2, pp. 320–334, Mar. 2003.

[112] S. Durrani and M. E. Bialkowski, “Effect of mutual coupling on the interference rejection capabilities of linear and circular arrays in CDMA systems,” *IEEE Transactions on Antennas and Propagation*, vol. 52, no. 4, pp. 1130–1134, Apr. 2004.

[113] ——, “Interference rejection capabilities of different types of antenna arrays in cellular systems,” *Electronics Letters*, vol. 38, pp. 617–619, June 2002.

[114] ——, “Investigation into the performance of a adaptive array in cellular environment,” in *Proc. IEEE International Symposium on Antennas and Propagation (APS)*, vol. 2, San Antonio, Texas, June 16-21, 2002, pp. 648–651.

[115] ——, “Effect of angular energy distribution of an incident signal on the spatial fading correlation of a uniform linear array,” in *Proc. 15th International Conference on Microwaves, Radar and Wireless Communications (MIKON)*, vol. 2, Warsaw, Poland, May 17-19, 2004, pp. 493–496.

[116] ——, “A simple model for performance evaluation of a smart antenna in a CDMA system,” in *Proc. Eighth IEEE International Symposium on Spread Spectrum Techniques and Applications (ISSSTA)*, Sydney, Australia, Aug. 30 - Sep. 2, 2004, pp. 379–383.

[117] ——, “Performance analysis of beamforming in ricean fading channels for CDMA systems,” in *Proc. 5th Australian Communications Theory Workshop (AusCTW)*, Newcastle, Australia, Feb. 4-6, 2004, pp. 1–5.

[118] ——, “Analysis of the error performance of adaptive array antennas for CDMA with noncoherent M-ary orthogonal modulation in nakagami fading,” *to appear in IEEE Communications Letters*, vol. 9, no. 2, Feb. 2005.

[119] ——, “Performance of hierarchical beamforming in a rayleigh fading environment with angle spread,” in *Proc. International Symposium on Antennas (ISAP)*, vol. 2, Sendai, Japan, Aug. 17-21, 2004, pp. 937–940.

[120] ——, “Development of CDMASIM: A link level simulation software for DS-CDMA systems,” in *Proc. 14th International Conference on Microwaves, Radar and Wireless Communications (MIKON)*, vol. 3, Gdansk, Poland, May 20-22, 2002, pp. 861–864.

[121] ——, "A smart antenna model incorporating an azimuthal dispersion of received signals at the base station of a CDMA system," in *Proc. IEEE International Multi Topic Conference (INMIC)*, Islamabad, Pakistan, Dec. 8-9, 2003, pp. pp. 218–223.

[122] ——, "BER performance of a smart antenna system for IS-95 CDMA," in *Proc. IEEE International Symposium on Antennas and Propagation (AP-S)*, vol. 2, Columbus, Ohio, June 22-27, 2003, pp. 855–858.

[123] ——, "Simulation of the performance of smart antennas in the reverse link of CDMA system," in *Proc. IEEE International Microwave Symposium (IMS)*, vol. 1, Philadelphia, Pennsylvania, June 8-13, 2003, pp. 575–578.

[124] ——, "An investigation into the interference rejection capability of a linear array in a wireless communications system," *Microwave and Optical Technology Letters*, vol. 35, no. 6, pp. 445–449, Dec. 2002.

[125] S. Durrani, M. E. Bialkowski, and J. Janapsatya, "Effect of mutual coupling on the interference rejection capabilities of a linear array antenna," in *Proc. Asia Pacific Microwave Conference (APMC)*, vol. 2, Kyoto, Japan, Nov. 19-22, 2002, pp. 1095–1098.

[126] *Using Matlab Version* 6.5, The Mathwoks Inc., 2003.

[127] L. C. Godara, Ed., *Handbook of Antennas in Wireless Communications*. CRC Press, 2002.

[128] R. A. Monzingo and T. W. Miller, *Introduction to Adaptive Arrays*. John Wiley, 1980.

[129] S. Anderson, M. Millnert, M. Vitberg, and B. Wahlberg, "An adaptive array for mobile communication systems," *IEEE Transactions on Vehicular Technology*, vol. 40, no. 1, pp. 230–236, Feb. 1991.

[130] R. S. Elliott, *Antenna Theory and Design*, Revised ed. IEEE Press, 2003.

[131] R. F. Harrington, *Field Computation by Moment Method*. IEEE Press, 1993.

[132] *IE3D Electronic Simulator: User Manual*, 5th ed., Zealand Software Inc., 1999.

[133] M. R. Spiegel, *Mathematical Handbook of Formulas and Tables*. McGraw-Hill, 1968.

[134] T. Svantesson, "Modelling and estimation of mutual coupling in a uniform linear array of dipoles," in *Proc. ICASSP 99*, Phoenix, Arizona, Mar. 1999, pp. 2961–2964.

[135] J.-A. Tsai, R. M. Buehrer, and B. D. Woerner, "BER performance of a uniform circular array versus a uniform linear array in a mobile radio environment," *IEEE Transactions on Wireless Communications*, vol. 3, no. 3, pp. 695–700, May 2004.

[136] N. Blaunstein and J. B. Andersen, *Multipath Phenomena in Cellular Networks*. Artech House, 2002.

[137] K. Wesolowski, *Mobile Communication Systems*. John Wiley, 2002.

[138] C. Tepedelenlioglu, A. Adbi, and G. B. Giannakis, "The ricean *K* factor: Estimation and performance analysis," *IEEE Transactions on Wireless Communications*, vol. 2, no. 4, pp. 799–809, July 2003.

[139] M. Wittmann, J. Marti, and T. Kurner, "Impact of the power delay profile shape on the bit error rate in mobile radio systems," *IEEE Transactions on Vehicular Technology*, vol. 46, no. 2, pp. 329–339, May 1997.

[140] "COST 207: Digital land mobile radio communications," Office for Official Publications of the European Communities, Luxembourg, Final report, 1989.

[141] R. L. Peterson, R. E. Ziemer, and D. E. Broth, *Introduction to Spread Spectrum Communications*. Prentice Hall, 1995.

[142] Y. Akaiwa, *Introduction to Digital Mobile Communication*. John Wiley, 1997.

[143] D. Hong and T. S. Rappaport, "Traffic model and performance analysis for cellular mobile radio telephone systems with prioritized and nonprioriotized handoff procedures," *IEEE Transactions on Vehicular Technology*, vol. 35, pp. 77–92, Aug. 1986.

[144] R. Prasad, *CDMA for Wireless Personal Communications*. Artech House, 1996.

[145] M. Lotter and P. V. Rooyen, "Modelling spatial aspects of cellular CDMA/SDMA systems," *IEEE Communications Letters*, vol. 3, no. 5, pp. 128–131, May 1999.

[146] A. Abdi, J. A. Barger, and M. Kaveh, "A parametric model for the distribution of the angle of arrival and the associated correlation function and power spectrum at the mobile station," *IEEE Transactions on Vehicular Technology*, vol. 51, no. 3, pp. 425–433, May 2002.

[147] A. Abdi and M. Kaveh, "A space-time correlation model for multielement antenna systems in mobile fading channels," *IEEE Transactions on Communications*, vol. 20, no. 3, pp. 550–560, Apr. 2002.

[148] J. Salz and J. H. Winters, "Effect of fading correlation on adaptive arrays in digital mobile radio," *IEEE Transactions on Vehicular Technology*, vol. 43, no. 4, pp. 1049–1057, Nov. 1994.

[149] J. Fuhl, A. F. Molisch, and E. Bonek, "Unified channel model for mobile radio systems with smart antennas," *Proc. Inst. Elect. Eng. Radar, Sonar, Navigation*, vol. 145, no. 1, pp. 32–42, Feb. 1998.

[150] J. Luo, J. R. Zeidler, and S. McLaughlin, "Performance analysis of compact antenna arrays with MRC in correlated nakagami fading channels," *IEEE Transactions on Vehicular Technology*, vol. 50, no. 1, pp. 267–277, Jan. 2001.

[151] K. I. Pedersen, P. E. Mogensen, and B. H. Fleury, "Power azimuth spectrum in outdoor environments," *IEE Electronics Letters*, vol. 33, no. 18, pp. 1583–1584, 1997.

[152] ——, “Spatial channel characteristics in outdoor environments and their impact on BS antenna system performance,” in *Proc. IEEE Vehicular Technology Conference (VTC)*, Ottawa, Canda, May 1998, pp. 719–724.

[153] S. K. Yong and J. S. Thompson, “The impact of angle of arrival distribution on the performance analysis of different antenna array architectures,” in *Proc. IEE International Conference on Antennas and Propagation(ICAP)*, vol. 2, no. 491, UK, Mar. 2003, pp. 840–843.

[154] T. S. Pollock, T. D. Abhayapala, and R. A. Kennedy, “Introducing space into MIMO capacity calculations,” *Telecommunication Systems*, vol. 24, no. 2-4, pp. 415–436, Oct.-Dec. 2003.

[155] J. A. Tsai, R. M. Buehrer, and B. D. Woerner, “The impact of AOA energy distribution on the spatial fading correlation of linear antenna array,” in *Proc. IEEE Vehicular Technology Conference (VTC)*, vol. 2, May 6-9 2002, pp. 933–937.

[156] P. D. Teal, T. D. Abhayapala, and R. A. Kennedy, “Spatial correlation for general distributions of scatterers,” *IEEE Signal Processing Letters*, vol. 9, no. 10, pp. 305–308, Oct. 2002.

[157] M. Abramowitz and I. A. Stegun, Eds., *Handbook of Mathematical Functions: With Formulas, Graphs, and Mathematical Tables*. Dover, 1965.

[158] T. Ihara, S. Tanaka, M. Sawahashi, and F. Adachi, “Fast two-step beam tracking algorithm of coherent adapative antenna array diversity receiver in W-CDMA reverse link,” *IEICE Transactions on Communications*, vol. E84-B, no. 7, pp. 1835–1848, July 2001.

[159] J. S. Lee and L. E. Miller, *CDMA Systems Engineering Handbook*. Artech House, 1998.

[160] J. E. Hudson, *Adaptive Array Principles*. Peter Peregrinus Ltd., 1981.

[161] R. Price and P. E. Green, "A communication technique for multipath channels," *Proceedings of Institute of Radio Engineers (IRE)*, vol. 46, pp. 555–570, Mar. 1958.

[162] B. Sklar, *Digitial Communications Fundamentals and Applications*, 2nd ed. Prentice Hall, 2001.

[163] R. Steele, *Mobile Radio Communications*. John Wiley, 1992.

[164] D. J. Torrieri, "Performance of direct-sequence systems with long psuedonoise sequences," *IEEE Journal on Selected Areas in Communications*, vol. 10, no. 4, pp. 770–781, May 1992.

[165] P. J. Crepeau, "Uncoded and coded performance of MFSK and DPSK in nakagami fading channels," *IEEE Transactions on Communications*, vol. 40, no. 3, pp. 487–493, Mar. 1992.

[166] A. Poloni and U. Spagnolini, "A simple method to calculate the error probability for 2D RAKE receivers," in *Proc. IEEE Vehicular Technology Conference (VTC)*, vol. 1, May 2001, pp. 590–594.

[167] C. Z. W. H. Sweatman, B. Mulgrew, J. S. Thompson, and P. M. Grant, "Spatial equivalence classes for CDMA array processing," in *Proc. IEEE International Conference on Communications (ICC)*, Vancouver, Canada, June 199, pp. 544–548.

[168] H. Harada and R. Prasad, *Simulation and Software Radio for Mobile Communications*. Artech House, 2002.

[169] M. C. Jeruchim, P. Balaban, and K. S. Shanmugan, *Simulation of Communication Systems*. Plenum Press, 1992.

[170] P. J. Smith, M. Shafi, and H. Gao, "Quick simulation: A review of importance sampling techniques in communications systems," *IEEE Journal on Selected Areas in Communications*, vol. 15, no. 4, pp. 579–613, May 1997.

[171] S. C. Yang, *CDMA RF System Engineering*. Artech House, 1998.